Thesis for The Degree of Licentiate of Engineering

An Isolated Integrated Charger for Electric or Plug-in Hybrid Vehicles

Saeid Haghbin

Division of Electric Power Engineering
Department of Energy and Environment
Chalmers University of Technology
Göteborg, Sweden, 2011

An Isolated Integrated Charger for Electric or Plug-in Hybrid Vehicles

Saeid Haghbin

Division of Electric Power Engineering
Department of Energy and Environment
Chalmers University of Technology
Göteborg, Sweden

This thesis has been prepared using LaTeX.
Printed by Chalmers Reproservice,
Göteborg, Sweden 2011.

To my family and friends

Abstract

For electric and hybrid vehicles using grid power to charge the battery, traction circuit components are not normally engaged during the charging time, so there is a possibility to use them in the charger circuit to have an on-board integrated charger.

In this Licentiate thesis, an isolated high power integrated charger is proposed, designed and constructed based on a special ac machine with a double set of stator windings called motor/generator. The charger is capable of unit power factor operation as well as bi-directional power operation for grid to vehicle application.

The mathematical electromechanical model of the motor/generator is derived and presented. Based on the developed model, new controller schemes are developed and designed for the grid synchronization and charge control. The machine windings are re-arranged for the traction and charging by a controllable relay-based switching device that is designed for this purpose.

A laboratory system is designed and implemented based on a 4 pole 25 kW interior permanent magnet synchronous motor and a frequency converter considering the integrated charging features for winding re-configuration. The practical results will be added in the next step of the project. The charging power is limited to 12.5 kW due to the machine thermal limit (half of the motor full power in the traction mode) for this system.

The whole system is simulated in Matlab/Simulink based on the developed model and controllers to verify the system operation for the charge control. Simulation results show that the system has good performance during the charging time for a load step change. The simulation results show also a good performance of the controllers leading to machine speed stability and smooth grid synchronization. Moreover, the unit power factor operation is achieved for battery charging in the simulations.

Keywords

Integrated Battery Charger, Galvanic Isolation, Vehicle Applications, Grid Synchronization

Acknowledgment

I would like to take this opportunity to thank my supervisor Ola Carlson for his great support, constant guidance, encouragement and for giving me the opportunity to start PhD education in the Division of Electric Power Engineering. Also, I would like to thank Sonja Lundmark, my co-supervisor, for her friendship, continuous help and excellent support.

Thanks to the Swedish Hybrid Vehicle Center (SHC), the partners inside SHC, the Swedish Energy Agency and Chalmers University of Technology for the project financial support.

The current project was part of theme 2 inside SHC. We have a good working group lead by Mats Alaküla from Lund University. Thanks to Mats for his valuable attitude and great support to form such a nice working group. Mats Leksell, Oskar Wallmark, Kashif Khan, Shuang Zhao, all from Royal Institute of Technology (KTH), and Fadi Abdallah from Lund University were our academic partners of the project. I would like thank to them all for all discussions, meetings and co-operations. Some parts of the hardware including the electrical machine designed in KTH was valuable help in this project. Moreover, we had nice time together in the context of the project that I have a good reminiscence of it.

Thanks to Lennart Josefson, director of SHC, for his nice support. It was exciting to attend to events conducted by SHC like test drives in Volvo and Scania. I never dream of driving a truck or a bus before! Thanks to our industrial project partners for support and discussions during the project. I would like to mention Robert Eriksson (Volvo Car Corporation), Niklas Edvinsson (Saab Automobile AB), Mats Hilmersson (Saab Automobile AB), Olof Martander (Saab Automobile AB), Anders Kroon (AB Volvo), Jörgen Engström (Scania CV AB), Lars Stenqvist (Scania CV AB), Jonas Hofstedt (Scania CV AB), Svante Bylund (BAE Systems Hägglunds AB) and Viktor Lassila (BAE Systems Hägglunds AB).

My special thanks go to Torbjörn Thiringer, my examiner, for his time and valuable comments. I am very grateful to Lina Bertling for her support at the division and nice co-operation regarding different activities.

Several people helped us to bring the idea to practice that without their support it was not possible to finish the job. Thanks to Robert Eriksson and his colleagues to provide and prepare us a car to install our hardware in. Rickard Larsson, Magnus Ellsen, Mikael Alatalo, Oskar Josefsson and Robert Karlsson had great contribution to develop the hardware. We also had a good IT support from Jan-Olov Lantto. Thank you all!

I express my sincere thanks to David Steen as a valuable friend and room-

mate. Thanks to Valborg and Eva for their kind help and support. In addition, I would like to thank Stefan Lundberg for his valuable technical support. Special thanks go to Tarik for his excellent support and nice time we spent together specially in our sport activities. Thanks to Johan, Andreas, Ali, Poopak and Emma for their friendship and support.

As an international student I faced tough times regarding different issues. I am indebt of many friends for their valuable support, help and synergy. I would like to give my sincere regards and thanks to Sima, Maziar, Fariba, Hadi, Mohsen, Mohammad Reza Shoaie, Mohammad Reza Gholami and other friends.

Heartfelt and special thanks go to Maliheh, my wife, for endless love, support and patience.

Saeid Haghbin
Göteborg, January 2011

Preface

The Swedish Hybrid Vehicle Center (SHC) was formed in spring 2007 to serve as a center of excellence in Sweden in research and development of sustainable hybrid electric vehicle systems. The mission of the center is to do research and development in hybrid electric vehicles to enhance education and cooperation between industry and academia. Several industrial and academic partners have active participation in the center activities.

The research in the center categorizes to three main themes: the control of the hybrid vehicle, the electric drive line and the energy storage. Theme 2 projects deal with electrical drive systems for the traction system inside the vehicle.

Three projects were defined in theme 2: Sensorless control of the motor in traction, integrated battery chargers (subject of this thesis) and electromagnetic compatibility design. These three projects are running together and share the same target vehicle specifications.

List of Publications and Patents

Appended papers

This thesis is based on the following papers:

[I] Saeid Haghbin, Sonja Lundmark, Mats Alaküla and Ola Carlson, "Grid-Connected Integrated Battery Chargers in Vehicle Applications: Review and New Solution,"
submitted to the IEEE Transactions on Industrial Electronics, 2011.

[II] Saeid Haghbin, Sonja Lundmark, Mats Alaküla and Ola Carlson, "An isolated high power integrated charger in electrified vehicle applications,"
submitted to the IEEE Transactions on Vehicular Technology, 2011.

[III] Saeid Haghbin, Sonja Lundmark and Ola Carlson, "Performance of a Direct Torque Controlled IPM Drive System in the Low Speed Region,"
Proc. of IEEE International Symposium on Idustrial Electronics (ISIE), Bari, Italy, July 2010.

Other papers

The following papers are published or submitted but not appended to the thesis, in some cases due to contents overlapping that of appended papers.

[i] Saeid Haghbin, Sonja Lundmark, Ola Carlson and Mats Alaküla, "A Combined Motor/Drive/Battery Charger Based on a Split-Windings PMSM,"
submitted to the IEEE Vehicle Power and Propulsion Conference (VPPC 2011), 2011.

[ii] Saeid Haghbin, Kashif Khan, Sonja Lundmark, Mats Alaküla, Ola Carlson, Mats Leksell and Oskar Wallmark, "Integrated Chargers for EVs and PHEVs: Examples and New Solutions,"
Proc. of XIX IEEE International Conference on Electrical Machines (ICEM), ISBN/ISSN: 978-1-4244-4174-7, Rome, Italy, Sep. 2010.

[iii] Saeid Haghbin, Mats Alaküla, Kashif Khan, Sonja Lundmark, Mats Leksell, Oskar Wallmark and Ola Carlson, "
An Integrated Charger for Plug-in Hybrid Electric Vehicles Based on a

Special Interior Permanent Magnet Motor,"
Proc. of IEEE Vehicle Power and Propulsion Conference (VPPC 2010), Lille, France, 1-3 Sep. 2010.

[iv] Saeid Haghbin and Torbjörn Thiringer, "Impact of inverter switching pattern on the performance of a direct torque controlled synchronous reluctance motor drive,"
Proc. of International Conference on Power Engineering, Energy and Electrical Drives (POWERENG 09), ISBN/ISSN: 978-1-4244-4611-7, 18-20 March 2009, Lisboa, Portugal, pp. 337-341.

[v] Kashif Khan, Saeid Haghbin, Mats Leksell and Oskar Wallmark, "Design and performance analysis of a permanent-magnet assisted synchronous reluctance machine for an integrated charger application,"
Proc. of XIX IEEE International Conference on Electrical Machines (ICEM), ISBN/ISSN: 978-1-4244-4174-7, Rome, Italy, Sep. 2010.

Patents

The following patent is filed as a result of the current project:

[i] Saeid Haghbin (Chalmers University of Technology) and Mats Alaküla (Lund University), "Elektrisk Appart," Swedish Pattent Office, Patent no 1050607-9, filed in 14 June 2010.

Contents

Chapter 1

Introduction

The project background and important related results regarding previous works are presented in this chapter. Moreover, the scope of the project and main contributions are also explained.

1.1 Background and Previous Work

The battery has an important role in the development of electric vehicles (EV) or plug-in hybrid electric vehicles (PHEV) [1–5]. The performance of battery modules depends not only on the design of modules, but also on how the modules are used and charged. In this sense, battery chargers play a critical role in the evolution of this technology. Generally there are two types of battery chargers: on-board type and stand-alone (off-board) type [2,3]. The on-board type would be appropriate for nighttime charging from a household utility outlet, or for charging during daytime at workplaces, malls or for emergency charging where no off-board charger is available. On the other hand, the off-board charger can be compared to a gas station used for an internal combustion engine vehicle, thus it is aimed at rapid charging. Because the on-board type of charger always should be carried by the vehicle, the weight and space have to be minimized. Of course, it is very important to minimize charger cost (especially the on-board versions). For on-board chargers, it is difficult to have high power level because of its weight, space and in total cost. Another difficulty is to assure galvanic isolation. Although it is a very favorable option in the charger circuits for safety reasons [6–8], it is usually avoided due to its cost impact on the system.

During charging the vehicle is parked so there is a possibility to use available traction hardware, mainly the electric motor and the inverter, for the charger circuit and thus to have an integrated motor/drive/battery charger to decrease the system weight, space and cost [9]. Several different types of integrated chargers are reported by industry or academia regarding vehicle applications (subject of appended Paper I). For those integrated chargers, the electric motor is used as inductors or as an isolated transformer while the machine is in standstill during charging time. All but one of the reported integrated chargers are non-isolated and they need extensive protection and shielding for safe and proper operation [6]. For the one isolated charger, a

wound rotor induction machine is used as an isolated transformer [9]. So for this solution the system has low efficiency due to the need of a high magnetization current.

So, among the reported integrated chargers, there is no version that combines galvanic isolation and high efficiency features. Moreover, few of them are high power chargers [9].

1.2 Purpose of the Thesis and Contributions

The main objective of the work reported in this thesis is to develop a high power isolated integrated charger for EVs or PHEVs that is 12.5 kW in this case (subject of appended paper II). It is also an objective to investigate the impact of different inverter switching patterns on the performance of a direct torque control (DTC) based drive system (subject of appended paper III). In summary the main contributions can be listed as:

- Proposition, design and implementation of an isolated high power integrated charger based on a special machine winding configuration.
- Mathematical modeling, controllers development and simulation of different system parts including a six terminal electrical machine called motor/generator, grid synchronization and charge control.

1.3 Thesis Outline

The thesis is divided into two parts. The first part gives an introduction to the subject and the second part includes three appended papers. The target vehicle specification including the charging system is presented in the second chapter. The review of integrated chargers is described in chapter 3. The proposed integrated charger with galvanic isolation is described in chapter 4. Chapter 5 is dedicated to conclusions and future work.

Chapter 2

Electrical Driveline Specification of the Target Vehicle

The hybrid electric vehicle (HEV) can, just like the pure electric vehicle (EV), give a higher energy efficiency and reduced emissions when compared with conventional vehicles but compared to the EV, it can also be driven for a longer range by using an internal combustion engine (ICE). A plug-in hybrid means that the HEV can be charged from a power supply off-board. In this project, the electric driveline of a PHEV have been considered with the charger specification. The system configuration and specification is presented in this chapter.

2.1 Plug-in Hybrid Electric Vehicles

Fig. 2.1 shows a schematic diagram of a PHEV with a parallel configuration. The electrical part includes the grid connected battery charger, battery, inverter, motor and control system [1]. During charging time the vehicle is not driven and during driving time the charger is not intended to charge the battery pack. However, it is possible to use the inverter and motor in the charger circuit to reduce the system components, space and weight which means a cost reduction. This is what is referred to as an integrated charger in this thesis.

2.2 Traction System Specification

The traction system specification was set by the project working group and industrial partners. The target vehicle is a passenger car with parallel configuration (PHEV). Table 2.1 shows the traction system specifications.

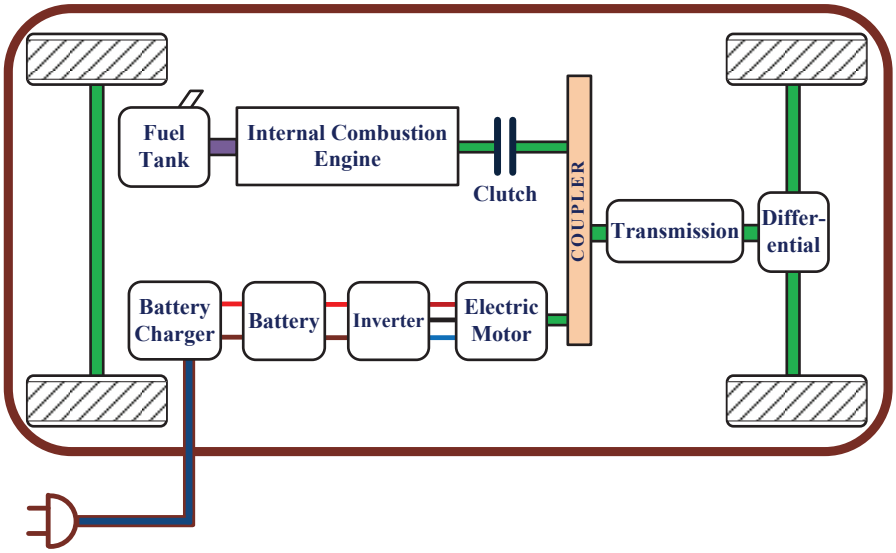

Figure 2.1: Simplified schematic diagram of a PHEV.

Table 2.1: Electrical driveline specification of target vehicle in traction mode.

Continuous traction power of the electric motor (kW)	25
Electric motor peak traction power for 3 seconds (kW)	45
Battery voltage level (V)	400
Electric motor speed range (rpm)	0 ... 6500
Electric motor base speed(rpm)	1500
Electric motor maximum speed (rpm)	6500
Electric motor maximum torque (Nm)	270

2.3 Charger Specification

Three-phase supply is available in most residential areas in Sweden. For a three-phase 400 V and 32 A supply, the maximum available power is 22 kW. So the primary level of charging power was set to 22 kW with the three-phase utility grid supply. Later on, the charging power level reduced to half of the traction power due to the integration, that is 12.5 kW in this case.

Although galvanic isolation is not mandatory in the charging circuit according to related standards [10], it is a very interesting option due to the safety and EMC issues. It was thus included in the specifications.

Additionally unit power factor operation was another functionality that was set as mandatory in the specification. Further, bi-directional charger operation, which would allow vehicle to grid (V2G) operation was regarded as an interesting operational feature.

Chapter 3

Review of Integrated Chargers in Vehicle Applications

Different types of integrated chargers are reported by academia or industry [11–14, 19, 20, 20, 21, 21, 22, 22, 23, 27–31, 33–39, 39–43]. Some of them that are more relevant to the current project are reviewed and compared in this chapter.

Different power levels of chargers are briefly presented in the first section and the examples of integrated chargers are described and compared in the second section.

3.1 Battery Chargers in Vehicle Applications

Chargers can be classified in terms of power levels and time of charging [40,41]. The choice of classification depends naturally on nationally available power levels. One example of classification that suits the US residential power source is given in [40]:

Level 1: Common household type of circuit in US rated to 120 V and up to 15 A.

Level 2: Permanently wired electric vehicle supply equipment used specially for electric vehicle charging and it is rated up to 240 V, up to 60 A, and up to 14.4 kW.

Level 3: Permanently wired electric vehicle supply equipment used specially for electric vehicle charging and it is rated greater than 14.4 kW.

Equivalently, above categories are known as emergency charger which charges the battery pack of a vehicle in six to eight hours, standard charger which charges the battery pack in two to three hours, and rapid charger which charges the battery pack in ten to fifteen minutes (fast chargers). Chargers can also be described as either conductive or inductive.

For a conductive charger, the power flow take place through metal-to-metal contact between the connector on the charge port of the vehicle and charger

(off-board charging) or grid (on-board charging). Conductive chargers may have different circuit configurations but the common issues concern safety and the design of the connection interface.

Inductive coupling is a method of transferring power magnetically rather than by direct electrical contact and the technology offers advantages of safety, power compatibility, connector robustness and durability to the users of electric vehicles but on the expense of a lower efficiency and the need of new equipment at charging sites. The electric vehicle user may physically insert the coupler into the vehicle inlet where the ac power is transformer coupled, rectified and fed to the battery, or the charging could be done almost without driver action by wireless charging [42]. For inductive charging, among the most critical parameters are the frequency range, the low magnetizing inductance, the high leakage inductance and the significant discrete parallel capacitance [5, 43].

Different topologies and schemes are reported for both single-phase and three-phase input conductive battery chargers. Usually the three-phase input solutions are used in high power applications [44–47].

3.2 Examples of Integrated Chargers

The electrical system inside a grid-connected hybrid electric vehicle mainly includes the grid connected battery charger, battery, inverter, motor and control system. It is here assumed that during charging time the vehicle is not driven and during driving time it is not possible to charge the battery pack from the grid.

In a classical electrical device arrangement in the vehicle, there are separate inverter and charger circuits for traction and charging from an external source. However, it is possible to integrate both hardware to reduce the system components, space and weight which is equivalent to cost reduction. For instance, the three-phase three-wire boost AC/DC converter that can be used as a battery charger is very similar to the hardware that is available in the traction system. See [44, 45] for different AC/DC rectifier schemes.

Another example of the use of integration is to use the electric motor windings as inductors in the charger circuit. This reduces weight as high current inductors are large components compared to other components like switches for example.

A traction system based on an ac motor and a three-phase inverter is shown in Fig. 3.1. In some schemes a DC/DC converter is used in the system also [48]. The battery power is transferred to the motor through the inverter. Bidirectional operation of the inverter allows energy restoration during braking to the battery. Regarding different drive systems, different types of integrated chargers are reported both within academia and industry and some of them are assessed here.

3.2.1 A Combined Motor Drive and Battery Recharge System Based on an Induction Motor

An integrated motor drive and charger based on an induction machine was patented 1994 by AC Propulsion Inc. [12] and is currently in use in the car

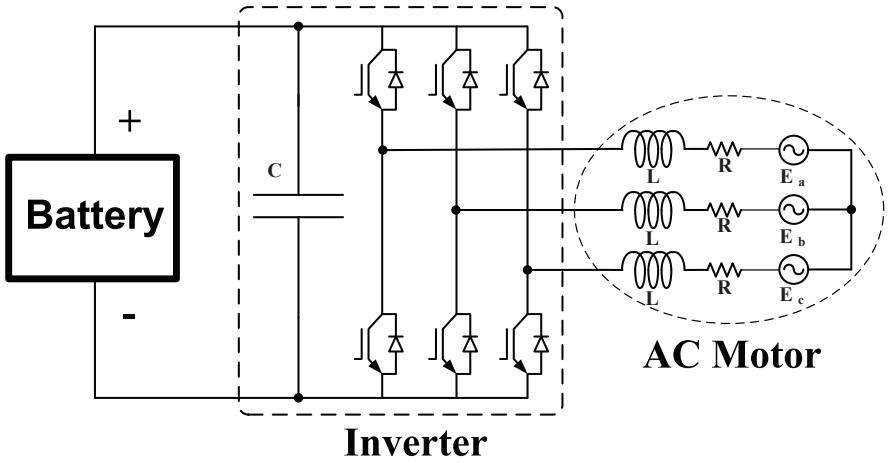

Figure 3.1: Electrical traction in a vehicle.

industry [49]. The main idea is to use the motor as a set of inductors during charging time to constitute a boost converter with the inverter to have unit power factor operation. Fig. 3.2 shows the functional schematic diagram of this non-isolated integrated charger system. By the means of inexpensive relays the machine windings are reconfigured to be inductors in the charging mode.

It is possible to have a three-phase input supply with this scheme, but there will be developed torque in the machine during charging that should be considered. The single-phase charger can charge from any source, $100 - 250\ Vac$, from 200 W up to 20 kW and can be used for V2G (vehicle to grid) and for backup power and energy transfer to other electric vehicles. The filter bank at the front of the ac supply will smooth the harmonic contents of the charger line current also.

Other similar alternatives have been patented in the US [13, 14]. All of these solutions are bidirectional non-isolated type of chargers with unit power factor operation and single-phase ac supply.

3.2.2 Non-isolated Integrated Charger Based on a Split-Winding AC Motor

A non-isolated high power three-phase integrated charger is reported by Luis De Sousa et al. in Valeo Engine and Electrical Systems in 2010 [19–21]. Fig. 3.3 shows the proposed integrated charger. In traction mode a 3H-bridge topology is used with a DC/DC converter. The DC/DC converter consists of inductor L and two switches. The inverter dc bus voltage is 900 Vdc while the battery voltage is maximum 420 Vdc for the proposed system.

Fig. 3.4 shows the system equivalent circuit in charging mode. For charging, the three-phase supply is connected to the middle point of the stator windings. A small EMI filter is used to improve the grid current waveforms. As is shown in this figure, there are two three-phase boost converters sharing a common dc bus. By using a split-winding configuration and regulating the

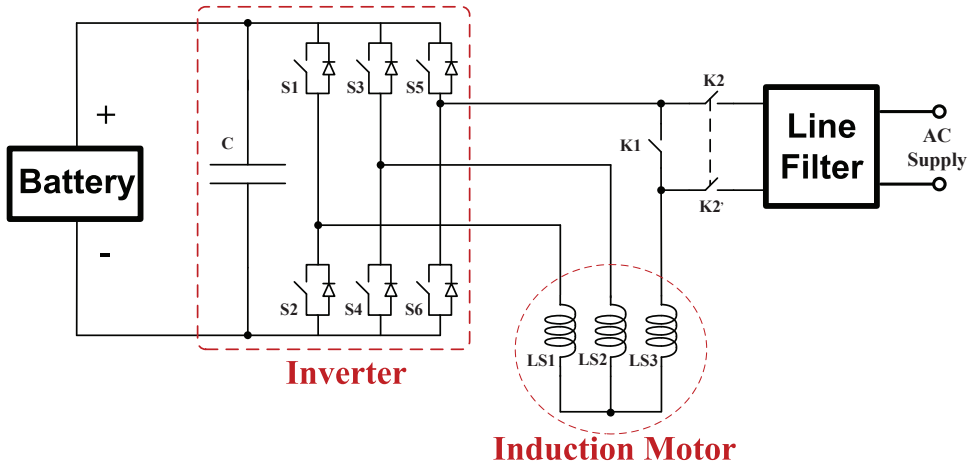

Figure 3.2: Non-isolated single-phase integrated charger based on an induction motor drive system.

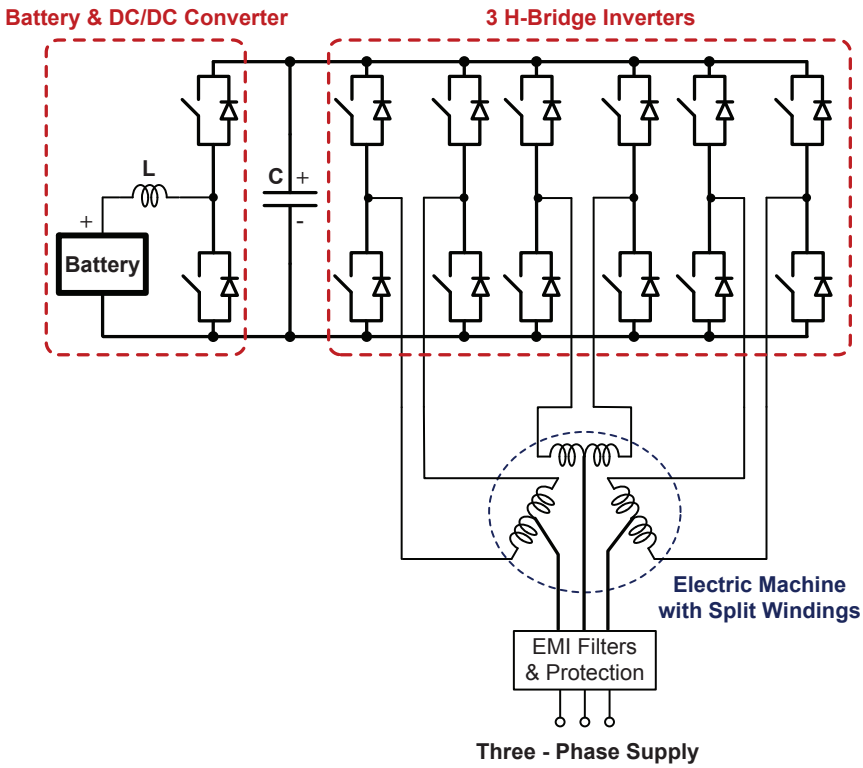

Figure 3.3: Three-phase non-isolated integrated charger based on a split-winding ac motor.

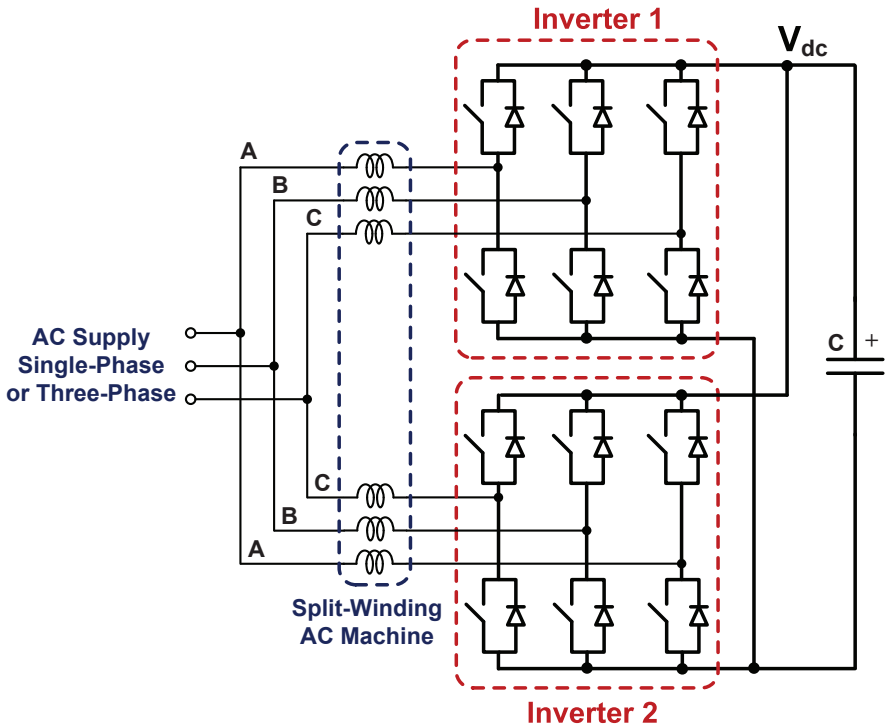

Figure 3.4: Charging mode equivalent circuit of the three-phase integrated charger based on a split-winding ac motor.

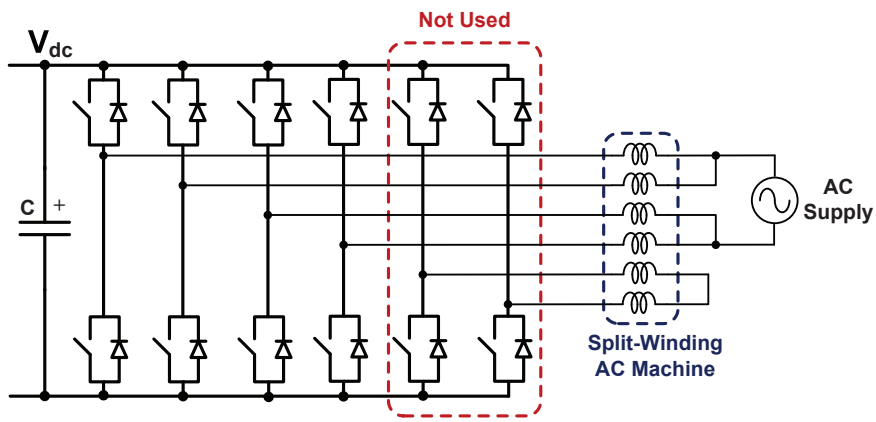

Figure 3.5: Charging mode equivalent circuit of the single-phase integrated charger based on a split-winding ac motor.

same current in the same phases of the two boost converters, the developed stator magnetomotive force (MMF) of the machine is eliminated so there is not any rotational magnetic field in the motor during charging.

The proposed charger is a high power non-isolated version capable of unit power factor operation. There is no need to use a switch like contactor for the charger to grid connection. A plug can be used for this purpose. Two international patents are received for the proposed scheme [22, 23].

It is shown that it is possible to use the same strategy for a single-phase supply by S. Lacroix et al. [21]. Fig. 3.5 shows the system in charging mode for the single-phase supply. Four legs of bridges in the inverter and inductances of two phases are used in this mode. As is shown in this figure, the third H-bridge inverter is not used. The currents will be regulated to be equal for each phase. Unit power factor operation is possible in this case also due to the boost converter topology.

3.2.3 An Integral Battery Charger for a Four-Wheel Drive Electric Vehicle

An integral battery charger is reported for a four-wheel motor driven EV by Seung-Ki Sul and Sang-Joon Lee [20]. The propulsion system includes four induction motors and four three-leg inverters with a battery on the system dc bus. By the use of an extra transfer switch the whole system is reconfigured to a single-phase battery charger. Fig. 3.6 shows the system configuration in traction and charging mode. In traction mode, four inverters are connected to the system dc bus drive motors (each motor neutral point is float in this mode). In the charging mode (the transfer switch is in position 2) the single-phase ac source is connected between the neutral points of two motors. Utilizing the switches in inverter one and two, this configuration will be a single-phase boost converter with unit power factor operation capability. The third and fourth inverters with the use of two other motors constitute two buck-type converters. Fig. 3.7 shows the system equivalent circuit in charging mode where the motors are used as inductors. For each motor the winding currents are the same for each phase so there is no developed electromagnetic torque in the motors during the charging time. Further, in the charging mode, by controlling the PWM boost converter, the dc link voltage is kept constant. The constant current battery charging profile is achieved by the control of the two buck-type choppers. Of course, this integrated charger solution is a high cost solution and only appropriate for vehicles with four-wheel motors.

3.2.4 An Integrated Charger for an Electric Scooter

A non-isolated single-phase (110 Vac and 60 Hz) integrated charger for an electrical scooter is another example described in [21]. The authors use the three-phase inverter as a single switch in the charging mode, see Fig. 3.8 Thus, the switches S2, S4 and S6 seen in Fig. 3.8 are to be operated all together as a simple switch. In turn, the circuit is a single-phase boost converter. All three windings of the motor are used in the charging process. A power rectifier and line filter are also used as extra components for the charging operation. It is expected to have unit power factor operation as is expected for the boost

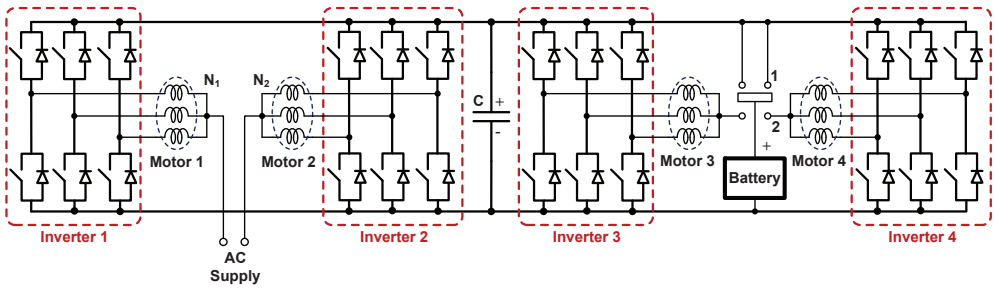

Figure 3.6: Power circuit of integrated battery charger for a four wheel drive.

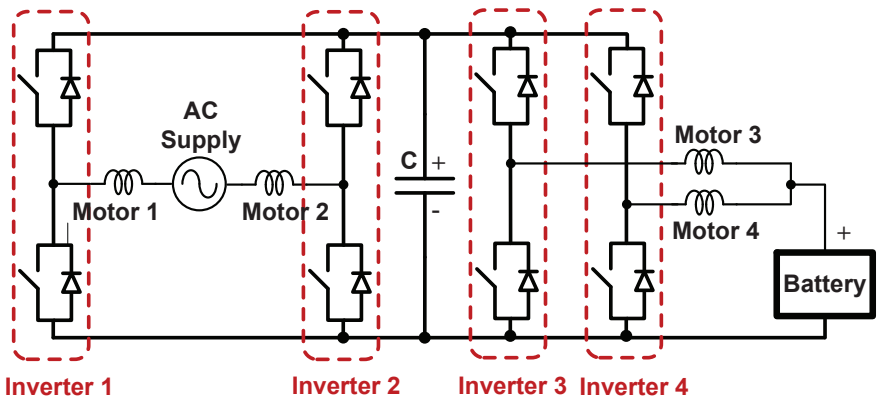

Figure 3.7: System equivalent circuit in charging mode.

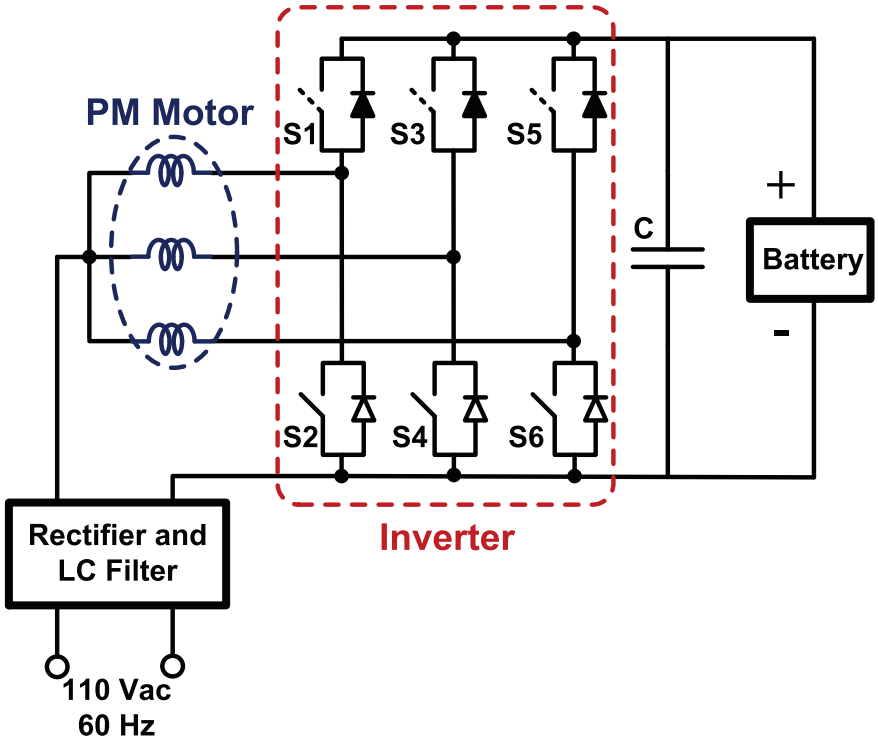

Figure 3.8: Single-phase integrated charger for an electric scooter.

converter and low THD in the ac line current due to use of the line filter. A 180 Vdc lead acid battery (12 Ah) is used as the traction power source and the motor is a 6 kW axial flux permanent magnet motor. Moreover, 50 A and 600 V IGBT modules are used with a switching frequency of 25 kHz. At charging mode, the motor is used as three parallel connected 0.1 mH inductances. The currents through the inductances are thus unidirectional, thus no torque is developed in the motor, and the rotor can be at standstill. Of course, only slow, low power charging is possible with this solution.

3.2.5 Isolated Integrated Charger Based on a Wound-Rotor Induction Motor

An integrated drive/charger system has been reported in 2005 for a fork lift truck [22] in which an induction motor is used as a step down transformer in the charging mode. In the traction mode a 6 kW induction machine is used to drive the truck. The battery voltage and rated motor voltage is nominal 48 V. A three-phase inverter is utilized for motor control based on the space vector modulation (SVM) scheme.

In charging mode, the motor is used as a low frequency step-down transformer. A wound-type rotor is used in the drive system and for the charging mode the rotor winding is used as a primary side of the transformer with the secondary side (the stator) connected to the grid (three-phase 400 Vac).

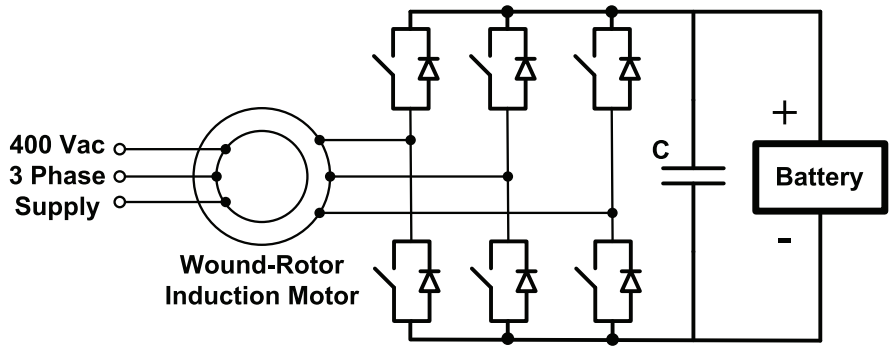

Figure 3.9: Integrated charger based on the operation of an induction machine as a three-phase transformer.

Naturally, there is a galvanic insolation between the grid and battery by the means of this transformer. Fig. 3.9 shows the system in charging mode. The air-gap in the motor (transformer in charging mode) will affect the system performance regarding the loss due to the need of large magnetization currents. Other disadvantages are the extra cost of the wound rotor (compared to a squirrel cage rotor), need of contactors and the need to adapt the motor windings to the charge voltage. Advantages include the possibility of bidirectional power flow, low harmonic distortion and a unit power factor. The rotor is at standstill during charging and a mechanical lock is used.

3.2.6 Comparison of Integrated Chargers

All but one of the presented examples of chargers are non-isolated versions. The presented integrated chargers are compared and summarized in Table 3.1. Type of supply (three-phase or single phase), galvanic isolation of the grid, unit power factor operation capability, efficiency, and extra components for integration are considered in this comparison.

Table 3.1: Comparison of integrated charger examples.

Solution	**Supply**	**Isolation**	**Efficiency**	**PFC Operation**	**Extra Components for Charging**	**Comments**
A Combined Motor Drive and Battery Recharge System Based on an Induction Motor (3.2.1)	single-phase or three-phase	non-isolated	high	feasible	few relays and a line filter	is currently used in car industry
Non-isolated Integrated Charger Based on a Split-Winding AC Motor (3.2.2)	single-phase or three-phase	non-isolated	high	feasible	an extra inverter	will be used in car industry
An Integral Battery Charger for a Four-Wheel Drive Electric Vehicle (3.2.3)	single-phase	non-isolated	high	feasible	a position switch	4 motors and inverters are used in traction mode
An Integrated Charger for an Electric Scooter (3.2.4)	single-phase	non-isolated	high	feasible	a line filter	—
Isolated Integrated Charger Based on a Wound-Rotor IM (3.2.5)	single-phase or three-phase	isolated	low due to the motor air gap	feasible	mechanical rotor lock	feasible for wound type rotor induction motor

Chapter 4

An Integrated Charger Based on a Special ac Machine

A high power isolated integrated battery charger based on a special winding configuration of an ac machine is described in this section. First, the system diagram of the proposed solution is described and then the mathematical model of the machine with double set of stator windings is presented. Further, the system operation in charging mode is explained. Different developed controllers for grid synchronization and charge control are also explained. Simulation results are presented to show the system operation in charging mode for the proposed integrated charger. Moreover, the drive system performance of a DTC based IPM machine is presented as an example that can be applied for the charger grid synchronization and charge control.

4.1 Proposed Isolated Integrated Charger

By reconfiguration of the electric motor windings, an integrated charger scheme is proposed where the machine is used as a special grid connected generator. The main idea is to introduce a multi terminal device called motor/generator set to act like a motor in traction mode and like an isolated generator/transformer in charging mode. The so called motor/generator acts as an isolated three-phase power source after synchronization with the utility grid in charging mode. This rotary three-phase isolated power source constitutes a three-phase boost rectifier (battery charger) with full utilization of the inverter.

All machine windings are used in traction mode and are then reconnected in charging mode through a simple switching device. Fig. 4.1 shows a schematic diagram of the integrated charger for a PHEV first proposed in [11]. Different motor topologies are possible both concerning motor types and winding arrangement. One option with an internal permanent magnet synchronous motor was reported in [11, 50].

Fig. 4.2 shows a simple schematic diagram of the system in the charging mode. This solution has bidirectional capability so it is possible to bring back

power to the grid from the battery. Moreover, unit power factor operation is feasible. Depending on the type of machine and winding configuration, a single-phase solution is also possible. The charging power will be limited by the motor thermal limit and inverter power limit and limit of the supply, so high power charging is feasible in this configuration.

The motor rotates at synchronous speed during charging so a mechanical clutch is used to disconnect the motor from the transmission system. Before connection to the grid, through the inverter-side stator windings, the battery and inverter will synchronize the voltage at the grid-side windings to the grid voltage.

After grid synchronization, the grid-side stator windings are connected to grid voltage. Now the inverter side windings are an isolated three-phase voltage source and the inverter can control the dc voltage and current at the battery side. One control objective is to keep the torque zero during synchronization with the grid. Another control objective is unit power factor operation.

To have proper boost converter operation the dc bus voltage should be more than peak ac line voltage. This can be solved in two ways: using an extra DC/DC converter or $Y - \Delta$ connection of the stator windings to reduce the voltage at the inverter side. The second approach has been selected to reduce the system hardware in this case. The detailed motor design is presented in [50].

4.2 The IPMSM Machine with Split Stator Windings

In a two-pole three-phase IPMSM there are three windings in the stator shifted 120 electrical degrees [51]. Assume that each phase winding is divided into two equivalent parts and moreover they are shifted symmetrically around the stator periphery. Basically there will be six windings inside the stator instead of three for a two pole machine. Fig. 4.3 shows the cross section of the motor in this configuration.

As is shown in this figure, there are six windings shifted 30 electrical degrees while the rotor has a two-pole configuration. Other number of pole pairs are also possible for the machine with this integrated charger.

These six windings can be considered as two sets of three-phase windings. Let say a_1, b_1 and c_1 are the first set of windings (the same as classical three-phase windings). Consequently, a_2, b_2 and c_2 are the second set of three-phase windings. These two sets of three-phase windings are shifted 30 electrical degrees (angle between magnetic axis of $a_1'a_1$ and $a_2'a_2$) in this configuration to have a symmetric winding placement around the stator periphery.

4.2.1 Mathematical Model of the IPMSM with Six Stator Windings

A mathematical model of this machine is developed based on the assumption that all windings and rotor magnets magnetomotive forces are sinusoidally distributed. To model this machine with six stator windings, the inductance matrix is first calculated (a 6×6 matrix including self inductances and mutual

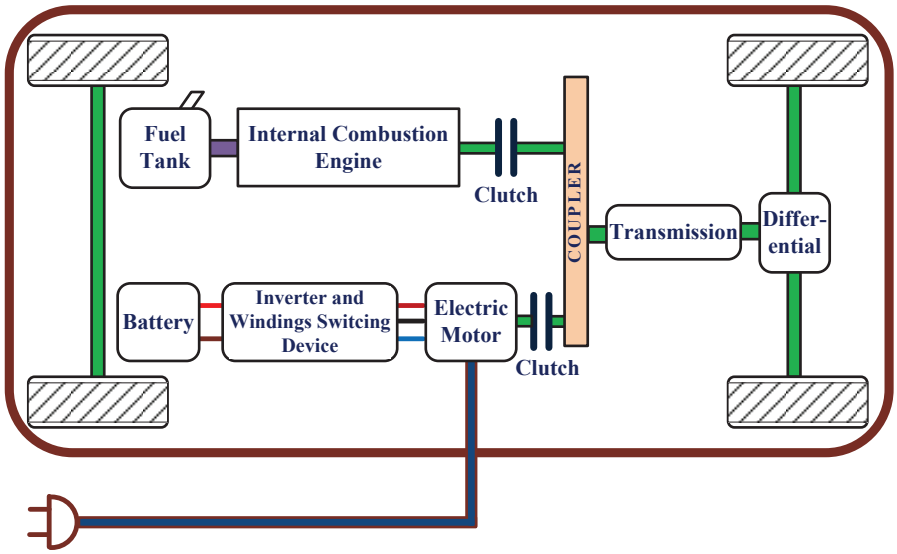

Figure 4.1: Integrated charger based on the special electric motor configuration.

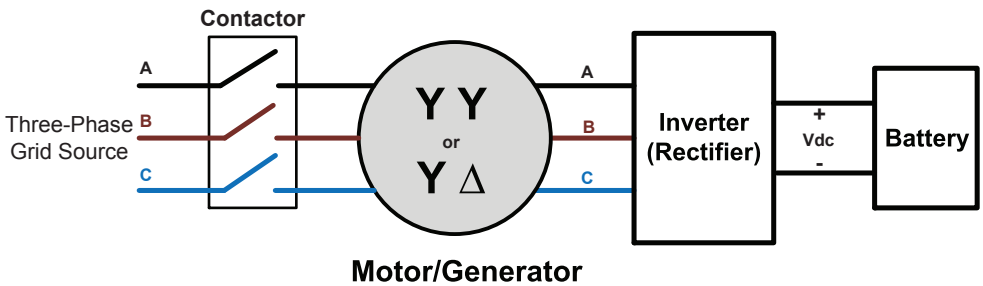

Figure 4.2: Simplified system diagram of the proposed integrated charger.

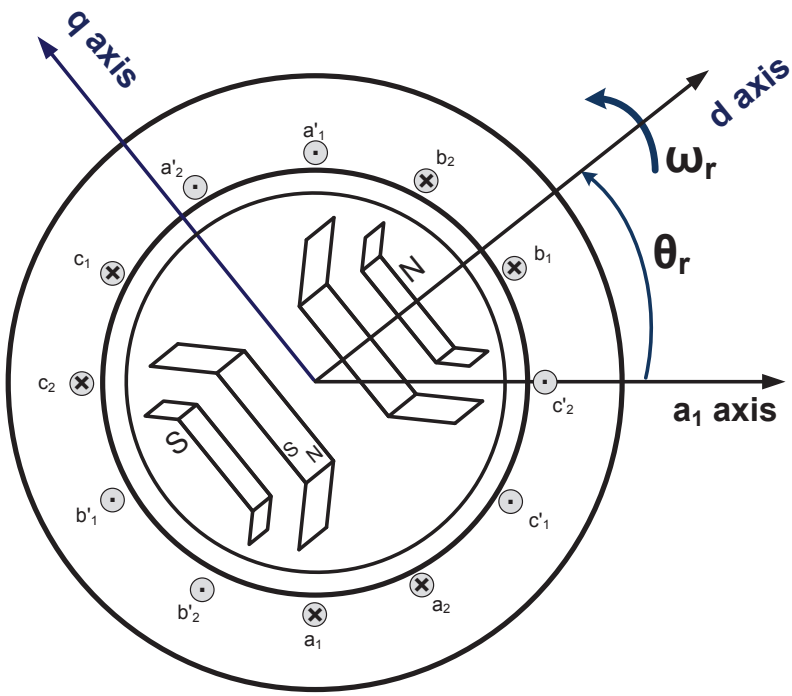

Figure 4.3: Cross section of a IPMSM with split stator windings.

inductances). Afterwards, the flux and voltage equations are written to model the electrical system [51]. The derivative of the co-energy is calculated to obtain the developed electromagnetic torque. The order of system is eight that is six electrical equations and two mechanical equations in the phase domain.

A special *abc* to *dq* transformation is used that is based on the Park transformation but an extended version for six variables instead of three. The system equations in the *dq* frame is reduced to a six order system while all sin and cos terms are eliminated from the equations.

The voltage equations for six windings can be described by the following equations:

$$v_{a_1} = r_s i_{a_1} + \frac{d}{dt}\psi_{a_1} \tag{4.1}$$

$$v_{b_1} = r_s i_{b_1} + \frac{d}{dt}\psi_{b_1} \tag{4.2}$$

$$v_{c_1} = r_s i_{c_1} + \frac{d}{dt}\psi_{c_1} \tag{4.3}$$

$$v_{a_2} = r_s i_{a_2} + \frac{d}{dt}\psi_{a_2} \tag{4.4}$$

$$v_{b_2} = r_s i_{b_2} + \frac{d}{dt}\psi_{b_2} \tag{4.5}$$

$$v_{c_2} = r_s i_{c_2} + \frac{d}{dt}\psi_{c_2} \tag{4.6}$$

where v_{a_1}, v_{b_1}, v_{c_1}, v_{a_2}, v_{b_2}, v_{c_2}, i_{a_1}, i_{b_1}, i_{c_1}, i_{a_2}, i_{b_2}, i_{c_2},ψ_{a_1}, ψ_{b_1}, ψ_{c_1}, ψ_{a_2}, ψ_{b_2}, ψ_{c_2} and r_s are windings voltages, currents, flux linkages and resistance.

The windings flux linkages can be expressed as:

$$\begin{aligned}\psi_{a_1} =&L_{a_1a_1}i_{a_1} + L_{a_1b_1}i_{b_1} + L_{a_1c_1}i_{c_1} + L_{a_1a_2}i_{a_2}+\\ &L_{a_1b_2}i_{b_2} + L_{a_1c_2}i_{c_2} + \psi_{pm}cos(\theta_r)\end{aligned} \tag{4.7}$$

$$\begin{aligned}\psi_{b_1} =&L_{b_1a_1}i_{a_1} + L_{b_1b_1}i_{b_1} + L_{b_1c_1}i_{c_1} + L_{b_1a_2}i_{a_2}+\\ &L_{b_1b_2}i_{b_2} + L_{b_1c_2}i_{c_2} + \psi_{pm}cos(\theta_r - \frac{2\pi}{3})\end{aligned} \tag{4.8}$$

$$\begin{aligned}\psi_{c_1} =&L_{c_1a_1}i_{a_1} + L_{c_1b_1}i_{b_1} + L_{c_1c_1}i_{c_1} + L_{c_1a_2}i_{a_2}+\\ &L_{c_1b_2}i_{b_2} + L_{c_1c_2}i_{c_2} + \psi_{pm}cos(\theta_r + \frac{2\pi}{3})\end{aligned} \tag{4.9}$$

$$\begin{aligned}\psi_{a_2} =&L_{a_2a_1}i_{a_1} + L_{a_2b_1}i_{b_1} + L_{a_2c_1}i_{c_1} + L_{a_2a_2}i_{a_2}+\\ &L_{a_2b_2}i_{b_2} + L_{a_2c_2}i_{c_2} + \psi_{pm}cos(\theta_r - \frac{\pi}{6})\end{aligned} \tag{4.10}$$

$$\begin{aligned}\psi_{b_2} =&L_{b_2a_1}i_{a_1} + L_{b_2b_1}i_{b_1} + L_{b_2c_1}i_{c_1} + L_{b_2a_2}i_{a_2}+\\ &L_{b_2b_2}i_{b_2} + L_{b_2c_2}i_{c_2} + \psi_{pm}cos(\theta_r - \frac{2\pi}{3} - \frac{\pi}{6})\end{aligned} \tag{4.11}$$

$$\begin{aligned}\psi_{c_2} =&L_{c_2a_1}i_{a_1} + L_{c_2b_1}i_{b_1} + L_{c_2c_1}i_{c_1} + L_{c_2a_2}i_{a_2}+\\ &L_{c_2b_2}i_{b_2} + L_{c_2c_2}i_{c_2} + \psi_{pm}cos(\theta_r + \frac{2\pi}{3} - \frac{\pi}{6})\end{aligned} \tag{4.12}$$

where $L_{a_1a_1}$, $L_{b_1b_1}$, $L_{c_1c_1}$, $L_{a_2a_2}$, $L_{b_2b_2}$ and $L_{c_2c_2}$ are windings self inductances. Moreover, $L_{a_1b_1}$, $L_{a_1c_1}$, $L_{a_1a_2}$, $L_{a_1b_2}$, $L_{a_1c_2}$, $L_{b_1bc_1}$, $L_{b_1c_2}$, $L_{c_1b_2}$, $L_{a_2b_2}$, $L_{a_2c_2}$ and $L_{b_2c_2}$ are windings mutual inductances. ψ_{pm} is the permanent magnet flux (the rotor flux) and θ_r is the angel between the rotor d axis and the magnetic axes of winding $a_1'a_1$.

The inductance values are calculates as (see appended paper II):

$$L_{a_1a_1} = L_{ls} + \bar{L}_m - L_{\Delta m}cos(2\theta_r) \tag{4.13}$$

$$L_{a_1b_1} = L_{b_1a_1} = -\frac{1}{2}\bar{L}_m - L_{\Delta m}cos2(\theta_r - \frac{\pi}{3}) \tag{4.14}$$

$$L_{a_1c_1} = L_{c_1a_1} = -\frac{1}{2}\bar{L}_m - L_{\Delta m}cos2(\theta_r + \frac{\pi}{3}) \tag{4.15}$$

$$L_{a_1a_2} = L_{a_2a_1} = \frac{\sqrt{3}}{2}\bar{L}_m - L_{\Delta m}cos2(\theta_r - \frac{\pi}{12}) \tag{4.16}$$

$$L_{a_1b_2} = L_{b_2a_1} = -\frac{\sqrt{3}}{2}\bar{L}_m - L_{\Delta m}cos2(\theta_r - \frac{\pi}{3} - \frac{\pi}{12}) \tag{4.17}$$

$$L_{a_1c_2} = L_{c_2a_1} = L_{\Delta m}sin2\theta_r = L_{\Delta m}cos2(\theta_r - \frac{\pi}{4}) \tag{4.18}$$

$$L_{b_1b_1} = L_{ls} + \bar{L}_m - L_{\Delta m}cos2(\theta_r - \frac{2\pi}{3}) \tag{4.19}$$

$$L_{b_1c_1} = L_{c_1b_1} = -\frac{1}{2}\bar{L}_m - L_{\Delta m}cos2\theta_r \tag{4.20}$$

$$L_{b_1a_2} = L_{a_2b_1} = L_{\Delta m}cos2(\theta_r + \frac{\pi}{12}) \tag{4.21}$$

$$L_{b_1b_2} = L_{b_2b_1} = \frac{\sqrt{3}}{2}\bar{L}_m + L_{\Delta m}cos2(\theta_r - \frac{\pi}{4}) \tag{4.22}$$

$$L_{b_1c_2} = L_{c_2b_1} = -\frac{\sqrt{3}}{2}\bar{L}_m - L_{\Delta m}cos2(\theta_r - \frac{\pi}{12}) \tag{4.23}$$

$$L_{c_1c_1} = L_{ls} + \bar{L}_m - L_{\Delta m}cos2(\theta_r + \frac{2\pi}{3}) \tag{4.24}$$

$$L_{c_1a_2} = L_{a_2c_1} = -\frac{\sqrt{3}}{2}\bar{L}_m - L_{\Delta m}cos2(\theta_r + \frac{\pi}{4}) \tag{4.25}$$

$$L_{c_1b_2} = L_{b_2c_1} = L_{\Delta m}cos2(\theta_r + \frac{5\pi}{12}) \tag{4.26}$$

$$L_{c_1c_2} = L_{c_2c_1} = \frac{\sqrt{3}}{2}\bar{L}_m + L_{\Delta m}cos2(\theta_r + \frac{\pi}{12}) \tag{4.27}$$

$$L_{a_2a_2} = L_{ls} + \bar{L}_m - L_{\Delta m}cos2(\theta_r - \frac{\pi}{6}) \tag{4.28}$$

$$L_{a_2b_2} = L_{b_2a_2} = -\frac{1}{2}\bar{L}_m - L_{\Delta m}cos2(\theta_r - \frac{\pi}{2}) \tag{4.29}$$

$$L_{a_2c_2} = L_{c_2a_2} = -\frac{1}{2}\bar{L}_m - L_{\Delta m}cos2(\theta_r + \frac{\pi}{6}) \tag{4.30}$$

$$L_{b_2b_2} = L_{ls} + \bar{L}_m - L_{\Delta m}cos2(\theta_r - \frac{2\pi}{3} - \frac{\pi}{6}) \tag{4.31}$$

$$L_{b_2c_2} = L_{c_2b_2} = -\frac{1}{2}\bar{L}_m - L_{\Delta m}cos2(\theta_r - \frac{\pi}{6}) \tag{4.32}$$

$$L_{c_2c_2} = L_{ls} + \bar{L}_m - L_{\Delta m}cos2(\theta_r + \frac{2\pi}{3} - \frac{\pi}{6}) \tag{4.33}$$

where $\bar{L}_m$, $L_{\Delta m}$ and L_{ls} are average values of magnetization inductance, half-amplitude of the sinusoidal variation of the magnetization inductance and the leakage inductance of each winding. It is assumed that all windings have the same number of turns.

If we define the vectors and matrixes for the inductances, currents, voltages, fluxes, and resistance as following:

$$\mathbf{L_s} = \begin{bmatrix} L_{a_1a_1} & L_{a_1b_1} & L_{a_1c_1} & L_{a_1a_2} & L_{a_1b_2} & L_{a_1c_2} \\ L_{b_1a_1} & L_{b_1b_1} & L_{b_1c_1} & L_{b_1a_2} & L_{b_1b_2} & L_{b_1c_2} \\ L_{c_1a_1} & L_{c_1b_1} & L_{c_1c_1} & L_{c_1a_2} & L_{c_1b_2} & L_{c_1c_2} \\ L_{a_2a_1} & L_{a_2b_1} & L_{a_2c_1} & L_{a_2a_2} & L_{a_2b_2} & L_{a_2c_2} \\ L_{b_2a_1} & L_{b_2b_1} & L_{b_2c_1} & L_{b_2a_2} & L_{b_2b_2} & L_{b_2c_2} \\ L_{c_2a_1} & L_{c_2b_1} & L_{c_2c_1} & L_{c_2a_2} & L_{c_2b_2} & L_{c_2c_2} \end{bmatrix},$$

$$\mathbf{i_s} = \begin{bmatrix} i_{a_1} & i_{b_1} & i_{c_1} & i_{a_2} & i_{b_2} & i_{c_2} \end{bmatrix}^T,$$

$$\mathbf{v_s} = \begin{bmatrix} v_{a_1} & v_{b_1} & v_{c_1} & v_{a_2} & v_{b_2} & v_{c_2} \end{bmatrix}^T,$$

$$\psi_\mathbf{s} = \begin{bmatrix} \psi_{a_1} & \psi_{b_1} & \psi_{c_1} & \psi_{a_2} & \psi_{b_2} & \psi_{c_2} \end{bmatrix}^T \text{ and}$$

$$\mathbf{R_s} = \begin{bmatrix} r_s & 0 & 0 & 0 & 0 & 0 \\ 0 & r_s & 0 & 0 & 0 & 0 \\ 0 & 0 & r_s & 0 & 0 & 0 \\ 0 & 0 & 0 & r_s & 0 & 0 \\ 0 & 0 & 0 & 0 & r_s & 0 \\ 0 & 0 & 0 & 0 & 0 & r_s \end{bmatrix}$$

the voltage and flux equations can be written as [51]:

$$\mathbf{v_s} = \mathbf{R_s i_s} + \frac{d}{dt}\psi_\mathbf{s}. \tag{4.34}$$

The developed electromagnetic torque in the machine can be calculated as [51]:

$$T_e = \frac{P}{2}(\frac{1}{2}\mathbf{i_s^T}\frac{\partial \mathbf{L_s}}{\partial \theta_r}\mathbf{i_s} + \mathbf{i_s^T}\frac{\partial \psi_\mathbf{pm}}{\partial \theta_r}) \tag{4.35}$$

where P is the machine number of poles. $\psi_\mathbf{pm}$ is stator winding fluxes due to rotor magnets. The mechanical dynamical equations describing the machine are:

$$\frac{d\omega_r}{dt} = \frac{P}{2J}(T_e - \frac{2B_m}{P}\omega_r - T_L) \tag{4.36}$$

$$\frac{d\theta_r}{dt} = \omega_r \tag{4.37}$$

where J, B_m, T_L and ω_r are the moment of inertia, viscous friction coefficient, load torque and speed of the machine.

To simplify the machine equations a special version of the Park transformation (it is called extended Park transformation here) is used to reduce the system order and remove all sinusoidal terms. The transformation matrix, $\mathbf{K_s}$, is applied to machine equations to transform them to the synchronous dq0 reference frame. This matrix is defined as:

$$\mathbf{K_s} = \frac{2}{3}\begin{bmatrix} cos\theta_r & cos(\theta_r - \frac{2\pi}{3}) & cos(\theta_r + \frac{2\pi}{3}) & \dots \\ -sin\theta_r & -sin(\theta_r - \frac{2\pi}{3}) & -sin(\theta_r + \frac{2\pi}{3}) & \dots \\ \frac{1}{2} & \frac{1}{2} & \frac{1}{2} & \dots \\ 0 & 0 & 0 & \dots \\ 0 & 0 & 0 & \dots \\ 0 & 0 & 0 & \dots \end{bmatrix}$$

$$\begin{bmatrix} 0 & 0 & 0 \\ 0 & 0 & 0 \\ 0 & 0 & 0 \\ cos(\theta_r - \frac{\pi}{6}) & cos(\theta_r - \frac{2\pi}{3} - \frac{\pi}{6}) & cos(\theta_r + \frac{2\pi}{3} - \frac{\pi}{6}) \\ -sin(\theta_r - \frac{\pi}{6}) & -sin(\theta_r - \frac{2\pi}{3} - \frac{\pi}{6}) & -sin(\theta_r + \frac{2\pi}{3} - \frac{\pi}{6}) \\ \frac{1}{2} & \frac{1}{2} & \frac{1}{2} \end{bmatrix}.$$

The inverse of the matrix $\mathbf{K_s}$,$\mathbf{K_s}^{-1}$, can be calculated as:

$$\mathbf{K_s^{-1}} = \begin{bmatrix} cos\theta_r & -sin\theta_r & 1 & \dots \\ cos(\theta_r - \frac{2\pi}{3}) & -sin(\theta_r - \frac{2\pi}{3}) & 1 & \dots \\ cos(\theta_r + \frac{2\pi}{3}) & -sin(\theta_r + \frac{2\pi}{3}) & 1 & \dots \\ 0 & 0 & 0 & \dots \\ 0 & 0 & 0 & \dots \\ 0 & 0 & 0 & \dots \end{bmatrix}$$

$$\begin{bmatrix} 0 & 0 & 0 \\ 0 & 0 & 0 \\ 0 & 0 & 0 \\ cos(\theta_r - \frac{\pi}{6}) & -sin(\theta_r - \frac{\pi}{6}) & 1 \\ cos(\theta_r - \frac{2\pi}{3} - \frac{\pi}{6}) & -sin(\theta_r - \frac{2\pi}{3} - \frac{\pi}{6}) & 1 \\ cos(\theta_r + \frac{2\pi}{3} - \frac{\pi}{6}) & -sin(\theta_r + \frac{2\pi}{3} - \frac{\pi}{6}) & 1 \end{bmatrix}.$$

By transforming the phase variables to the rotor reference frame by applying the transformation matrix $\mathbf{K_s}$, the machine equations will be simplified with reduced number of equations. In the rotor reference frame the variables are superscripted by letter r and are defined as:

$$\mathbf{i_s^r} = \begin{bmatrix} i_{d_1} & i_{q_1} & i_{0_1} & i_{d_2} & i_{q_2} & i_{0_2} \end{bmatrix}^T,$$

$$\mathbf{v_s^r} = \begin{bmatrix} v_{d_1} & v_{q_1} & v_{0_1} & v_{d_2} & v_{q_2} & v_{0_2} \end{bmatrix}^T \textit{ and}$$

$$\psi_\mathbf{s}^\mathbf{r} = \begin{bmatrix} \psi_{d_1} & \psi_{q_1} & \psi_{0_1} & \psi_{d_2} & \psi_{q_2} & \psi_{0_2} \end{bmatrix}^T.$$

The indexes d, q and 0 denote the direct axis, quadrature axis and zero component of the variables. Moreover, there are two set of three-phase quantities that are denoted by the numbers 1 and 2 respectively. For example the voltage can be transformed from the abc domain to the dq domain by $\mathbf{v_s^r} = \mathbf{K_s v_s}$.

By transforming machine voltage, flux linkage and torque equations to the dq reference frame, the following equations describe the electrical system dynamics:

$$v_{d_1} = r_s i_{d_1} + \frac{d}{dt}\psi_{d_1} - \omega_r \psi_{q_1} \tag{4.38}$$

$$v_{q_1} = r_s i_{q_1} + \frac{d}{dt}\psi_{q_1} + \omega_r \psi_{d_1} \tag{4.39}$$

$$v_{d_2} = r_s i_{d_2} + \frac{d}{dt}\psi_{d_2} - \omega_r \psi_{q_2} \tag{4.40}$$

$$v_{q_2} = r_s i_{q_2} + \frac{d}{dt}\psi_{q_2} + \omega_r \psi_{d_2} \tag{4.41}$$

$$\psi_{d_1} = L_d i_{d_1} + L_{md} i_{d_2} + \psi_{pm} \tag{4.42}$$

$$\psi_{q_1} = L_q i_{q_1} + L_{mq} i_{q_2} \tag{4.43}$$

$$\psi_{d_2} = L_{md} i_{d_1} + L_d i_{d_2} + \psi_{pm} \tag{4.44}$$

$$\psi_{q_2} = L_{mq} i_{q_1} + L_q i_{q_2} \tag{4.45}$$

where L_d, L_q, L_{md}, L_{mq} are direct and quadrature axis winding self and mutual inductances respectively. Moreover, $L_d = L_l + L_{md}$ and $L_q = L_l + L_{mq}$. It is assumed that the zero components are zero due to symmetrical three-phase quantities.

The developed electromagnetic torque can be expressed as:

$$T_e = \frac{3}{2}\frac{P}{2}[\psi_{pm}(i_{q_1} + i_{q_2}) + (L_d - L_q)(i_{d_1} i_{q_1} + i_{d_1} i_{q_2} + i_{d_2} i_{q_1} + i_{d_2} i_{q_2}]. \tag{4.46}$$

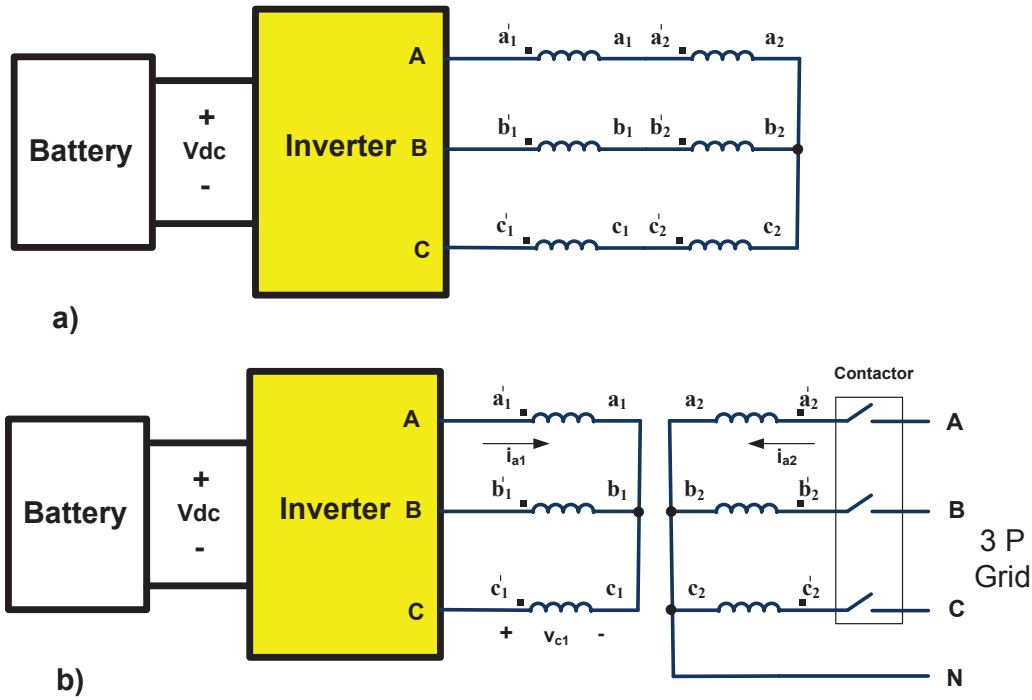

Figure 4.4: System modes of operation: a) traction and b) charging.

4.3 System Operation in Traction and Charging

As mentioned before, the system has two modes of operation: traction and charging. In traction mode, each two windings are connected to each other in series to constitute a three-phase winding set. These three windings can be connected to each other in Δ or Y to form a classical three-phase machine. Moreover, the motor is powered by the battery through the inverter. Fig. 4.4.a shows the system diagram in this mode. Sensorless schemes for example can be employed to run the motor in traction mode [52].

For charging, the system is reconfigured according to the scheme shown in Fig. 4.4.b. A simple relay based device re-connects the windings and a contactor is needed to connect the system to the utility grid.

If the machine would be kept in standstill as in [22], the magnetization current will be high due to the air-gap. So it is expected to have lower system efficiency depending on the air-gap length. However, if the machine rotates with the grid synchronous speed, the magnets will induce voltages in the inverter-side windings that emulates an isolated PM ac generator for the inverter. The idea is thus to connect the machine to the grid via the grid-side three-phase windings, a_2, b_2 and c_2. These three windings can be used to run the machine as a classical motor. The inverter side windings, a_1, b_1 and c_1 pick up the induced voltage due to the developed flux inside the machine (since they are located on the same pole-pair as are the grid-side windings). The inverter uses

this isolated voltage source to charge the battery by the means of machine leakage inductances as the converter energy storage component (yielding a three-phase boost converter).

4.3.1 Motor/Generator Grid Synchronization

At first, the inverter-side windings are used to drive the motor by the means of the battery and proper inverter operation while the grid-side windings are open connected. The electric machine must be rotated at the synchronous speed and produce the same voltage as the grid does (both amplitude and phase) for the grid connection. Before closing the contactor, the dc link voltage, motor/generator primary side currents and the rotor position/speed are measured to have a classical field oriented speed control of the IPM motor [53]. The position/speed can be estimated instead of using a sensor, but here for simplicity it is assumed that the position and speed signals are available.

Both grid-side winding voltages, and grid voltages are measured and transformed to the dq reference frame. Both voltage vectors magnitude and angle of the grid voltage and motor/generator grid-side windings should be equal as an index of synchronization. The magnitude of voltage is a function of the motor speed and flux (refer to motor/generator equations), so by controlling the flux, the voltage level can be adjusted. In a classical IPM motor usually the reference value for the d component of the machine is zero (for flux weakening operation this value will be modified), but at this scheme this value is used as a control parameter to change the induced voltage magnitude. The d component of the voltage is close to zero so the angle error is replaced by the voltage d components error ($v_{dg} - v_{d2}$) in the controller for the phase synchronization.

The motor/generator will rotate at the synchronous speed to meet the frequency synchronization requirement. So the speed reference will be $2\pi 50\ rad/s$ for a grid with $50\ Hz$ frequency supply. Moreover, to match the voltage angles, a PI controller is used to adjust the motor/generator speed reference due to the angle error signal. This speed reference will be tracked by the field oriented speed control part of the system. Fig. 4.5 shows the schematic diagram of the control system in the synchronization phase.

When both voltage magnitude and angle error signals are small values within predefined bands, the motor/generator set is synchronized and the contactor is closed. Now the system is ready for the charge operation.

4.3.2 Battery Charge Control

Fig. 4.6 shows a basic diagram of a three-phase boost converter. This scheme is very similar to the proposed integrated charger system. The voltage equations describing the converter in the dq reference frame are [54]:

$$u_{Ld} = Ri_{Ld} + L\frac{d}{dt}i_{Ld} - \omega L i_{Lq} + u_{Id} \tag{4.47}$$

$$u_{Lq} = Ri_{Lq} + L\frac{d}{dt}i_{Lq} + \omega L i_{Ld} + u_{Iq} \tag{4.48}$$

where u_{Ld}, u_{Lq}, u_{Id} and u_{Iq} are line and inverter dq voltage components respectively. R, L and ω are the resistance, inductance and source frequency

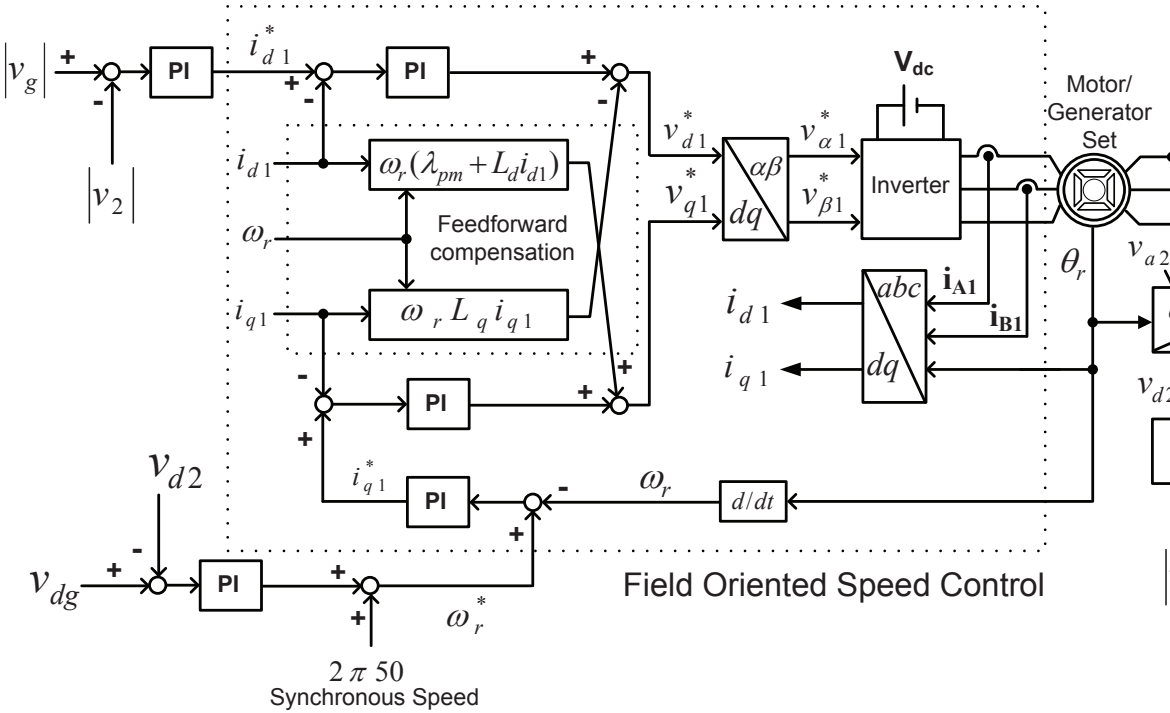

Figure 4.5: Grid synchronization scheme of IPM motor/generator se

also. i_{Ld} and i_{Lq} are d an q components of the line currents. The active and reactive power going to the converter from the grid can be written as [54]:

$$p = \frac{3}{2}(u_{Ld}i_{Ld} + u_{Lq}i_{Lq}) \tag{4.49}$$

$$q = \frac{3}{2}(u_{Lq}i_{Ld} - u_{Ld}i_{Lq}) \tag{4.50}$$

Different control strategies have been proposed for this three-phase boost converter operation [12]. If $i_{Lq} = 0$ and $u_{Lq} = 0$ in the equations above, then the active and reactive power will be simplified to $p = \frac{3}{2}u_{Ld}i_{Ld}$ and $q = 0$. Based on these equations, the feedforward current control method is one of the widely used schemes for power control. Fig. 4.7 shows the basic diagram of the controller. The dq current control and feedforward compensation are the main parts of this decoupled control scheme. The controller has an outer loop for the dc bus voltage regulation. This controller output sets the reference value for the d component of the current that controls the power. Two independent PI controllers have been used to generate reference values for the converter, u_α and u_β. The feedforward terms are added to this reference values to the decoupled system in d and q axes to improve the system performance.

At grid synchronization the contactor is closed and the grid voltages are applied to the grid-side motor/generator windings. Thus it is a constant voltage source over the windings. The motor/generator voltage equations can be written as below after some mathematical manipulations:

$$v_{d_2} = r_s(i_{d_2} - i_{d_1}) + L_l\frac{d}{dt}(i_{d_2} - i_{d_1}) - \omega_r L_l(i_{d_2} - i_{d_1}) + v_{d_1} \tag{4.51}$$

$$v_{q_2} = r_s(i_{q_2} - i_{q_1}) + L_l\frac{d}{dt}(i_{q_2} - i_{q_1}) + \omega_r L_l(i_{q_2} - i_{q_1}) + v_{q_1}. \tag{4.52}$$

The equations above are very similar to (4.47) and (4.48) that describe the classical three-phase boost converter. The difference is that currents are replaced by the difference of the primary and secondary winding currents. So the same control strategy is adopted with small modifications (adjusting the currents by the current differences). Moreover, due to existence of a battery in the dc link, the dc bus voltage controller is eliminated from the scheme.

Fig. 4.8 shows the proposed control system diagram in charging mode. This scheme is an extension of the classical control (Fig. 4.7) with some modifications. Two sets of three-phase machine currents and rotor position are measured and used in the controller. The grid voltage is also measured and used in the controller for proper operation (feed-forward compensation). When the system starts to charge, there are some mechanical oscillations in the rotor. The rotor speed error (the difference between the synchronous speed and true speed) is added to the controller by the means a proportional controller to reduce these oscillations.

With assumption of the symmetrical three-phase currents and voltages for the inverter-side and grid-side windings, each three-phase quantity can be represented by a classical two-dimensional vector with the extended dq transformation (there is no coupling in the matrix transformation between the two systems).

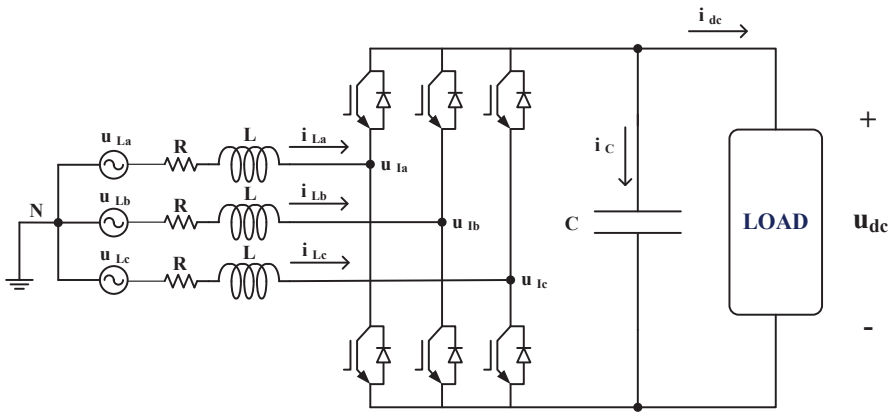

Figure 4.6: The power stage of the three-phase boost converter.

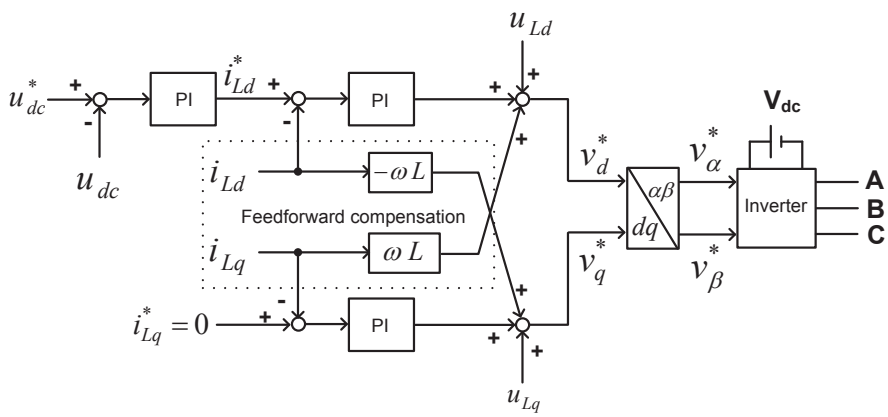

Figure 4.7: Decoupled current control of the three-phase boost converter.

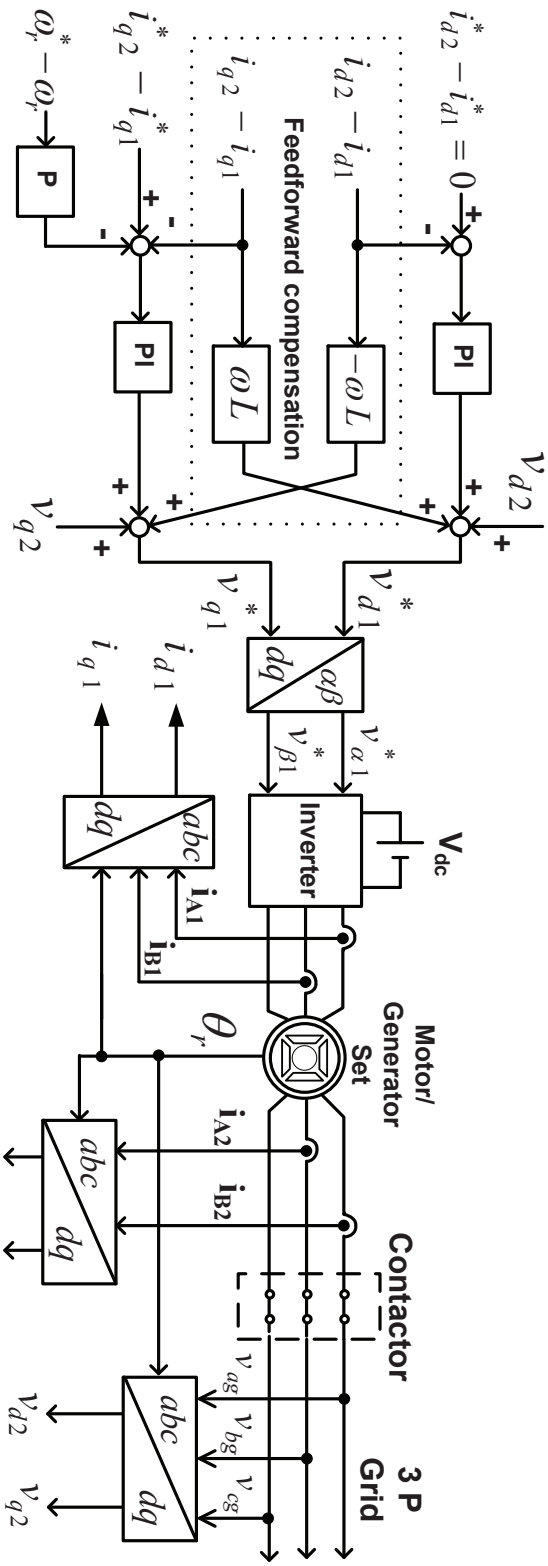

Figure 4.8: Block diagram for the charge control of proposed integrated charger.

The system has a bidirectional power flow capability that is inherent in the system because of the bidirectional operation of the three-phase inverter. Moreover, by changing the set point of the d component of the current, there is also a possibility of production/generation of reactive power. The system power limitation is mainly a thermal limitation of the machine in the classical vehicle drive systems. Half of the machine's full power can be used in the charging mode (the converter withstands this power level because it is designed for machine full power operation).

4.4 Integrated Charger Simulation Results

A 4 pole IPM machine is designed, optimized and constructed for a 25 kW traction system with a possibility to reconnect the windings for charging [50]. Fig. 4.9.a shows the windings configuration (in delta) in traction mode. The dc bus voltage (battery voltage) is 400 Vdc in this case. The machine base speed is 1500 rpm while the maximum speed is 6500 rpm. For charging, the windings are re-arranged according to Fig. 4.9.b. The charge power is limited to 12.5 kW due to the machine thermal limit. The motor parameters are shown in Table 4.1. The whole system has been simulated by the use of

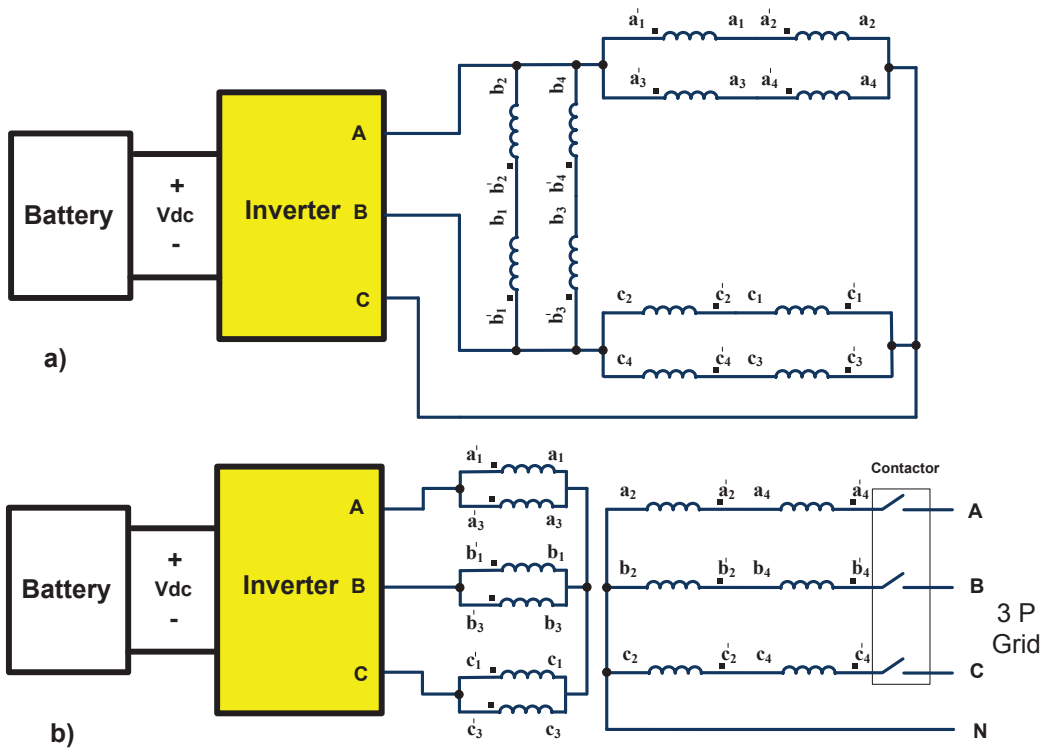

Figure 4.9: 25 kW system modes of operation: a) traction and b) charging.

Matlab/Simulink software based on the before mentioned system equations. The ideal converter is used in the simulation (no PWM or SVM is used for

Table 4.1: IPM motor parameters.

Rated power (kW)	25
Rated line voltage (V)	270
Rated phase current (A)	30
Rated speed(rev/min)	1500
No of poles	4
Permanent magnet flux (Wb)	0.6
Stator resistance (Ohm)	0.45
d axis inductance (mH)	12
q axis inductance (mH)	42
Inertia (Kg.m2)	0.1
Viscous friction coefficient (Nms/rad)	0.002

the inverter). Before simulation starts, it is assumed that the system is reconfigured for charging but the grid contactor is open. The charging process starts with that the inverter starts to rotate the motor by the means of the battery and inverter side motor windings. The motor will then rotate at grid synchronous speed.

When the motor speed is close to synchronous speed, the voltage level of the grid-side winding is adjusted by controlling the motor flux level (d component of the current). Afterwards, the voltage angle is adjusted by speed control of the motor (equivalently torque control) by the means of the q component of the current in this case. After synchronization, both voltage amplitude and angle adjustment, the contactor is closed and the machine grid-side windings are directly connected to the grid. One second after closing the contactor (the system continues the synchronization while the contactor is closed for more stability), the charge control is started for a power level of 12.5 kW. In order to show the system transient response, the charge power is reduced to 7 kW after two seconds.

System operation during different time intervals can be summarized as:

- $t = 0$ s till $t = 0.5$ s: The speed is regulated close to the synchronous speed, $2\pi 50$ rad/s. The system is in synchronization mode and the contactor is open.
- $t = 0.5$ s till $t = 0.9$ s: The grid side windings voltage amplitudes are adjusted. The system is in synchronization mode and the contactor is open.
- $t = 0.9$ s till $t = 3.6$ s: The grid side windings voltage angles are adjusted. The system is in synchronization mode and the contactor is open.
- $t = 3.6$ s till $t = 5$ s: Synchronization is finished and the contactor is closed, but the charging is not started.
- $t = 5$ s till $t = 7$ s: The system is charging full power (12.5 kW).
- $t = 7$ s till $t = 9$ s: The system is charging with 7 kW power.

Fig. 4.10 shows the power from the grid to the charger system. At first, while the motor/generator is in synchronization mode (the first 3.6 seconds), the grid power is zero. Then the contactor is closed and charging is started after 1.4 seconds (t=5 s). After additional two seconds (t=7 s), the charging power is reduced to 7 kW. The electrical speed is shown in Fig. 4.11. As is shown in this figure, the rotor speed oscillations are damped quickly by the proper operation of the controller as it was expected. The system efficiency is around 89%. However, the machine iron losses and inverter losses are neglected in this simulation. This efficiency level is acceptable compared to a similar isolated version of integrated charger. Even though motor losses are the same and inverter losses are lower in charging mode compared to traction mode, the efficiency of the system in charging mode is lower than the efficiency of the system in traction mode since with the same amount of losses the output power in charging is half that of traction. Thus, with improved design of the motor it is possible to increase the system efficiency for both charging and traction.

The motor/generator torque is shown in Fig. 4.12. The machine develops constant torque in the first 0.35 seconds to increase the speed to become close to the synchronous speed ($2\pi 50$ rad/s in this case). Then there are some oscillations around times $t = 0.5$ s and $t = 0.9$ s. First the voltage magnitude is adjusted and then the voltage angle is adjusted for synchronization. Moreover, there are some oscillations in torque around the times that the contactor is closed ($t = 3.6$ s), start of charging ($t = 5$ s) and step changes of the charge power level ($t = 7$ s). The developed torque compared to its nominal value is almost negligible (less than 1%) because there is no mechanical load connected to the machine during charging.

As is mentioned before, unit power factor operation is possible for the charger. Fig. 4.13 shows grid side phase A winding voltage and current. The voltage is scaled to half its value for more figure clarity.

Grid side and inverter side windings are shifted 30 electrical degrees (refer to Fig. 4.3). Therefore, phase shifted voltages for grid side and inverter side windings are expected. This phase shift can be seen in Fig. 4.14 which shows phase A voltages for the grid side and inverter side windings.

Fig. 4.15 shows the phase A current of the grid during the charge operation. For more clarity, the three-phase currents are shown in Fig. 4.16, 4.17 and 4.18 during the time when the contactor is closed, at full power charging and at the step change in charging power. As is shown in these figures, the system has good dynamic performance.

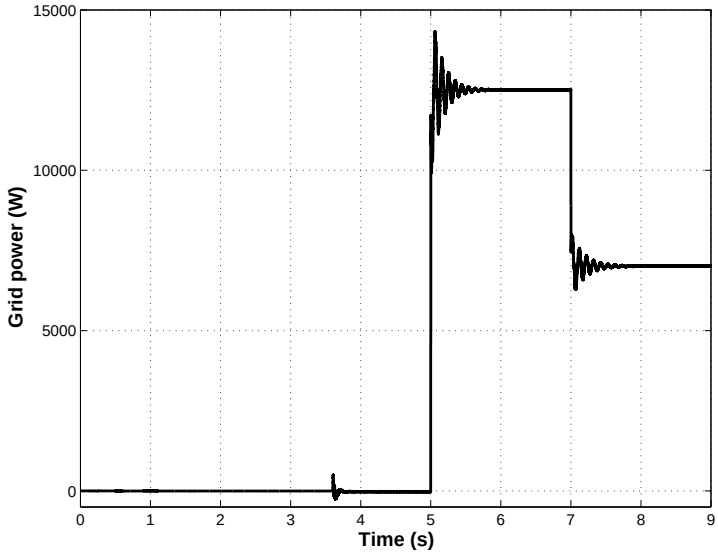

Figure 4.10: Grid power to the charger system.

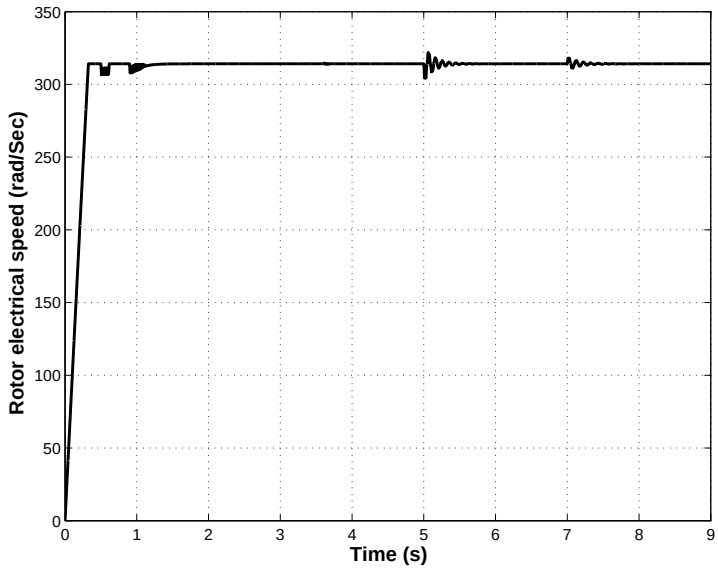

Figure 4.11: Electrical speed of the motor/generator.

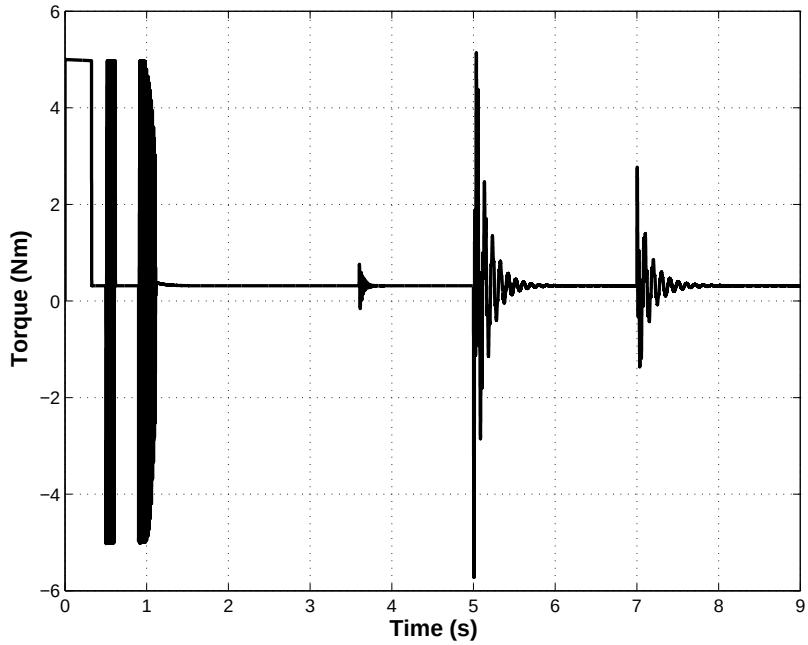

Figure 4.12: Motor/generator torque during charge time.

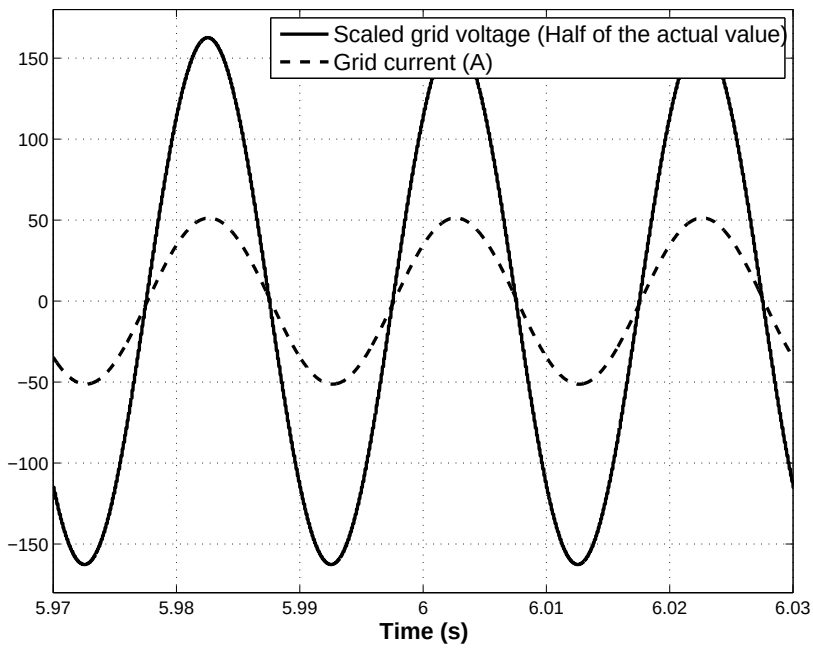

Figure 4.13: Grid side phase A voltage and current: unit power factor operation.

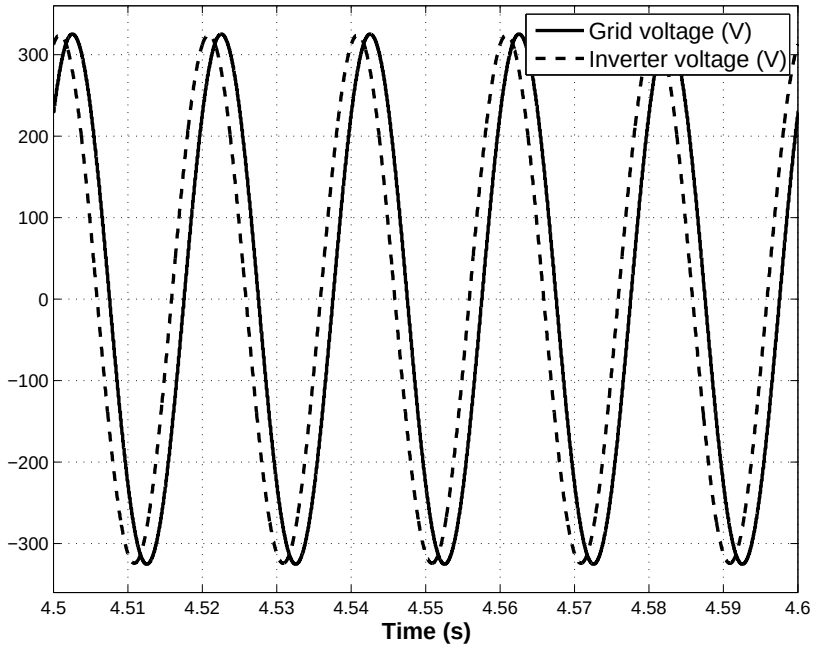

Figure 4.14: Grid side and inverter side winding voltages for phase A.

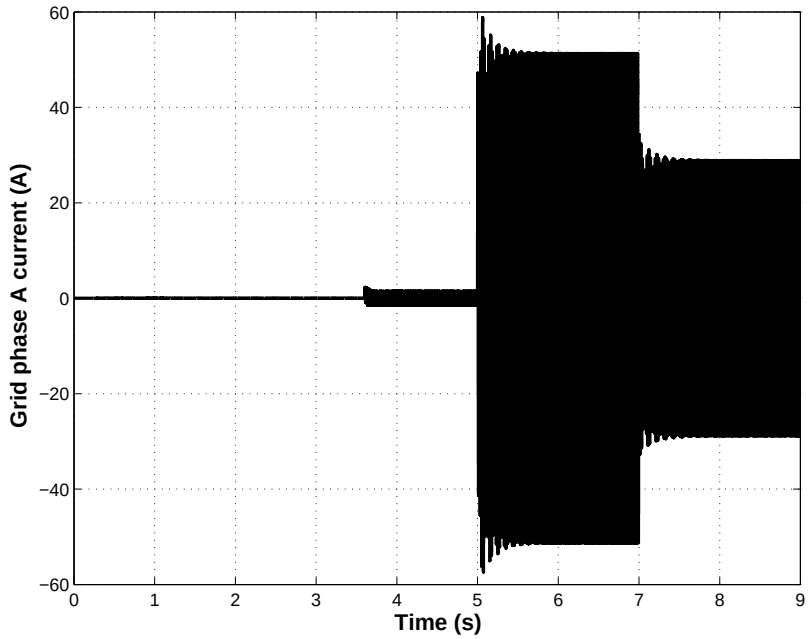

Figure 4.15: Grid side phase A current during charge time.

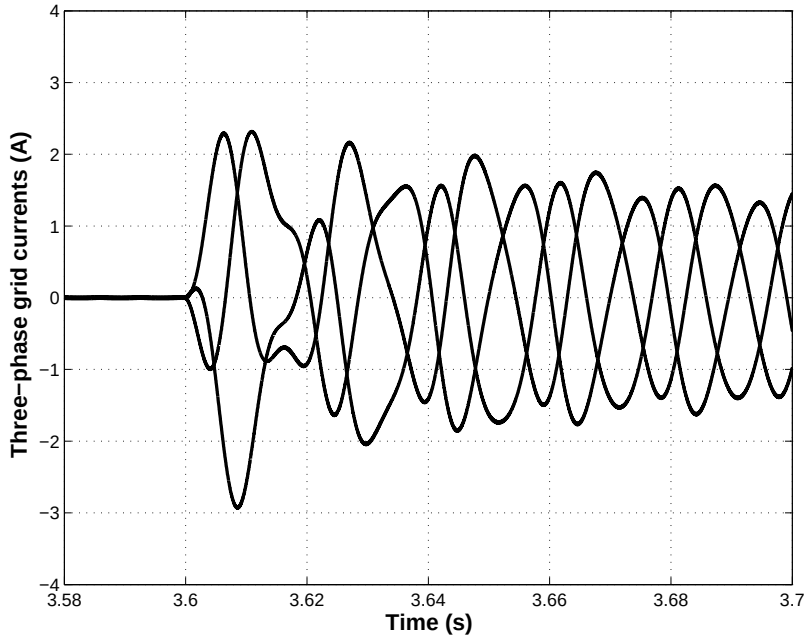

Figure 4.16: Grid three-phase currents during closing the contactor and before charge start-up.

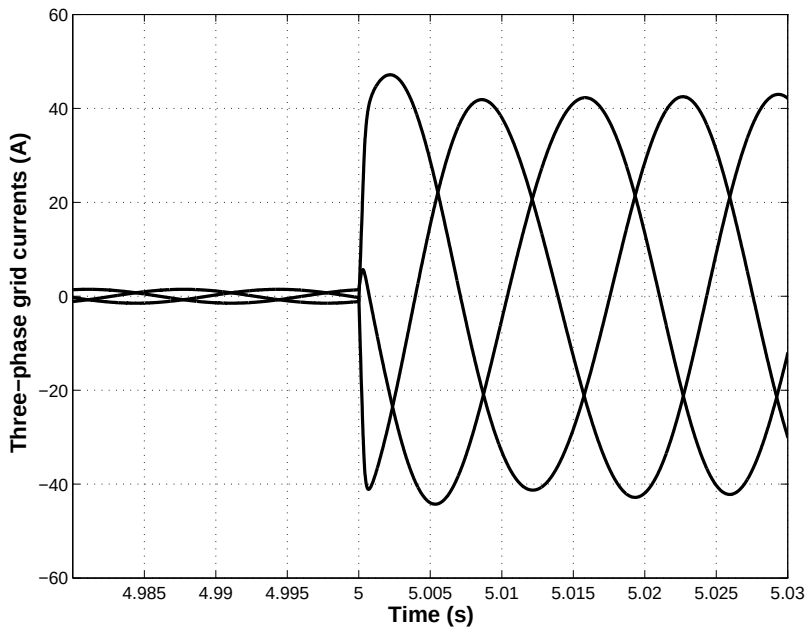

Figure 4.17: Grid three-phase currents after closing the contactor and during charge start-up.

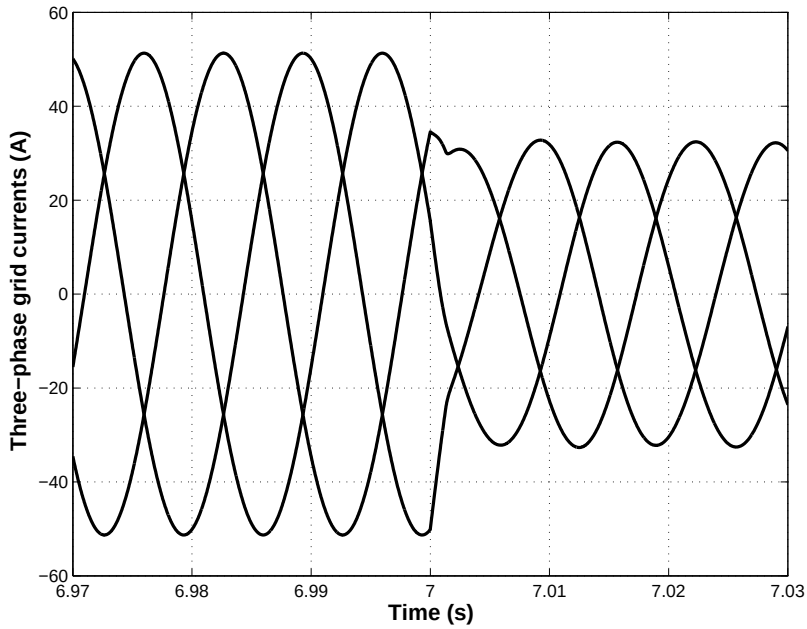

Figure 4.18: Grid three-phase currents during the step change of the charging power.

4.5 Drive System Performance of a DTC Based IPM Machine

As mentioned in previous sections, the field-oriented control method used for both synchronization and charge control is a widely-used method [55]. Other alternatives can be employed to improve the overall system performance like system response time or improved dynamic behavior. Direct torque control is one of these techniques gained a lot of interest due to its simplicity and fast dynamic response [56]. A 25 kW IPM machine is used in this project as traction motor and motor/generator device in charging mode. The drive system performance for a IPM machine is introduced in this section while the detail discussions are presented in appended paper [III].

Direct torque control method first introduced by Takahashi [57] and Depenbrock [58] gained a lot of attentions thanks to its simple structure and fast torque dynamics. In the DTC method, six non-zero and two zero voltage vectors generated by the inverter are selected to keep the motor flux and torque within the limits of two hysteresis bands [59]. The DTC method has been widely studied for induction machines. For the induction machines there are four different switching patterns for the selection of the inverter voltage vector [52]. Each switching method affects the drive system performance [60]. The same concept is applied to the IPM synchronous machine [56], so most of the methods developed for DTC based induction motor drive systems can be applied for the DTC based IPM synchronous motor drives.

The impact of different inverter switching patterns on the performance of a DTC based IPM drive system is investigated in terms of torque ripple, flux ripple, current ripple and inverter switching frequency at low speeds. Applying a zero voltage vector by the inverter has an important role on the overall drive system performance that will be addressed in the sequel.

Fig. 4.19 shows the block diagram of a IPM synchronous motor drive system based on the DTC method. During each sample interval the stator currents, i_A and i_B, are measured along with the dc bus voltage V_{dc}. Using the inverter switching states ($S_A S_B S_C$), the stator voltage and current vector components in the stationary reference frame can be calculated as [52]:

$$u_\alpha = \frac{2}{3} V_{dc} (S_A - \frac{S_A + S_B}{2}) \tag{4.53}$$

$$u_\beta = \frac{1}{\sqrt{3}} V_{dc} (S_B - S_C) \tag{4.54}$$

$$i_\alpha = i_A \tag{4.55}$$

$$i_\beta = \frac{i_A + 2i_B}{\sqrt{3}} \tag{4.56}$$

where u_α, u_β, i_α and i_β are α and β components of the stator voltage and current in the stationary reference frame. The α and β components of the stator flux, ψ_α and ψ_β, can be obtained by the integration of the stator voltage minus the voltage drop in the stator resistance as:

$$\psi_\alpha = \int_0^t (u_\alpha - R i_\alpha) dt + \psi_{\alpha|t=0} \tag{4.57}$$

$$\psi_\beta = \int_0^t (u_\beta - Ri_\beta)dt + \psi_{\beta|t=0}. \tag{4.58}$$

The electromagnetic torque, T_e, can be written in terms of quantities in the stationary reference frame as:

$$T_e = \frac{3}{2}P(\psi_\alpha i_\beta - \psi_\beta i_\alpha). \tag{4.59}$$

This equation is used in the drive system to estimate the developed electromagnetic torque [52]. The stator flux vector magnitude and phase are given by:

$$|\overline{\psi}_s| = \sqrt{\psi_\alpha^2 + \psi_\beta^2} \tag{4.60}$$

$$\angle\overline{\psi}_s = \arctan(\frac{\psi_\beta}{\psi_\alpha}). \tag{4.61}$$

As shown in Fig. 4.19, estimated values of the stator flux vector magnitude, $|\overline{\psi}_s|$, and the electromagnetic torque, T_e, are compared with their reference values. Afterwards, the errors are provided to the flux and torque hysteresis controllers. The goal of the control system is to limit the flux and torque within the hysteresis bands around their reference values. By using the torque error, flux error and stator flux position the control can be done by applying a proper inverter voltage. For a three phase inverter, there are 6 power switches. It is not possible to turn on the upper and lower switches in a leg simultaneously. So there are 8 possible switching configurations where each state defines a voltage space vector. Fig. 4.20 shows six non-zero inverter voltage space vectors (there are two zero voltage vectors, $\overline{u}_7$ and $\overline{u}_8$, that are not shown in this figure). Moreover the $\alpha\beta$ plane can be divided into 6 sectors (k=1, 2, 3, 4, 5 and 6) in which the controller needs to know in what sector the stator flux is located. If two level hysteresis controllers are used for the flux and torque control, there will be four switching strategies for the selection of the appropriate stator voltage vector (these possible switching strategies are proposed for the DTC of induction motors originally). Assume that the stator flux vector is located in sector k, then these four switching strategies are listed in Table 4.2 [59]. Effects of the applied voltage vector on the motor flux and torque are summarized in Table 4.2 as well. For the DTC system based on the IPM synchronous motor mainly solution A and D are used [61].

Assume that the flux is located in sector k; then, to increase the torque the voltage vectors $\overline{u}_{k+1}$ or $\overline{u}_{k+2}$ will be applied (depending on if the flux increases or decreases, one of the two voltage vectors will be selected). Different voltage vectors can be applied to decrease the torque in different switching possibilities. $\overline{u}_k$, $\overline{u}_{k-1}$, $\overline{u}_{k-2}$, $\overline{u}_{k+3}$, $\overline{u}_7$ and $\overline{u}_8$ can be applied according to Table 4.2. As is seen in Table 4.2, different switching patterns are only different in the torque decrement case, regardless of the flux increase or decrease demand in the motor. To decrease the torque, the simplest way is applying a zero voltage (solution A). The main difference between switching algorithms is in applying the zero vector or non-zero vector to decrease the torque. The motor current ripple, torque ripple and inverter switching frequency will vary for each switching strategy. This will affect the whole drive system performance for each switching method.

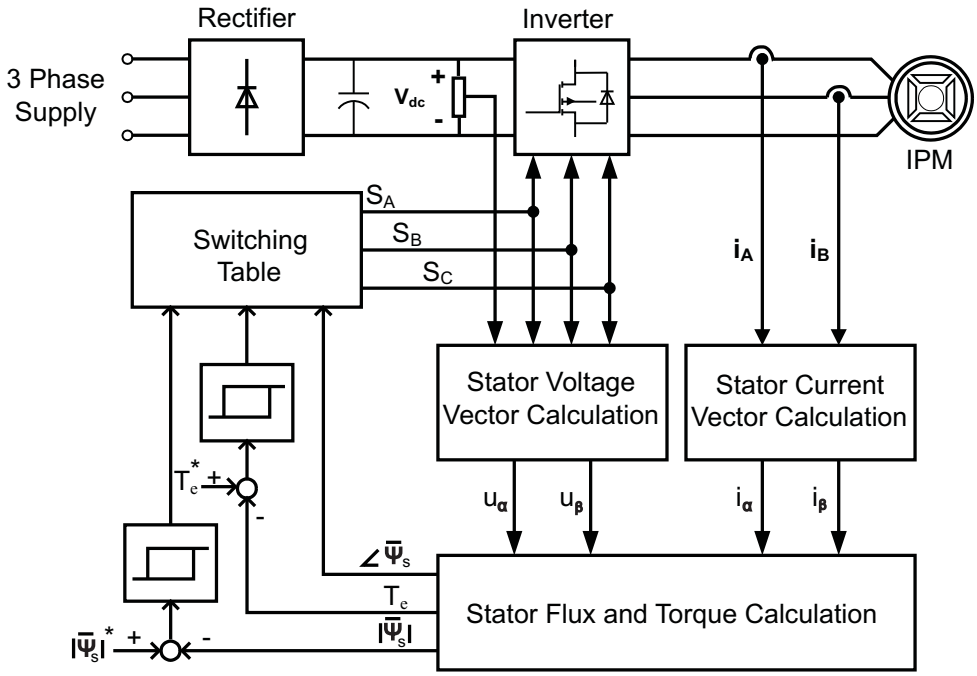

Figure 4.19: Block diagram of the direct torque control of IPM synchronous motor.

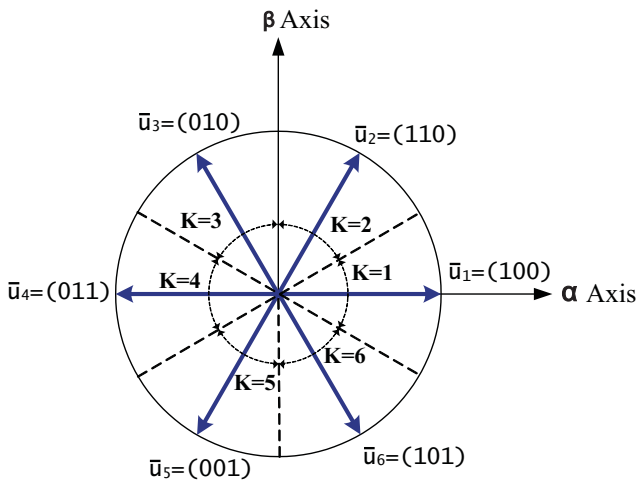

Figure 4.20: Inverter voltage space vectors.

To evaluate the drive system performance at low speed for different inverter switching algorithms according to Table 4.2, the motor torque ripple, stator current ripple, stator flux ripple and inverter switching frequency have been considered. Using the same motor, controller and load parameters, simulations have been conducted for different inverter switching patterns. The normalized torque ripple, normalized stator current ripple, normalized stator flux ripple and average inverter switching frequency have been determined.

Thus, after removing the average part of the signals (torque, magnitude of the stator current and flux vectors), the root mean square (rms) values are calculated. Moreover, the values are normalized by dividing with the related average values. The results are presented in Table 4.3.

As is presented in Table 4.3, the torque ripple and average inverter switching frequency are lower in solution A compared to the other switching patterns. For solution D, the inverter switching frequency is the highest, making inverter loss higher than those of the other switching algorithms. Thus, high values of the torque ripple and inverter switching frequency make this solution (solution D) an unfavorable choice for the drive system at low speeds. The inverter switching pattern A which employs the zero voltage vector to reduce the torque has better performance compared to the other switching methods at low speeds.

Table 4.2: Inverter switching strategies for the DTC system.

	$T_e \uparrow \lvert\overline{\psi}_s\rvert \uparrow$	$T_e \uparrow \lvert\overline{\psi}_s\rvert \downarrow$	$T_e \downarrow \lvert\overline{\psi}_s\rvert \uparrow$	$T_e \downarrow \lvert\overline{\psi}_s\rvert \downarrow$
Solution A	$\overline{u}_{k+1}$	$\overline{u}_{k+2}$	$\overline{u}_7$,$\overline{u}_8$	$\overline{u}_7$,$\overline{u}_8$
Solution B	$\overline{u}_{k+1}$	$\overline{u}_{k+2}$	$\overline{u}_k$	$\overline{u}_7$,$\overline{u}_8$
Solution C	$\overline{u}_{k+1}$	$\overline{u}_{k+2}$	$\overline{u}_k$	$\overline{u}_{k+3}$
Solution D	$\overline{u}_{k+1}$	$\overline{u}_{k+2}$	$\overline{u}_{k-1}$	$\overline{u}_{k-2}$

Table 4.3: Impact of switching algorithm on the drive system performance.

Switching algorithm	Normalized torque ripple (%)	Normalized stator current ripple (%)	Normalized stator flux ripple (%)	Inverter switching frequency [kHz]
Solution A	5.31	6.81	7.54	0.35
Solution B	11.15	10.36	7.50	0.27
Solution C	10.11	7.81	8.91	1.46
Solution D	8.84	7.48	7.57	2.47

Chapter 5

Conclusions and Future Work

5.1 Conclusions

In this Licentiate thesis, it is shown and thoroughly explained how it is possible to use the electric drive system components in a plug-in vehicle for fast high power charging, with charging power restricted to half the traction power. The electric motor stator windings are re-configured for the traction and charging modes by the means of a relay-based switching device which together with a clutch, due to the machine rotation in charging mode, are the only extra components needed to yield a very cost-effective and compact on-board three-phase insulated charger with unit power factor capability. All motor windings are used in both traction and charging so there is no extra winding in the motor. Bi-directional power operation for the grid to vehicle application is possible also.

By the use of an exclusive Park type transformation, a mathematical electromechanical model of the electric machine is derived and presented. Also, new controller schemes are developed and designed for the necessary grid synchronization and for the charge control. The torque reference is zero, as the machine is rotating in the charging mode, and the torque ripple is shown to be less than 1% of rated torque. It is also shown that smooth grid synchronization can be achieved and that the system has good performance during the charging time, also for a load step change.

To verify the system operation for the modeled integrated charger, a practically designed system is simulated, with 25 kW traction power and with an IPM motor with double set of windings. The charge power is thus limited to 12.5 kW in this case and the system efficiency was found to be 89%, neglecting iron losses and converter losses. The efficiency of the system in charging mode is lower than the efficiency of the system in traction mode since with the same amount of losses the output power in charging is half that of traction.

A patent is filed as a result of the current project [62].

5.2 Future Work

Basically there are two areas that will be focused on for the continuation of the current study: theory development and practical implementation.

Further development can be done in the theoretical side by applying the principle to different machines with different winding configurations. Moreover, the overall system can be optimized by considering the impact of the integration on the system performance to have a more efficient system in charging mode.

The machine rotation is the key point in the proposed integrated charger, because it will avoid high magnetization currents compared to the methods employing the machine as a stationary transformer. A IPM machine is analyzed in this thesis as an example, but it is possible to apply the method to other type of machines like PMSM with different winding arrangements. For example in the IPM machine two set of windings are shifted $\pi/6$ degree in the stator periphery. It is possible to have double set of windings without space shift.

When the machine is rotating at the synchronous speed in the charging mode, the machine produced voltage should be the same as the grid voltage in the synchronization. With the d component of the current it is possible to adjust the voltage level. By an accurate machine design it is possible to have very low d component current that is equivalent to more system efficiency. So, with better machine design the system efficiency can be improved.

For the grid synchronization and charge control more advanced controllers can be employed to improve system performance. Another example is controlling the reactive power during the charging that can broaden the application of the proposed charger concerning grid issues like reactive power compensation.

The grid supply is assumed to be three-phase. It is possible to investigate system operation for the single-phase supply also. More theoretical development is needed to address the system operation for the single-phase supply.

And finally the system validation will be checked in an experimental set up developed for this purpose.

Bibliography

[1] A. Emadi, Y. J. Lee, and K. Rajashekara, "Power electronics and motor drives in electric, hybrid electric, and plug-in hybrid electric vehicles," *Industrial Electronics, IEEE Transactions on*, vol. 55, no. 6, pp. 2237 –2245, 2008.

[2] I. Khan, "Battery chargers for electric and hybrid vehicles," in *Power Electronics in Transportation, 1994. [Proceedings]*, Oct. 1994, pp. 103 – 112.

[3] J. Hayes, "Battery charging systems for electric vehicles," in *Electric Vehicles - A Technology Roadmap for the Future (Digest No. 1998/262), IEE Colloquium on*, May 1998, pp. 4/1 –4/8.

[4] C. Chan and K. Chau, "An overview of power electronics in electric vehicles," *Industrial Electronics, IEEE Transactions on*, vol. 44, no. 1, pp. 3 –13, Feb. 1997.

[5] C. Toepfer, "Charge! evs power up for the long haul," *Spectrum, IEEE*, vol. 35, no. 11, pp. 41 –47, Nov. 1998.

[6] P. Krein, "Electrostatic discharge issues in electric vehicles," *Industry Applications, IEEE Transactions on*, vol. 32, no. 6, pp. 1278 –1284, 1996.

[7] S. Y. Kim, I. Jeong, K. Nam, and H.-S. Song, "Three-port full bridge converter application as a combined charger for phevs," in *Vehicle Power and Propulsion Conference, 2009. VPPC '09. IEEE*, 2009, pp. 461 –465.

[8] M. Dumenjo, S. Monge, J. Yus, J. Delgado, M. Espadaler, J. Apruzzese, and J. Pereira, "A novel pulsewidth modulation to operate a bidirectional two-stage dc-ac converter with high-frequency isolation in discontinuous conduction mode for photovoltaic applications," in *Power Electronics and Applications, 2009. EPE '09. 13th European Conference on*, 2009, pp. 1 –8.

[9] S. Haghbin, K. Khan, S. Lundmark, M. Alakula, O. Carlson, M. Leksell, and O. Wallmark, "Integrated chargers for ev's and phev's: examples and new solutions," in *Electrical Machines (ICEM), 2010 XIX International Conference on*, 2010, pp. 1 –6.

[10] *SAE-J1772 Standard: Electric Vehicle And Plug In Hybrid Electric Vehicle Conductive Charge Coupler*, Society of Automotive Engineers, 2010.

[11] S. Haghbin, M. Alakula, K. Khan, S. Lundmark, M. Leksell, O. Wallmark, and O. Carlson, "An integrated charger for plug-in hybrid electric vehicles based on a special interior permanent magnet motor," *in Vehicle Power and Propulsion Conference (VPPC) Proceedings, in Lille, France*, 2010.

[12] A. G. Cocconi, "Combined motor drive and battery recharge system," *US Patent no. 5,341,075*, 23 August 1994.

[13] W. E. Rippel, "Integrated traction inverter and battery charger apparatus," *US Patent no. 4,920,475*, 24 April 1990.

[14] ——, "Integrated motor drive and recharge system," *US Patent no. 5,099,186*, 24 March 1992.

[15] L. De Sousa, B. Silvestre, and B. Bouchez, "A combined multiphase electric drive and fast battery charger for electric vehicles," in *IEEE Vehicle Power and Propulsion Conference (VPPC) Proceedings, 2010, France*, Oct. 2010.

[16] A. Bruyre, L. De Sousa, B. Bouchez, P. Sandulescu, X. Kestelyn, and E. Semail, "A multiphase traction/fast-battery-charger drive for electric or plug-in hybrid vehicles," in *IEEE Vehicle Power and Propulsion Conference (VPPC) Proceedings, 2010, France*, Oct. 2010.

[17] S. Lacroix, E. Laboure, and M. Hilairet, "An integrated fast battery charger for electric vehicle," in *IEEE Vehicle Power and Propulsion Conference (VPPC) Proceedings, 2010, France*, Oct. 2010.

[18] L. De-Sousa and B. Bouchez, "Combined electric device for powering and charging," *International Patent WO 2010/057892 A1*, 2010.

[19] ——, "Method and electric combined device for powering and charging with compensation means," *International Patent WO 2010/057893 A1*, 2010.

[20] S. J. Lee and S. K. Sul, "An integral battery charger for 4 wheel drive electric vehicle," in *Industry Applications Society Annual Meeting, 1994., Conference Record of the 1994 IEEE*, Oct. 1994, pp. 448 –452 vol.1.

[21] L. Solero, "Nonconventional on-board charger for electric vehicle propulsion batteries," *Vehicular Technology, IEEE Transactions on*, vol. 50, no. 1, pp. 144 –149, Jan. 2001.

[22] F. Lacressonniere and B. Cassoret, "Converter used as a battery charger and a motor speed controller in an industrial truck," in *Power Electronics and Applications, 2005 European Conference on*, 0 2005.

[23] H.-C. Chang and C.-M. Liaw, "Development of a compact switched-reluctance motor drive for ev propulsion with voltage-boosting and pfc charging capabilities," *Vehicular Technology, IEEE Transactions on*, vol. 58, no. 7, pp. 3198 –3215, 2009.

[24] M. Barnes and C. Pollock, "New class of dual voltage converters for switched reluctance drives," *Electric Power Applications, IEE Proceedings* -, vol. 145, no. 3, pp. 164 –168, May 1998.

[25] ——, "Forward converters for dual voltage switched reluctance motor drives," *Power Electronics, IEEE Transactions on*, vol. 16, no. 1, pp. 83 –91, Jan. 2001.

[26] W. K. Thong and C. Pollock, "Low-cost battery-powered switched reluctance drives with integral battery-charging capability," *Industry Applications, IEEE Transactions on*, vol. 36, no. 6, pp. 1676 – 1681, 2000.

[27] R. M. Davis and W. F. Ray, "Battery chargers in variable reluctance electric motor systems," *U.K. Patent GB 1604066*, 1978.

[28] G. Pellegrino, E. Armando, and P. Guglielmi, "An integral battery charger with power factor correction for electric scooter," *Power Electronics, IEEE Transactions on*, vol. 25, no. 3, pp. 751 –759, 2010.

[29] ——, "An integral battery charger with power factor correction for electric scooter," in *Electric Machines and Drives Conference, 2009. IEMDC '09. IEEE International*, May 2009, pp. 661 –668.

[30] C. Stancu, S. Hiti, and E. Mundt, "Mobile electric power for medium and heavy duty hybrid electric vehicles," in *Power Electronics Specialists Conference, 2004. PESC 04. 2004 IEEE 35th Annual*, vol. 1, 2004, pp. 228 – 234 Vol.1.

[31] F. J. Perez-Pinal and I. Cervantes, "Multi -reconfigurable power system for ev applications," in *Power Electronics and Motion Control Conference, 2006. EPE-PEMC 2006. 12th International*, 30 2006.

[32] S. Y. Kim, I. Jeong, K. Nam, and H.-S. Song, "Three-port full bridge converter application as a combined charger for phevs," in *Vehicle Power and Propulsion Conference, 2009. VPPC '09. IEEE*, 2009, pp. 461 –465.

[33] L. Tang and G.-J. Su, "Control scheme optimization for a low-cost, digitally-controlled charger for plug-in hybrid electric vehicles," in *Energy Conversion Congress and Exposition (ECCE), 2010 IEEE*, 2010, pp. 3604 –3610.

[34] G.-J. Su and L. Tang, "Control of plug-in hybrid electric vehicles for mobile power generation and grid support applications," in *Applied Power Electronics Conference and Exposition (APEC), 2010 Twenty-Fifth Annual IEEE*, 2010, pp. 1152 –1157.

[35] D. Thimmesch, "An scr inverter with an integral battery charger for electric vehicles," *Industry Applications, IEEE Transactions on*, vol. IA-21, no. 4, pp. 1023 –1029, 1985.

[36] C. Liaw and H. Chang, "An integrated driving/charging switched reluctance motor drive using three-phase power module," *Industrial Electronics, IEEE Transactions on*, 2010.

[37] A.-T. Avestruz, J. Holloway, R. Cox, and S. Leeb, "Voltage regulation in induction machines with multiple stator windings by zero sequence harmonic control," in *Applied Power Electronics Conference and Exposition, 2005. APEC 2005. Twentieth Annual IEEE*, vol. 2, 2005, pp. 746 –752 Vol. 2.

[38] H. Plesko, J. Biela, J. Luomi, and J. Kolar, "Novel concepts for integrating the electric drive and auxiliary dc x2013;dc converter for hybrid vehicles," *Power Electronics, IEEE Transactions on*, vol. 23, no. 6, pp. 3025–3034, 2008.

[39] Y.-J. Lee, A. Khaligh, and A. Emadi, "Advanced integrated bidirectional ac/dc and dc/dc converter for plug-in hybrid electric vehicles," *Vehicular Technology, IEEE Transactions on*, vol. 58, no. 8, pp. 3970 –3980, 2009.

[40] M. Rawson and S. Kateley, "Electric vehicle charging equipment design and health and safety codes," *California Energy Commission Report*, 1998.

[41] K. Klontz, A. Esser, P. Wolfs, and D. Divan, "Converter selection for electric vehicle charger systems with a high-frequency high-power link," in *Power Electronics Specialists Conference, 1993. PESC '93 Record., 24th Annual IEEE*, Jun. 1993, pp. 855 –861.

[42] C.-S. Wang, O. Stielau, and G. Covic, "Design considerations for a contactless electric vehicle battery charger," *Industrial Electronics, IEEE Transactions on*, vol. 52, no. 5, pp. 1308 – 1314, 2005.

[43] H. Sakamoto, K. Harada, S. Washimiya, K. Takehara, Y. Matsuo, and F. Nakao, "Large air-gap coupler for inductive charger [for electric vehicles]," *Magnetics, IEEE Transactions on*, vol. 35, no. 5, pp. 3526 –3528, Sep. 1999.

[44] B. Singh, B. Singh, A. Chandra, K. Al-Haddad, A. Pandey, and D. Kothari, "A review of three-phase improved power quality ac-dc converters," *Industrial Electronics, IEEE Transactions on*, vol. 51, no. 3, pp. 641 – 660, 2004.

[45] ——, "A review of single-phase improved power quality ac-dc converters," *Industrial Electronics, IEEE Transactions on*, vol. 50, no. 5, pp. 962 – 981, 2003.

[46] E. Ismail and R. Erickson, "A new class of low-cost three-phase high-quality rectifiers with zero-voltage switching," *Power Electronics, IEEE Transactions on*, vol. 12, no. 4, pp. 734 –742, Jul. 1997.

[47] V. Vlatkovic, D. Borojevic, X. Zhuang, and F. Lee, "Analysis and design of a zero-voltage switched, three-phase pwm rectifier with power factor correction," in *Power Electronics Specialists Conference, 1992. PESC '92 Record., 23rd Annual IEEE*, 1992.

[48] R. Jayabalan, B. Fahimi, A. Koenig, and S. Pekarek, "Applications of power electronics-based systems in vehicular technology: state-of-the-art and future trends," in *Power Electronics Specialists Conference, 2004. PESC 04. 2004 IEEE 35th Annual*, vol. 3, 2004, pp. 1887 – 1894 Vol.3.

[49] "Ac propulsion electric vehicle drive system specifications," *AC Propulsion Inc. Technical Note*, 2008.

[50] K. Khan, S. Haghbin, M. Leksell, and O. Wallmark, "Design and performance analysis of a permanent-magnet assisted synchronous reluctance machine for an integrated charger application," in *Electrical Machines (ICEM), 2010 XIX International Conference on*, 2010, pp. 1 –6.

[51] S. E. Lyshevski, *Electromechanical Systems, Electric Machines, and Applied Mechatronics*. CRC Press, 1999.

[52] P. Vas, *Sensorless vector and direct torque control*. Oxford Press, 1998.

[53] B. K. Bose, *Modern power electronics and ac drives*. Prentice Hall, 2001.

[54] M. Malinowski, "Sensorless control strategies for three-phase pwm rectifiers," Ph.D. dissertation, Faculty of Electrical Engineering, Institute of Control and Industrial Electronics, Warsaw University of Technology, 2001.

[55] B. Bose, "A high-performance inverter-fed drive system of an interior permanent magnet synchronous machine," *Industry Applications, IEEE Transactions on*, vol. 24, no. 6, pp. 987 –997, 1988.

[56] Y. Wang, J. Zhu, and Y. Guo, "A survey of direct torque control schemes for permanent magnet synchronous motor drives," in *Power Engineering Conference, 2007. AUPEC 2007. Australasian Universities*, 2007, pp. 1 –5.

[57] I. Takahashi and T. Noguchi, "A new quick-response and high-efficiency control strategy of an induction motor," *Industry Applications, IEEE Transactions on*, vol. IA-22, no. 5, pp. 820 –827, 1986.

[58] M. Depenbrock, "Direct self-control (dsc) of inverter-fed induction machine," *Power Electronics, IEEE Transactions on*, vol. 3, no. 4, pp. 420 –429, Oct. 1988.

[59] G. Buja, D. Casadei, and G. Serra, "Direct torque control of induction motor drives," in *Industrial Electronics, 1997. ISIE '97., Proceedings of the IEEE International Symposium on*, vol. 1, Jul. 1997, pp. TU2 –TU8 vol.1.

[60] H. Yuwen, T. Cun, G. Yikang, Y. Zhiqing, L. Tang, and M. Rahman, "In-depth research on direct torque control of permanent magnet synchronous motor," in *IECON 02 [Industrial Electronics Society, IEEE 2002 28th Annual Conference of the]*, vol. 2, 2002, pp. 1060 – 1065 vol.2.

[61] M. Rahman and L. Zhong, "Voltage switching tables for dtc controlled interior permanent magnet motor," in *Industrial Electronics Society, 1999. IECON '99 Proceedings. The 25th Annual Conference of the IEEE*, 1999.

[62] S. Haghbin (Chalmers University of Technology) and M. Alakula (Lund University), "Elektrisk appart," *Swedish Patent Office, Patent no. 1050607-9*, filed in 14 June 2010.

Appendix A

Paper I: Grid-Connected Integrated Battery Chargers in Vehicle Applications: Review and New Solution

Saeid Haghbin, Sonja Lundmark, Mats Alaküla and Ola Carlson

Submitted to
the IEEE Transactions on Vehicular Technology, 2011

The layout has been revised.

Abstract

For vehicles using grid power to charge the battery, traction circuit components are not engaged during the charging time, so there is a possibility to use them in the charger circuit to have an on-board integrated charger. The battery charger can be galvanic isolated from the grid or non-isolated. Different examples of isolated or non-isolated integrated chargers are reviewed and explained. Moreover, a novel isolated high power three-phase battery charger based on a special ac motor design and its winding configuration is presented in this paper. The proposed charger is a bi-directional charger with unit power factor operation capability that has high efficiency.

A.1 Introduction

The battery has a vital role in the development of electrified vehicles. Its energy density, power density, charging time, lifetime, and cost are challenges for commercialization and subject of research. The charging time and lifetime of the battery have a strong dependency on the characteristics of the battery charger [1–10]. Several manufacturers are working worldwide on the development of various types of battery modules for electric and hybrid vehicles. However, the performance of battery modules depends not only on the design of modules, but also on how the modules are discharged and charged. In this sense, battery chargers play a critical role in the evolution of this technology.

Generally there are two types of battery chargers: on-board type and stand-alone (off-board) type. The on board charger gives flexibility to charge anywhere where there is an electric power outlet available. The on board charger has the drawback of adding weight, volume and cost to the vehicle, thus it is usually made for lower powers (< 3.5 kW). When higher charging powers is needed, the size and weight of the charger is easier to handle with an off board charger. Vehicles with a longer EV-range (e.g. > 100 km) may require filling large amounts of energy (e.g. > 20 kWh) in reasonably short time. Even a 30 minute charging time would require a charging power of 40 kW or more, which is on the high side and very well may be limited by the maximum allowed continuous battery power. With a significantly increased fleet of EV's the need for long charging times, compared to filling e.g. gasoline, implies the need for an un-proportionally large amount of charging stations - that will be expensive. High power on board charges are attractive if the weigh, volume and cost can be handled. In that case the infrastructure requirement would be reduced to rather simple high power outlets and thus the cost of these significantly lower than of board chargers.

Galvanic isolation is a favorable option in the charger circuits for safety reasons but isolated on-board chargers are usually avoided due to its cost impact on the system. There is a possibility of avoiding these problems of additional charger weight space and cost by using available traction hardware, mainly the electric motor and the inverter, for the charger circuit and thus to have an integrated drive system and battery charger. The integration may also allow galvanic isolation. Other aspects to consider regarding integrated chargers are voltage level adaption, unwanted developed torque in the motor during charging, efficiency, low harmonic content in the current from the grid and mandatory unit power factor operation.

Different types of integrated chargers reported [8,10,15–25,27–43] and some of are reviewed in this paper. In addition, a new isolated high power battery charger is described which integrate the traction drive system components (converter and motor) in such a way that most of the desired features are achieved [8].

A.2 Battery Chargers in Vehicle Applications

Chargers can be classified in terms of power levels and time of charging [44,45]. The choice of classification depends naturally on nationally available power levels. One example of classification that suits the US residential power source

is given in [44]:
Level 1: Common household type of circuit in the US rated to 120 V and up to 15 A.
Level 2: Permanently wired electric vehicle supply equipment used specially for electric vehicle charging and it is rated up to 240 V, up to 60 A, and up to 14.4 kW.
Level 3: Permanently wired electric vehicle supply equipment used specially for electric vehicle charging and it is rated greater than 14.4 kW.
Equivalently, above categories are known as; emergency charger which charges the battery pack of a vehicle in six to eight hours, standard charger which charges the battery pack in two to three hours, and rapid charger which charges the battery pack in ten to fifteen minutes (fast chargers).

Chargers can also be described as either conductive or inductive. For a conductive charger the power flow take place through metal-to-metal contact between the connector on the charge port of the vehicle and charger (off-board charging) or grid (on-board charging). Conductive chargers may have different circuit configurations but the common issues concern safety and the design of the connection interface.

Inductive coupling is a method of transferring power magnetically rather than by direct electrical contact and the technology offers advantages of safety, power compatibility, connector robustness and durability to the users of electric vehicles but on the expense of a lower efficiency and the need of new equipment at charging sites. The electric vehicle user may physically insert the coupler into the vehicle inlet where the ac power is transformer coupled, rectified and fed to the battery, or the charging could be done almost without driver action by wireless charging [46]. For inductive charging, among the most critical parameters are the frequency range, the low magnetizing inductance, the high leakage inductance and the significant discrete parallel capacitance [47, 48].

Different topologies and schemes are reported for both single-phase and three-phase input conductive battery chargers [12, 49, 50, 52–54]. Usually the three-phase input solutions are used in high power applications.

A.3 Integrated Chargers

Fig. A.1 shows a schematic diagram of a PHEV with parallel configuration (both internal combustion engine and electric motor can drive the vehicle simultaneously) as an example of a vehicle with grid-connected battery charger. The electrical part includes the grid connected battery charger, battery, inverter, motor and control system. It is here assumed that during charging time the vehicle is not driven and during driving time it is not possible to charge the battery pack except for regeneration at braking. In a classical electrical device arrangement in the vehicle, there are separate inverter and charger circuits for traction and charging from an external source. However, it is possible to integrate hardware to reduce the number of system components, space and weight which is equivalent to cost reduction. For instance, the three-phase three-wire boost AC/DC converter that can be used as a battery charger is very similar to what hardware is available in the traction system.

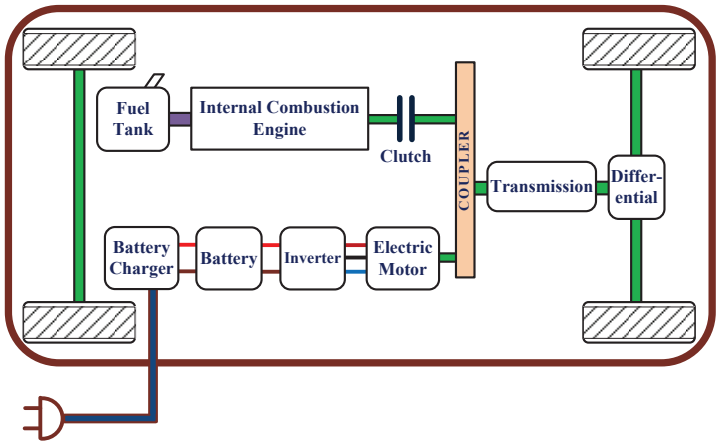

Figure A.1: A simple diagram of a parallel plug-in hybrid electric vehicle.

See [49,50] for different AC/DC rectifier schemes. Another example of the use of integration is to use the electric motor windings as inductors in the charger circuit. This reduces weight as high current inductors are large components compared to other components like switches for example.

A traction system based on an ac motor and a three-phase inverter is shown in Fig. A.2. In some schemes a DC/DC converter is used in the system also [59]. The battery power will be transferred to the motor through the inverter. Bi-directional operation of the inverter allows energy restoration to the battery during braking. Regarding different drive systems, different types of integrated chargers are reported both in academia and industry and some of them are assessed here.

A.3.1 A Combined Motor Drive and Battery Recharge System Based on Induction Motor

An integrated motor drive and charger based on an induction machine was patented 1994 by AC Propulsion Inc. [15] and is currently in use in the car industry [16]. The main idea is to use the motor as a set of inductors during charging time to constitute a boost converter with the inverter to have unit power factor operation. Fig. A.3 shows the functional schematic diagram of this non-isolated integrated charger system. By the means of inexpensive relays the machine windings are reconfigured to be inductors in the charging mode.

For example for a single-phase ac supply, LS2 and LS3 shown in Fig. A.3 are the induction motor phase to neutral leakage inductances of the windings that act as inductors in the single-phase boost converter circuit. The battery voltage should be more than maximum line-line peak voltage in the input to guarantee unit power factor operation. As an example they used a 336Vdc battery pack with a 220Vac input. The relays K1, K2 and K2' shown in Fig. A.3 are used to reconfigure the motor in motoring mode. Further, the inverter switches S1 and S2 are open in charging mode and switches S3-S6 are part of

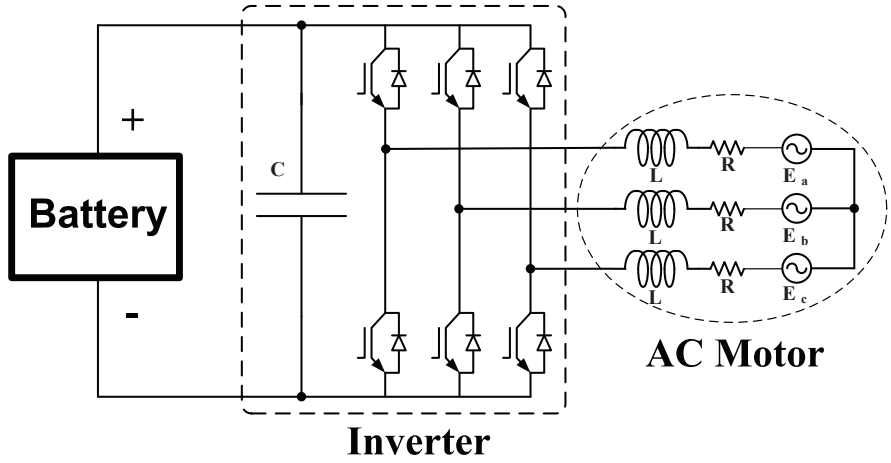

Figure A.2: Electrical traction in a vehicle.

the boost converter. A common/differential mode filter is used to eliminate the switching ripples and spikes from the line side current. Moreover, a lot of electrostatic shielding is used to decrease the ground current and high voltage transitions. In traction mode, relays K2 and K2' are open and K1 is closed, yielding a classical three-phase drive system.

It is possible to have a three-phase input supply with this scheme, but there will be developed torque in the machine during charging that should be considered. The one-phase charger can charge from any source, 100-250 VAC, from 200W up to 20kW and can be used for V2G (vehicle to grid) and for backup power and energy transfer to other electric vehicles. The filter bank at the front of the ac supply will smooth the harmonic contents of the charger line current. Other similar alternatives are patented in the US also. In some examples the motor, the inverter and the capacitor components are used in the charging system. All of these solutions are bidirectional non-isolated type of chargers with unit power factor operation and single-phase ac supply. In [17] two solutions are proposed by Rippel in 1990. In traction mode an inverter and a three-phase ac motor is used. in the first version the motor is not used in the charger circuit and instead an inductor is used to be the energy storage device in the front-end boost converter. The inverter switches are used in the system (part of the boost and DC/DC converter). In a later version, the inductors are eliminated and the machine leakage inductances are used as part of the charger circuit. When the machine is used as three inductors, the inductors have self and mutual couplings. So the inductance matrix should be considered in this case. The leakage inductances are the part of inductors that have no coupling to the other inductances. No switching devices like relays are used to reconfigure the circuit for traction and charging mode (the same hardware in the traction and charging mode).

Another solution patented by Rippel and Cocconi in 1992 (the patent assignee is General Motors Inc.) uses the same idea of integration but there are two independent inverters in the system [18]. They proposed two alternative

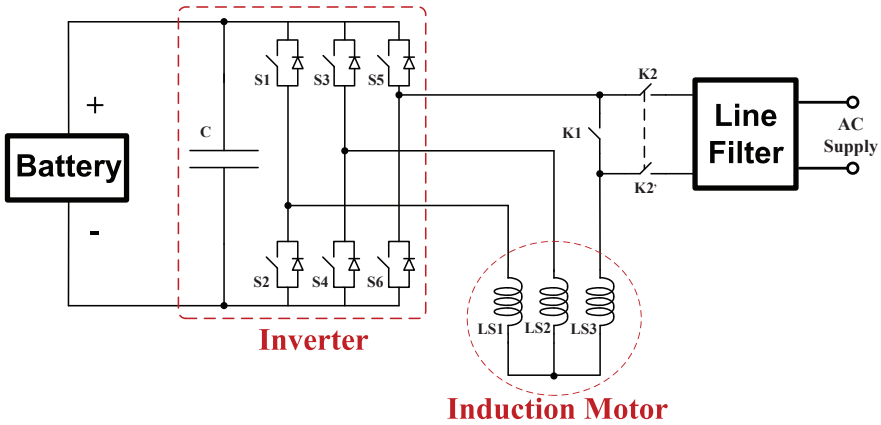

Figure A.3: Non-isolated single-phase integrated charger based on a induction motor drive system.

methods. One with two induction motors and another one with one induction motor (with double stator windings).

In the first alternative two induction motors and inverters are used for the traction force. Each motor can be controlled by its dedicated inverter independently. Each motor can be connected to the wheel directly or through a gear that eliminates the need for a transmission and differential in the mechanical system. For the charging mode the supply will be connected to the neutral point of the motors after EMI filtering.

The second alternative is using an induction motor with double set of stator windings comprising two motor halves. The rotor can be coupled to a single wheel or to two wheels by means of a reduction-differential gear or a transmission-differential gear. Each winding set is connected to an inverter (each winding set includes three windings). In the charging mode the supply is similarly connected to the neutral points of the double set of windings after EMI filtering.

A.3.2 Non-isolated Integrated Charger Based on a Split-Winding AC Motor

A non-isolated high power three-phase integrated charger is reported by Luis De Sousa et al. in Valeo Engine and Electrical Systems in 2010 [19–21]. Fig. A.4 shows the proposed integrated charger. In traction mode a 3H-bridge topology is used with a DC/DC converter. The DC/DC converter consists of inductor L and two switches. The inverter dc bus voltage is 900 Vdc while the battery voltage is maximum 420 Vdc for the proposed system.

Fig. A.5 shows the system equivalent circuit in charging mode. For charging, the three-phase supply is connected to the middle point of the stator windings. A small EMI filter is used to improve the grid current waveforms. As is shown in this figure, there are two three-phase boost converters sharing a common dc bus. By using a split-winding configuration and regulating the same current in the same phases of two boost converters, eliminates devel-

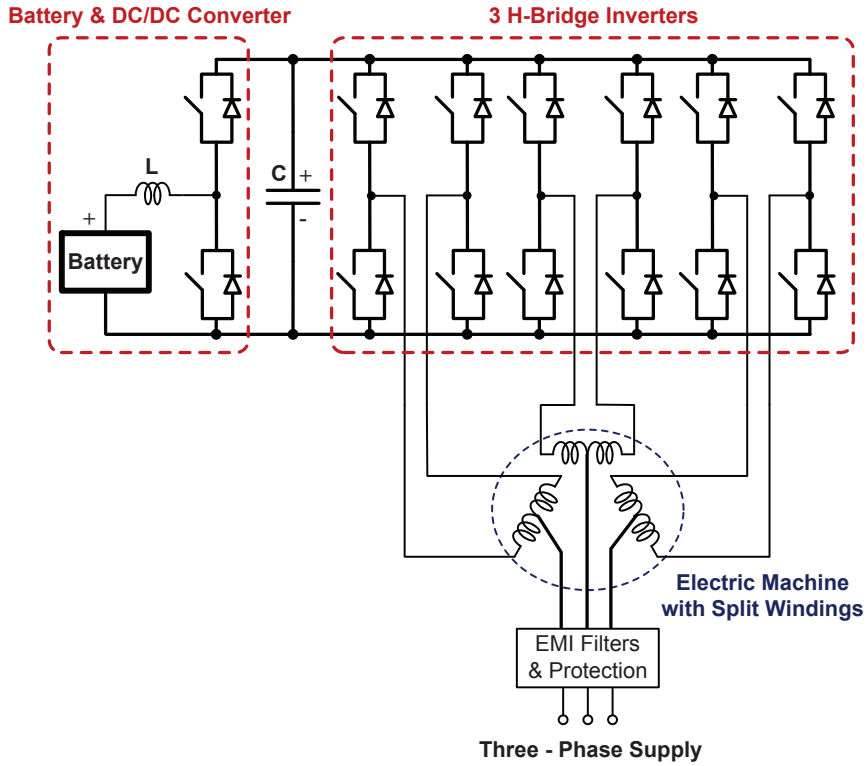

Figure A.4: Three-phase non-isolated integrated charger based on a split-winding ac motor.

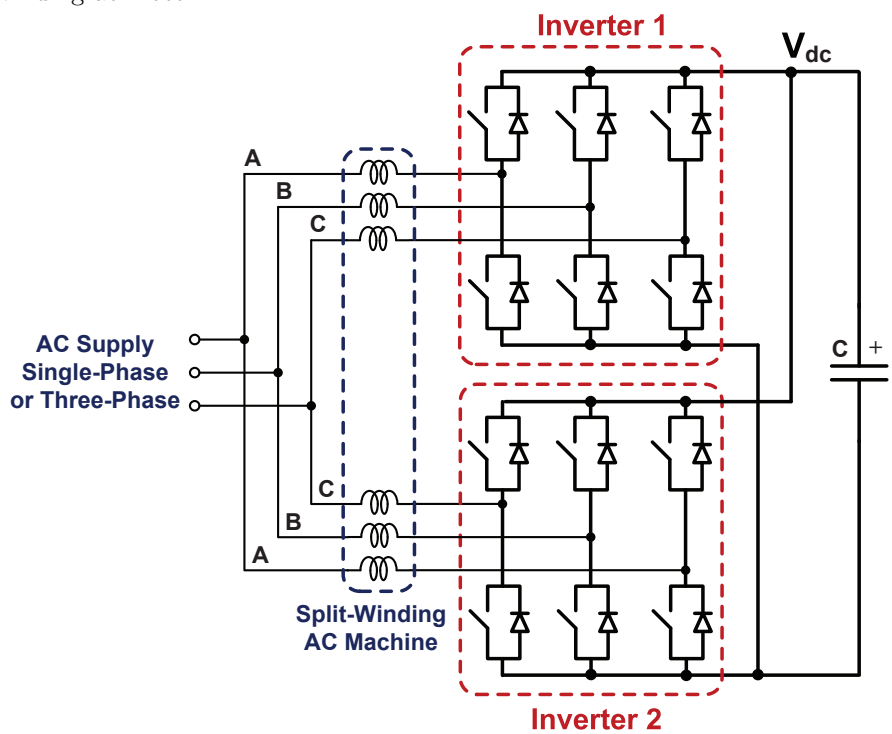

Figure A.5: Charging mode equivalent circuit of the three-phase integrated

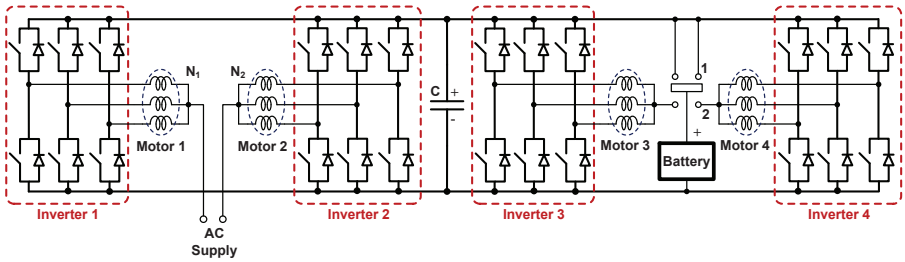

Figure A.7: Single-phase integrated battery charger for a four wheel drive system.

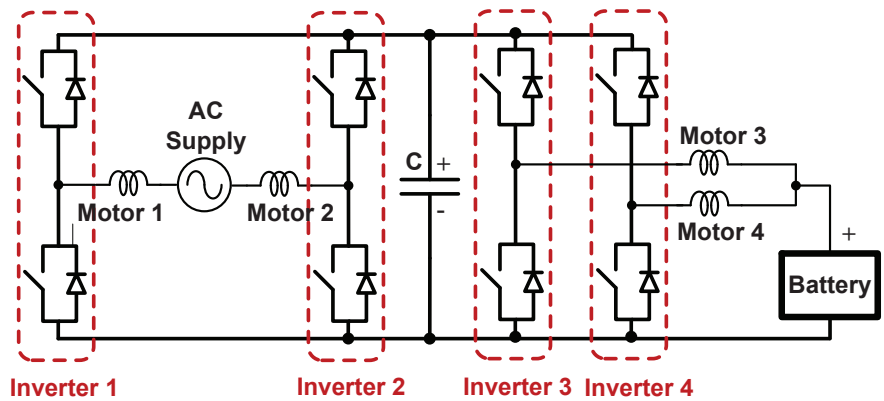

Figure A.8: System equivalent circuit for the four wheel drive integrated charger.

oped stator magnetomotive force (MMF) of the machine so there is not any rotational magnetic field in the motor during charging.

The proposed charger is a high power non-isolated version capable of unit power factor operation. There is no need to use a switch like contactor for the charger to grid connection. A plug can be used for this purpose. Two international patents are received for the proposed scheme [22, 23].

It is shown that it is possible to use the same strategy for a single-phase supply by S. Lacroix et al. [21]. Fig. A.6 shows the system in charging mode for the single-phase supply. Four legs of bridges in the inverter and inductances of two phases are used in this mode. As is shown in this figure, the third H-bridge inverter is not used. The currents will be regulated to be equal for each phase. Unit power factor operation is possible in this case also due to the boost converter topology.

A.3.3 An Integral Battery Charger for a Four-Wheel Drive Electric Vehicle

An integral battery charger has, in 1994, been reported for a four wheel-in motor driven EV by Seung-Ki Sul and Sang-Joon Lee [24]. The propulsion system includes four induction motors and four three-leg inverters with a battery on

the system dc bus. By the use of an extra transfer switch the whole system will be reconfigured to a single-phase battery charger. Fig. A.7 shows the system configuration in traction and charging mode. In the traction mode, four inverters connected to the system dc bus drive motors (each motor neutral point is float in this mode). In the charging mode (the transfer switch is in position 2) the single-phase ac source is connected between the neutral points of two motors. Utilizing the switches in inverter one and two, this configuration will be a single-phase boost converter with unit power factor operation capability. The third and fourth inverters with the use of two other motors constitute two buck-type converters. Fig. A.8 shows the system equivalent circuit in charging mode where the motors are used as inductors. For each motor the winding currents are the same for each phase so there is no developed electromagnetic torque in the motors during the charging time. Further, in the charging mode, by controlling the PWM boost converter, the dc link voltage is kept constant. The constant current battery charging profile is achieved by the control of the two buck-type choppers. Of course, this integrated charger solution is a high cost solution and only appropriate for vehicles with four motors.

A.3.4 An Integrated Charger for an Electric Scooter

A non-isolated single-phase (110 V ac and 60 Hz) integrated charger for an electrical scooter is another example described in [25]. The authors use the three-phase inverter as a single switch in the charging mode, see Fig. A.9. Thus, the switches S2, S4 and S6 seen in Fig. A.9 are to be operated all together as a simple switch. In turn, the circuit is a single-phase boost converter. All three windings of the motor are used in the charging process. A power rectifier and line filter are also used as extra components for the charging operation. It is expected to have unit power factor operation as is expected for boost converters, and low THD in the ac line current due to use of the line filter. A 180 V dc lead acid battery (12 Ah) is used as the traction power source and the motor is a 6 kW axial flux permanent magnet motor. Moreover the 50 A and 600 V IGBT modules are used with a switching frequency of 25 kHz. At charging mode, the motor is used as three parallel connected 0.1 mH inductances. The currents through the inductances are thus unidirectional, thus no torque is developed in the motor, and the rotor can be at standstill. Of course, only slow, low power charging is possible with this solution.

A.3.5 An Integrated Charger for a Fork Lift Truck

An integrated drive/charger system is reported in 2005 for a fork lift truck [10]. In traction mode a 6 kW induction machine is used to drive the truck. The battery voltage and rated motor voltage is nominal 48 V. A three-phase inverter is utilized for motor control based on the space vector modulation (SVM) scheme.

In charging mode, the motor is used as a low frequency step-down transformer. A wound-type rotor is used in the drive system and for the charging mode the rotor winding is used as a primary side of the transformer with the secondary side (the stator) connected to the grid (three-phase 400Vac). Naturally, there is a galvanic insulation between the grid and battery by the

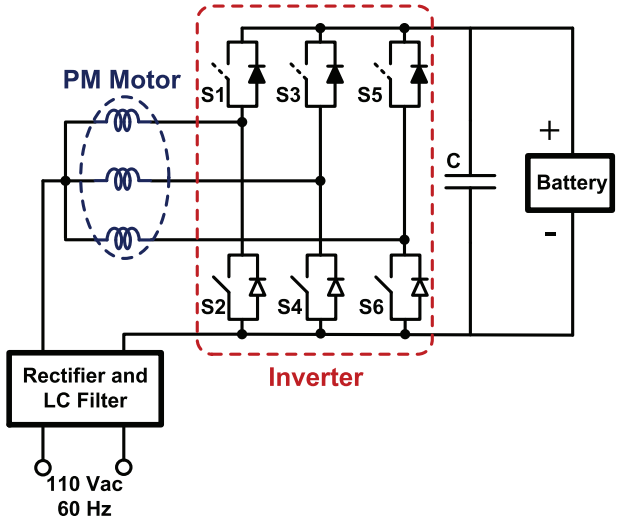

Figure A.9: Single-phase integrated charger for an electric scooter.

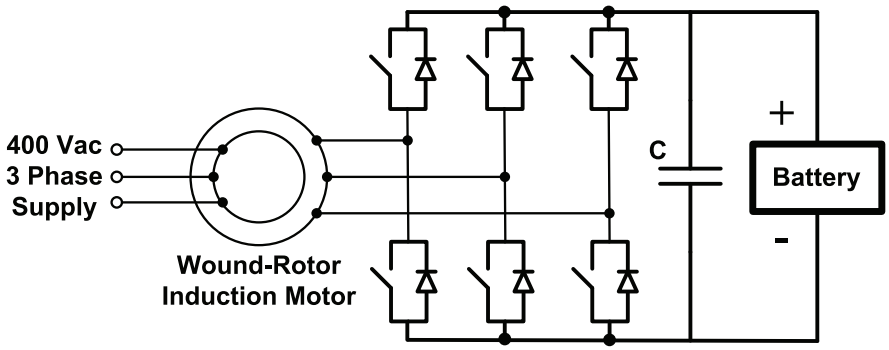

Figure A.10: Three-phase isolated integrated charger based on a wound-rotor induction motor.

means of this transformer. Fig. A.10 shows the system in charging mode. The air-gap in the motor (transformer in charging mode) will affect the system performance regarding the loss due to the need of large magnetization currents. Other disadvantages are the extra cost of the wound rotor (compared to a squirrel cage rotor), need of contactors and the need to adapt the motor windings to the charge voltage. Advantages include the possibility of bidirectional power flow, low harmonic distortion and a unit power factor. The rotor is at standstill during charging and a mechanical lock is used.

A.3.6 Single-Phase Integrated Charger Based on a Switched Reluctance Motor Drive

Switched reluctance motor (SRM) drive systems are interesting alternatives in vehicle applications due to motor robustness and control simplicity [55–58].

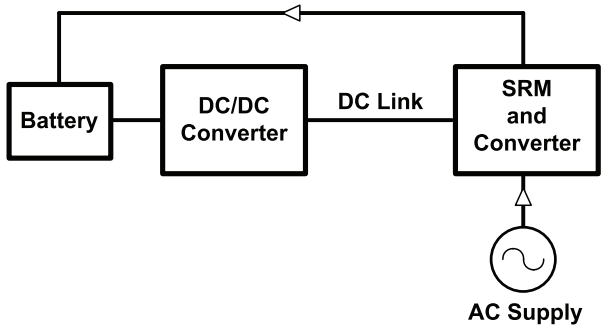

Figure A.11: Single-phase integrated charger based on a SRM drive system.

An integrated drive and charger system for a SRM is reported in [27] for an electric vehicle with voltage-boosting and on-board power-factor-corrected-charging capabilities. A boost DC/DC converter is used in the traction mode to boost and regulate the battery voltage for the motor driver. With slight modification in the traction mode a single-phase non-isolated battery charger is arranged. The DC/DC converter is not used in the charging mode and by the use of a switch the system is reconfigured from charging mode to traction mode and vice versa. Fig. A.11 shows a simplified diagram of the system in which the power flow in charging mode is through the SRM and its driver to the battery.

The SRM and its driver constitute a single phase buck-boost converter that insures unit power factor operation. Two windings of the SRM are used as line filter inductors and the third one is used as the energy storage inductor in the buck-boost converter.

A.3.7 Single-Phase Integrated Charger Based on a Dual Converter Switched Reluctance Motor Drive

By adding an extra winding tightly coupled to the stator windings it is possible to use it as a step down transformer. Different versions of single-phase integrated chargers reported by C. Pollock et al. are based on this principle [28–30]. Fig. A.12 shows a simple basic schematic diagram of the charger. The grid supply is rectified by a diode rectifier module to provide a dc link at the SR grid side winding (high voltage winding). By switching S1 is possible to have a flyback converter or a forward converter by the use of the SRM driver converter (switches S2 and S3 including their antibody diods). The SR grid side windings have more turns compared to its main winding to adjust battery voltage level and grid voltage.

The unit power factor operation is not feasible in this configuration. The machine core losses are high since the switching frequency is high compared to the 50 Hz nominal frequency. So the system efficiency is not high and in one example it was reported to be 25% [30]. The original application was low power application like electric shavers, but the topology improved to be used in vehicle application too [30]. The extra winding and switch S1 can drive the machine from the main in the electric shaver application.

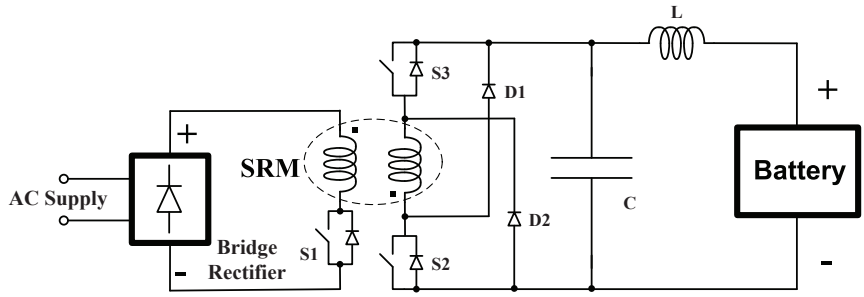

Figure A.12: Single-phase isolated integrated charger based on a dual converter SRM drive.

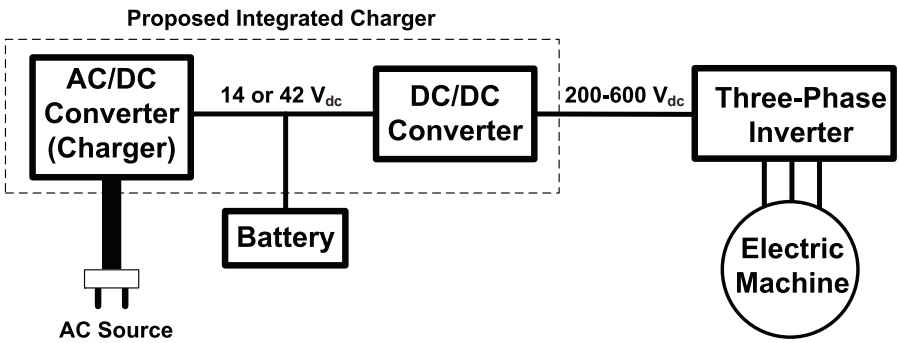

Figure A.13: System diagram of proposed integrated charger based on the combined bidirectional AC/DC and DC/DC converter.

A.3.8 Integrated Bidirectional AC/DC and DC/DC Converter for PHEVs

Conventional hybrid electric vehicles usually have two different voltage levels [60]. A 14 V dc bus supplied by a 12 V dc battery and a high-voltage 200-600 V dc bus that provides the propulsion power. Traditional loads like lightning systems and vipers are connected to the low voltage bus. The increasing number of additional loads motivates the car industries to replace the 14 V dc bus with a 42 V dc bus supplied by a 36 V battery. The high voltage and low voltage buses are connected to each other by the means of an isolated bidirectional DC/DC converter. Also, a DC/AC inverter is used to supply and control the ac drive system.

By combining the DC/DC converter and the battery charger (AC/DC converter) an integrated battery charger was proposed by Young-Joo Lee et al. 2009 in [32]. Fig. A.13 shows a simple schematic diagram of the system structure. Moreover the proposed integrated charger can be identified from this figure. The charger/converter is a non-isolated version with reduced number of inductors and current transducers for the single-phase input supply.

A.4 Isolated Integrated Charger Based on the AC Machine Operating as a Motor/Generator Set

As mentioned, isolated high power on board chargers are preferable from a safety viewpoint, but non-isolated are still used for cost and weight reasons, like several of those presented above. In the following, a drive system with a special machine winding configurations is proposed that can be reconnected into a isolated 3 phase integrated charging device in the charging mode through a simple switching device. Fig. A.14 shows a schematic diagram of the integrated charger first proposed in [8].

Different motor topologies are possible both concerning motor type and winding arrangement. One option with an internal permanent magnet (IPM) synchronous motor was reported in [8] and [6]. The main idea is to introduce a multi terminal device called motor/generator set to act like a motor in the traction mode and like an isolated generator/transformer in the charging mode. Fig. A.15 shows a simple schematic diagram of the system.

The so called motor/generator acts as an isolated three-phase power source after synchronization with the utility grid in the charging mode. This rotary three-phase isolated power source constitutes a three-phase boost rectifier (battery charger) with full utilization of the inverter.

This solution has bidirectional capability so it is possible to feed back power to the grid from the battery. Moreover, unit power factor operation is feasible. Depending on the type of machine and winding configuration, a single-phase solution is also possible. The charging power is limited by the motor thermal limit and inverter power limit and limit of the supply, so high power charging (fast charging) is feasible in this configuration.

A 4 pole IPM machine is designed and optimized for a $25kW$ traction system with a possibility to reconnect the windings for charging [8]. Fig. B.10.a shows the winding configuration (in delta) in the traction mode. The dc bus voltage (battery voltage) is $400Vdc$ in this case. The machine base speed is $1500rpm$ while the maximum speed is $6000rpm$. For the charging mode, the windings are re-arranged according to Fig. B.10.b. Charging power is restricted to half the traction power that is $12.5kW$ in this case.

A.4.1 System Modes of Operation: Traction and Charging

As mentioned before, the system has two modes of operation: traction and charging. In the traction mode, each two windings are connected to each other in series to constitute a three-phase winding set. These three windings can be connected to each other in Δ or Y to form a classical three-phase machine. Moreover, the motor is powered by the battery through the inverter.

If the machine would be kept in standstill as in [10], the magnetization current will be high due to the air-gap. So it is expected to have lower system efficiency depending on the air-gap length. However, if the machine rotates with the grid synchronous speed, the magnets will induce voltages in the inverter-side windings that emulates an isolated PM ac generator for the inverter. The

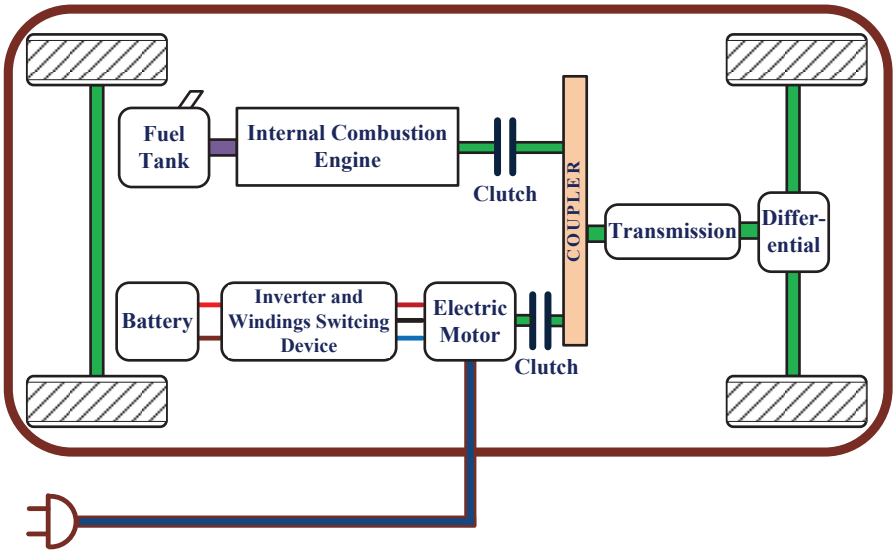

Figure A.14: System diagram of proposed integrated charger based on the electric machine windings configuration.

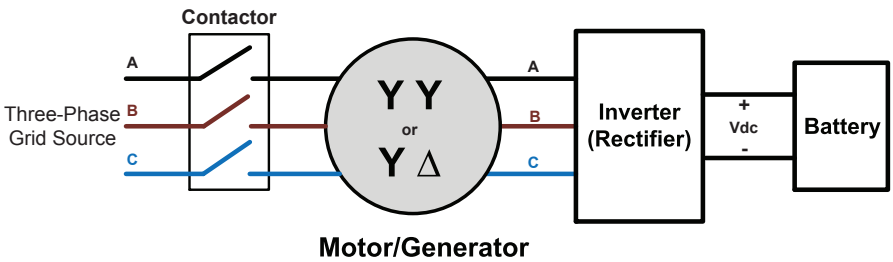

Figure A.15: Isolated high power three-phase integrated charger based on a rotating motor/generator device.

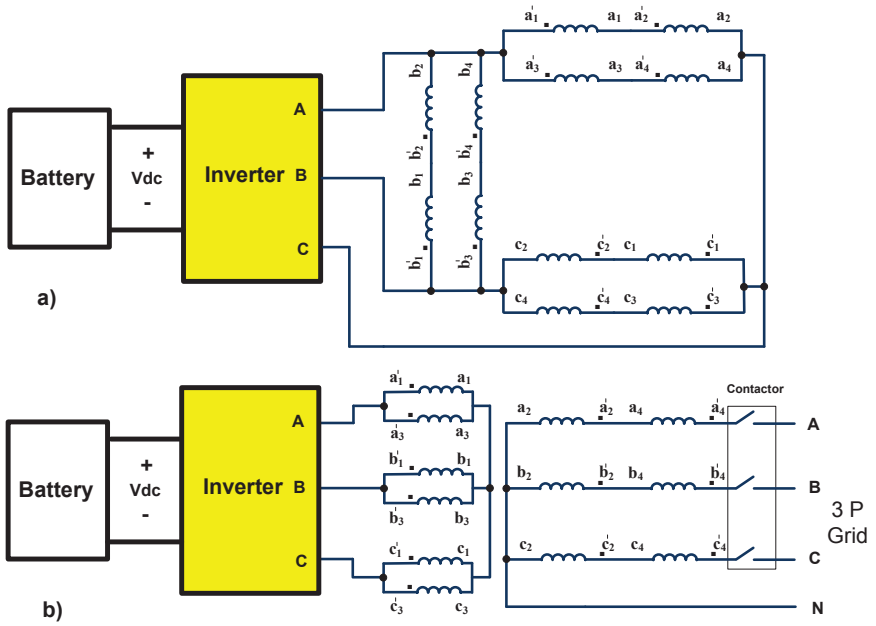

Figure A.16: Practical system modes of operation for proposed integrated charger: a) traction and b) charging.

idea is thus to connect the machine to the grid via the grid-side three-phase windings. These three windings can be used to run the machine as a classical motor. The inverter side windings will pick up the induced voltage due to the developed flux inside the machine (since they are located on the same pole-pair as are the grid-side windings). The inverter can use this isolated voltage source to charge the battery by the means of machine inductances as the converter energy storage component (yielding a three-phase boost converter).

To synchronize the machine to the grid, the inverter runs the motor by the means of the battery through the inverter-side windings. The grid-side windings are open circuited (contactor is open) but the induced voltage is measured to be synchronized with the grid voltage.

Grid-side winding voltages and grid voltages are measured and transformed to the *dq* reference frame. Both voltage vectors magnitude and angle of the grid voltage and motor/generator grid-side windings should be equal as an index of synchronization. The magnitude of voltage is a function of the motor speed and flux, so by controlling the flux, the voltage level can be adjusted. By controlling the machine speed the voltage angle is controlled in the grid-side windings.

The motor/generator will rotate at the synchronous speed to meet the frequency synchronization requirement. A clutch is needed to disconnect the motor from the mechanical transmission in charging operation. Moreover, to match the voltage angles, the motor/generator speed reference is controlled to reduce the voltages angle error to an acceptable level.

When the grid-side winding voltages are synchronized with the grid, the

contactor is closed and the grid voltage is thus applied to the grid-side windings. Afterwards, the inverter controls the inverter side winding voltages to charge the battery which is called charge control here. Now the inverter side windings are an isolated three-phase voltage source and the inverter can control the dc voltage and current at the battery side. One control objective is to keep the torque zero during synchronization with the grid. Another control objective is unit power factor operation. It is showed in [8] that it is possible to have unit power factor operation and current control.

To have proper boost converter operation the dc bus voltage should be more than the peak ac line voltage. This can be solved in two ways: using an extra DC/DC converter or $Y - \Delta$ connection of the stator windings to reduce the voltage at the inverter side. The second approach has been selected to reduce the system hardware in this case. The detailed motor design is presented in [6].

Instead of PM machines, an induction machine can be used with the same principle of operation. In that case the motor will not rotate at the synchronous speed. The motor rotation is a key point to solve the high magnetization problem (equivalently low efficiency) compared to the other solutions (discussed in section III) where the machine is used as an air-gapped transformer. It is also an advantage that the developed torque can be controlled by the control of the converter. At the other side, this solution needs a switching device for winding reconfiguration and, due to machine rotation in the charging mode, a clutch is needed to disconnect the motor from the mechanical system.

A.5 Conclusion

For vehicles using grid power to charge the battery, charging is happening during the time that the vehicle is parked, so there is a possibility to use the available traction hardware, inverter and motor, in the battery charger system to have an integrated battery charger and drive system. Different integrated chargers reported by industry or academia are reviewed and explained in this paper. Moreover, a novel galvanic isolated-high power bi-directional integrated charger based on a special electrical machine windings is described. The inverter is fully utilized in the proposed integrated charger so a minimum of extra components are needed, including a mechanical clutch used to disconnect the rotating machine from the transmission system during battery charging. Moreover, due to the galvanic isolation from the grid, the charger has higher safety compared to non-isolated versions.

Acknowledgment

The authors would like to thank Swedish Hybrid Vehicle Center (SHC) for financing the project and support. The IPM machine designed and optimized for fabrication considering the proposed integrated charger scheme by Kashif Khan, Mats Leksel and Oscar Wallmark in Royal Institute of Technology (KTH), Sweden, that authors would like to thank them also.

References

[1] Chan, C.C.; Chau, K.T.; , "Power electronics challenges in electric vehicles," Industrial Electronics, Control, and Instrumentation, 1993. Proceedings of the IECON '93., International Conference on , vol., no., pp.701-706 vol.2, 15-19 Nov 1993 doi: 10.1109/IECON.1993.338995.

[2] Emadi, A.; Young Joo Lee; Rajashekara, K.; , "Power Electronics and Motor Drives in Electric, Hybrid Electric, and Plug-In Hybrid Electric Vehicles," Industrial Electronics, IEEE Transactions on , vol.55, no.6, pp.2237-2245, June 2008 doi: 10.1109/TIE.2008.922768.

[3] Khan, I.A.; , "Battery chargers for electric and hybrid vehicles," Power Electronics in Transportation, 1994. [Proceedings] , vol., no., pp.103-112, 20-21 Oct 1994 doi: 10.1109/PET.1994.572365.

[4] Hayes, J.G.; , "Battery charging systems for electric vehicles," Electric Vehicles - A Technology Roadmap for the Future (Digest No. 1998/262), IEE Colloquium on , vol., no., pp.4/1-4/8, 5 May 1998 doi: 10.1049/ic:19980359.

[5] Mapelli, F.L.; Tarsitano, D.; Mauri, M.; , "Plug-In Hybrid Electric Vehicle: Modeling, Prototype Realization, and Inverter Losses Reduction Analysis," Industrial Electronics, IEEE Transactions on , vol.57, no.2, pp.598-607, Feb. 2010 doi: 10.1109/TIE.2009.2029520.

[6] Gomez, J.C.; Morcos, M.M.; , "Impact of EV battery chargers on the power quality of distribution systems," Power Delivery, IEEE Transactions on , vol.18, no.3, pp. 975- 981, July 2003 doi: 10.1109/TPWRD.2003.813873.

[7] van Hoek, Hauke; Boesing, Matthias; van Treek, Daniel; Schoenen, Timo; De Doncker, Rik W.; , "Power electronic architectures for electric vehicles," Emobility - Electrical Power Train, 2010 , vol., no., pp.1-6, 8-9 Nov. 2010 doi: 10.1109/EMOBILITY.2010.5668048

[8] Vazquez, S.; Lukic, S. M.; Galvan, E.; Franquelo, L. G.; Carrasco, J. M.; , "Energy Storage Systems for Transport and Grid Applications," Industrial Electronics, IEEE Transactions on , vol.57, no.12, pp.3881-3895, Dec. 2010 doi: 10.1109/TIE.2010.2076414.

[9] Amjadi, Z.; Williamson, S.S.; , "Power-Electronics-Based Solutions for Plug-in Hybrid Electric Vehicle Energy Storage and Management Systems," Industrial Electronics, IEEE Transactions on , vol.57, no.2, pp.608-616, Feb. 2010 doi: 10.1109/TIE.2009.2032195.

[10] Dixon, J.; Nakashima, I.; Arcos, E.F.; Ortuzar, M.; , "Electric Vehicle Using a Combination of Ultracapacitors and ZEBRA Battery," Industrial Electronics, IEEE Transactions on , vol.57, no.3, pp.943-949, March 2010 doi: 10.1109/TIE.2009.2027920.

[11] Haghbin, S.; Khan, K.; Lundmark, S.; Alakla, M.; Carlson, O.; Leksell, M.; Wallmark, O.; , "Integrated chargers for EV's and PHEV's: examples and new solutions," Electrical Machines (ICEM), 2010 XIX International Conference on , vol., no., pp.1-6, 6-8 Sept. 2010 doi: 10.1109/ICELMACH.2010.5608152.

[12] Lisheng Shi; Meintz, A.; Ferdowsi, M.; , "Single-phase bidirectional AC-DC converters for plug-in hybrid electric vehicle applications," Vehicle Power and Propulsion Conference, 2008. VPPC '08. IEEE , vol., no., pp.1-5, 3-5 Sept. 2008 doi: 10.1109/VPPC.2008.4677506.

[13] Khan, K.; Haghbin, S.; Leksell, M.; Wallmark, O.; , "Design and performance analysis of a permanent-magnet assisted synchronous reluctance machine for an integrated charger application," Electrical Machines (ICEM), 2010 XIX International Conference on , vol., no., pp.1-6, 6-8 Sept. 2010 doi: 10.1109/ICELMACH.2010.5607905.

[14] Haghbin, Saeid; Alakla, Mats; Khan, Kashif; Lundmark, Sonja; Leksell, Mats; Wallmark, Oskar; Carlson, Ola; , "An Integrated Charger for Plug-in Hybrid Electric Vehicles Based on a Special Interior Permanent Magnet Motor," in Vehicle Power and Propulsion Conference (VPPC) Proceedings, 2010, France.

[15] Cocconi, Alan G.; , "Combined Motor Drive and Battery Recharge System," US Patent no. 5,341,075 on 23 August 1994.

[16] AC Propulsion Inc. technical note, "AC Propulsion EV Drive System Specifications," 2008.

[17] Rippel, Wally E.; , "Integrated Traction Inverter and Battery Charger Apparatus," US Patent no. 4,920,475 on 24 April 1990.

[18] Rippel, Wally E.; Cocconi, Alan G.; , "Integrated Motor Drive and Recharge System," US Patent no. 5,099,186 on 24 March 1992.

[19] De Sousa, Luis; Silvestre, Benedicte; Bouchez, Boris; , "A Combined Multiphase Electric Drive and Fast Battery Charger for Electric Vehicles," in IEEE Vehicle Power and Propulsion Conference (VPPC) Proceedings, 2010, France.

[20] Bruyre, A.; De Sousa, L.; Bouchez, B; Sandulescu, P.; Kestelyn, X; Semail,E; , "A Multiphase Traction/Fast-Battery-Charger Drive for Electric or Plug-in Hybrid Vehicles," in IEEE Vehicle Power and Propulsion Conference (VPPC) Proceedings, 2010, France.

[21] Lacroix, S.; Laboure, E.; Hilairet, M.; , "An Integrated Fast Battery Charger for Electric Vehicle," in IEEE Vehicle Power and Propulsion Conference (VPPC) Proceedings, 2010, France.

[22] De-Sousa, L.; Bouchez, B.; , "Combined Electric Device for Powering and Charging," International Patent WO 2010/057892 A1.

[23] De-Sousa, L.; Bouchez, B.; , "Method and Electric Combined Device for Powering and Charging with Compensation Means," International Patent WO 2010/057893 A1.

[24] Seung-Ki Sul; Sang-Joon Lee; , "An integral battery charger for four-wheel drive electric vehicle ," Industry Applications, IEEE Transactions on , vol.31, no.5, pp.1096-1099, Sep/Oct 1995 doi: 10.1109/28.464524.

[25] Solero, L.; , "Nonconventional on-board charger for electric vehicle propulsion batteries," Vehicular Technology, IEEE Transactions on , vol.50, no.1, pp.144-149, Jan 2001 doi: 10.1109/25.917904.

[26] Lacressonniere, F.; Cassoret, B.; , "Converter used as a battery charger and a motor speed controller in an industrial truck," Power Electronics and Applications, 2005 European Conference on , vol., no., pp.7 pp.-P.7, 0-0 0 doi: 10.1109/EPE.2005.219286.

[27] Hung-Chun Chang; Chang-Ming Liaw; , "Development of a Compact Switched-Reluctance Motor Drive for EV Propulsion With Voltage-Boosting and PFC Charging Capabilities," Vehicular Technology, IEEE Transactions on , vol.58, no.7, pp.3198-3215, Sept. 2009 doi: 10.1109/TVT.2009.2017546.

[28] Barnes, M.; Pollock, C.; , "New class of dual voltage converters for switched reluctance drives ," Electric Power Applications, IEE Proceedings - , vol.145, no.3, pp.164-168, May 1998 doi: 10.1049/ip-epa:19981851.

[29] Barnes, M.; Pollock, C.; , "Forward converters for dual voltage switched reluctance motor drives," Power Electronics, IEEE Transactions on , vol.16, no.1, pp.83-91, Jan 2001 doi: 10.1109/63.903992.

[30] Weng Kwai Thong; Pollock, C.; , "Low-cost battery-powered switched reluctance drives with integral battery-charging capability," Industry Applications, IEEE Transactions on , vol.36, no.6, pp. 1676- 1681, Nov/Dec 2000 doi: 10.1109/28.887221.

[31] R. M. Davis; W. F. Ray; , "Battery chargers in variable reluctance electric motor systems," U.K. Patent GB 1604066, 1978.

[32] Young-Joo Lee; Khaligh, A.; Emadi, A.; , "Advanced Integrated Bidirectional AC/DC and DC/DC Converter for Plug-In Hybrid Electric Vehicles," Vehicular Technology, IEEE Transactions on , vol.58, no.8, pp.3970-3980, Oct. 2009 doi: 10.1109/TVT.2009.2028070.

[33] Pellegrino, G.; Armando, E.; Guglielmi, P.; , "An Integral Battery Charger With Power Factor Correction for Electric Scooter," Power Electronics, IEEE Transactions on , vol.25, no.3, pp.751-759, March 2010 doi: 10.1109/TPEL.2009.2033187.

[34] Pellegrino, G.; Armando, E.; Guglielmi, P.; , "Integrated battery charger for electric scooter," Power Electronics and Applications, 2009. EPE '09. 13th European Conference on , vol., no., pp.1-7, 8-10 Sept. 2009.

[35] Stancu, C.; Hiti, S.; Mundt, E.; , "Mobile electric power for medium and heavy duty hybrid electric vehicles," Power Electronics Specialists Conference, 2004. PESC 04. 2004 IEEE 35th Annual , vol.1, no., pp. 228-234 Vol.1, 20-25 June 2004 doi: 10.1109/PESC.2004.1355747.

[36] Perez-Pinal, Francisco J.; Cervantes, Ilse; , "Multi -Reconfigurable Power System for EV Applications," Power Electronics and Motion Control Conference, 2006. EPE-PEMC 2006. 12th International , vol., no., pp.491-495, Aug. 30 2006-Sept. 1 2006 doi: 10.1109/EPEPEMC.2006.4778447.

[37] Sung Young Kim; Ilsu Jeong; Kwanghee Nam; Hong-Seok Song; , "Three-port full bridge converter application as a combined charger for PHEVs," Vehicle Power and Propulsion Conference, 2009. VPPC '09. IEEE , vol., no., pp.461-465, 7-10 Sept. 2009 doi: 10.1109/VPPC.2009.5289810.

[38] Lixin Tang; Gui-Jia Su; , "Control scheme optimization for a low-cost, digitally-controlled charger for plug-in hybrid electric vehicles," Energy Conversion Congress and Exposition (ECCE), 2010 IEEE , vol., no., pp.3604-3610, 12-16 Sept. 2010 doi: 10.1109/ECCE.2010.5617711.

[39] Gui-Jia Su; Lixin Tang; , "Control of plug-in hybrid electric vehicles for mobile power generation and grid support applications," Applied Power Electronics Conference and Exposition (APEC), 2010 Twenty-Fifth Annual IEEE , vol., no., pp.1152-1157, 21-25 Feb. 2010 doi: 10.1109/APEC.2010.5433356.

[40] Thimmesch, David; , "An SCR Inverter with an Integral Battery Charger for Electric Vehicles," Industry Applications, IEEE Transactions on , vol.IA-21, no.4, pp.1023-1029, July 1985 doi: 10.1109/TIA.1985.349573.

[41] Liaw, C; Chang, H; , "An Integrated Driving/Charging Switched Reluctance Motor Drive using Three-Phase Power Module," Industrial Electronics, IEEE Transactions on , vol.PP, no.99, pp.1, 0 doi: 10.1109/TIE.2010.2051938.

[42] Avestruz, A.-T.; Holloway, J.W.; Cox, R.; Leeb, S.B.; , "Voltage regulation in induction machines with multiple stator windings by zero sequence harmonic control," Applied Power Electronics Conference and Exposition, 2005. APEC 2005. Twentieth Annual IEEE , vol.2, no., pp.746-752 Vol. 2, 6-10 March 2005 doi: 10.1109/APEC.2005.1453053

[43] Plesko, H.; Biela, J.; Luomi, J.; Kolar, J.W.; , "Novel Concepts for Integrating the Electric Drive and Auxiliary DC DC Converter for Hybrid Vehicles," Power Electronics, IEEE Transactions on , vol.23, no.6, pp.3025-3034, Nov. 2008 doi: 10.1109/TPEL.2008.2005384.

[44] Rawson, Mark; Kateley,Sue; , "Electric Vehicle Charging Equipment Design and Health and Safety Codes," California Energy Commission, 1998.

[45] Klontz, K.W.; Esser, A.; Wolfs, P.J.; Divan, D.M.; , "Converter selection for electric vehicle charger systems with a high-frequency high-power link," Power Electronics Specialists Conference, 1993. PESC '93 Record., 24th Annual IEEE , vol., no., pp.855-861, 20-24 Jun 1993 doi: 10.1109/PESC.1993.472021.

[46] Chwei-Sen Wang; Stielau, O.H.; Covic, G.A.; , "Design considerations for a contactless electric vehicle battery charger," Industrial Electronics, IEEE Transactions on , vol.52, no.5, pp. 1308- 1314, Oct. 2005 doi: 10.1109/TIE.2005.855672.

[47] Toepfer, C.B.; , "Charge! EVs power up for the long haul," Spectrum, IEEE , vol.35, no.11, pp.41-47, Nov 1998 doi: 10.1109/6.730519.

[48] Sakamoto, H.; Harada, K.; Washimiya, S.; Takehara, K.; Matsuo, Y.; Nakao, F.; , "Large air-gap coupler for inductive charger [for electric vehicles] ," Magnetics, IEEE Transactions on , vol.35, no.5, pp.3526-3528, Sep 1999 doi: 10.1109/20.800578.

[49] Singh, B.; Singh, B.N.; Chandra, A.; Al-Haddad, K.; Pandey, A.; Kothari, D.P.; , "A review of single-phase improved power quality AC-DC converters," Industrial Electronics, IEEE Transactions on , vol.50, no.5, pp. 962-981, Oct. 2003 doi: 10.1109/TIE.2003.817609.

[50] Singh, B.; Singh, B.N.; Chandra, A.; Al-Haddad, K.; Pandey, A.; Kothari, D.P.; , "A review of three-phase improved power quality AC-DC converters," Industrial Electronics, IEEE Transactions on , vol.51, no.3, pp. 641-660, June 2004 doi: 10.1109/TIE.2004.825341.

[51] Malinowski, M.; , "Sensorless control strategies for three-phase PWM rectifiers," Ph.D. Thesis, Warsaw Univ. of Technology, Poland, 2001.

[52] Ismail, E.H.; Erickson, R.; , "A new class of low-cost three-phase high-quality rectifiers with zero-voltage switching," Power Electronics, IEEE Transactions on , vol.12, no.4, pp.734-742, Jul 1997 doi: 10.1109/63.602569.

[53] Vlatkovic, V.; Borojevic, D.; Zhuang, X.; Lee, F.C.; , "Analysis and design of a zero-voltage switched, three-phase PWM rectifier with power factor correction," Power Electronics Specialists Conference, 1992. PESC '92 Record., 23rd Annual IEEE , vol., no., pp.1352-1360 vol.2, 29 Jun-3 Jul 1992 doi: 10.1109/PESC.1992.254720.

[54] Huang-Jen Chiu; Yu-Kang Lo; Hung-Chi Lee; Shih-Jen Cheng; Yeong-Chang Yan; Chung-Yi Lin; Tai-Hung Wang; Shann-Chyi Mou; , "A Single-Stage Soft-Switching Flyback Converter for Power-Factor-Correction Applications," Industrial Electronics, IEEE Transactions on , vol.57, no.6, pp.2187-2190, June 2010 doi: 10.1109/TIE.2009.2033622.

[55] Krishnamurthy, M.; Edrington, C.S.; Emadi, A.; Asadi, P.; Ehsani, M.; Fahimi, B.; , "Making the case for applications of switched reluctance motor technology in automotive products," Power Electronics, IEEE Transactions on , vol.21, no.3, pp.659-675, May 2006 doi: 10.1109/TPEL.2006.872371.

[56] Rahman, K.M.; Schulz, S.E.; , "High-performance fully digital switched reluctance motor controller for vehicle propulsion," Industry Applications, IEEE Transactions on , vol.38, no.4, pp. 1062- 1071, Jul/Aug 2002 doi: 10.1109/TIA.2002.800568.

[57] Hannoun, H.; Hilairet, M.; Marchand, C.; , "Design of an SRM Speed Control Strategy for a Wide Range of Operating Speeds," Industrial Electronics, IEEE Transactions on , vol.57, no.9, pp.2911-2921, Sept. 2010 doi: 10.1109/TIE.2009.2038396.

[58] Liang, J.; Lee, D.-H.; Xu, G.; Ahn, J.-W.; , "Analysis of Passive Boost Power Converter for Three-Phase SR Drive," Industrial Electronics, IEEE Transactions on , vol.57, no.9, pp.2961-2971, Sept. 2010 doi: 10.1109/TIE.2010.2040558.

[59] Jayabalan, R.; Fahimi, B.; Koenig, A.; Pekarek, S.; , "Applications of power electronics-based systems in vehicular technology: state-of-the-art and future trends," Power Electronics Specialists Conference, 2004. PESC 04. 2004 IEEE 35th Annual , vol.3, no., pp. 1887- 1894 Vol.3, 20-25 June 2004 doi: 10.1109/PESC.2004.1355405.

[60] Emadi, A.; Williamson, S.S.; Khaligh, A.; , "Power electronics intensive solutions for advanced electric, hybrid electric, and fuel cell vehicular power systems," Power Electronics, IEEE Transactions on , vol.21, no.3, pp.567-577, May 2006 doi: 10.1109/TPEL.2006.872378.

Appendix B

Paper II: An Isolated High Power Integrated Charger in Electrified Vehicle Applications

Saeid Haghbin, Sonja Lundmark, Mats Alaküla and Ola Carlson

Submitted to
the IEEE Transactions on Vehicular Technology, 2011

The layout has been revised.

Abstract

For vehicles using grid power to charge the battery, traction circuit components are not engaged during the charging time, so there is a possibility to use them in the charger circuit to have an on-board integrated charger. One solution of an isolated high power integrated charger is based on a special electrical machine with a double set of stator windings: By reconfiguration of the motor stator windings in the charging mode, a six-terminal machine is achieved. The so called motor/generator acts as an isolated three-phase power source after synchronization with the utility grid in the charging mode. This rotary three-phase isolated power source constitutes a three-phase boost rectifier (battery charger) with full utilization of the inverter. The motor windings are reconfigured by a relay-based switching device for the charging and traction modes. This paper presents the mathematical model of the motor/generator and explains the system functionality for the traction and charging modes. Further, the charger grid synchronization and charge control are described. Finally, simulation results are presented for a practically designed system with a traction power of 25 kW and with a possible charge power of 12.5 kW.

B.1 Introduction

The battery has an important role in the development of EVs and PHEVs. Its energy density, power density, charging time, lifetime, and cost are still behind practical applications and subject of research. The charging time and lifetime of the battery have a strong dependency on the characteristics of the battery charger [1] [2] [3] [4]. Several manufacturers are working worldwide on the development of various types of battery modules for electric and hybrid vehicles. However, the performance of battery modules depends not only on the design of modules, but also on how the modules are used and charged. In this sense, battery chargers play a critical role in the evolution of this technology.

An on-board battery charger is an interesting option for users since that allows them to charge their vehicles everywhere that a suitable power source is available. With requirements on galvanic isolation and 3-phase connection for high power charging the weight and cost of a separate on-board charging system becomes unrealistically high. If the traction and charging are not happening in the same time, it is possible to use the traction system components, like inverter and motor, in the charger system to have an integrated charging device with reduced weight, space and total cost. Several integrated chargers in vehicle applications have been reported by the academia or industry [5].

An innovative integrated charger was introduced in [8] which detail modeling and analysis of the proposed system is explained in this paper. Contrary to other solutions mentioned in [5], this is an isolated high power three-phase bi-directional integrated charger with unit power factor operation capability. Accordingly, an interior permanent magnet synchronous motor (IPMSM) was designed [6] with a special winding configuration with two functions: motor operation in traction mode and assistance of charging in the charging mode. Depending on the desired mode of operation the system hardware is reconfigured for the traction or charging operation. The traction-mode inverter acts like a rectifier in the charging mode.

In this paper system modes of operation in charging and traction is described first. Afterwards, the mathematical model of the IPMSM motor with double stator windings is presented. The grid synchronization and charging control are described also. Moreover, simulation results of the system for the charging mode will be presented.

B.2 Integrated Charger Based on a Special Motor Windings Configuration

Fig. B.1 shows a schematic diagram of a PHEV with a parallel configuration [4]. The electrical part includes the grid connected battery charger, battery, inverter, motor and control system. During charging time the vehicle is not driven and during driving time it is not intended to charge the battery pack except for regeneration at braking. However, it is possible to integrate both hardware to use the inverter and motor in the charger circuit to reduce the system components, space and weight which is equivalent to a cost reduction. This is what is referred to as an integrated charger in this paper.

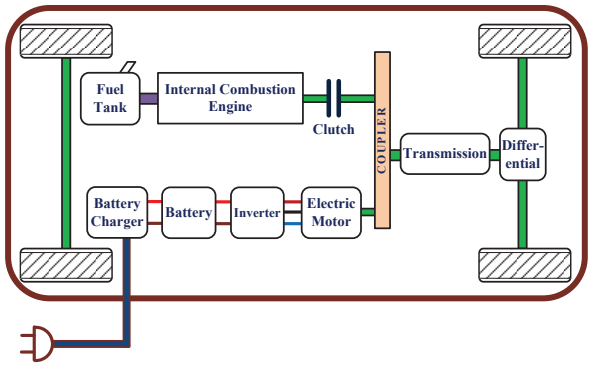

Figure B.1: Simplified schematic diagram of a PHEV.

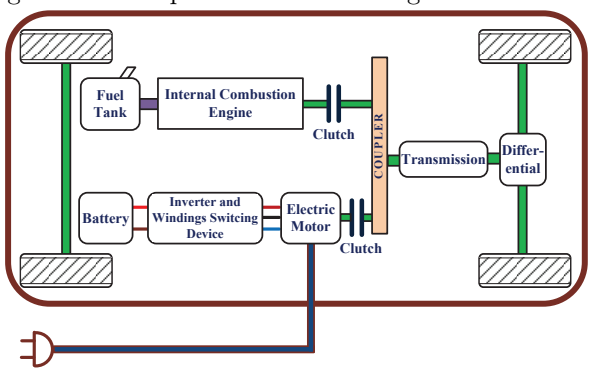

Figure B.2: Simplified schematic diagram of a PHEV using galvanic-isolated integrated charger.

The main idea [8] is to introduce a multi terminal device called motor/generator set to act like a motor in the traction mode and an isolated three-phase power source in the charging mode. The inverter can charge the battery by this power source as the three-phase boost rectifier assuming proper voltage levels are adopted. With this scheme the separate battery charger will be eliminated from the system. The inverter, motor with re-configured stator windings and a switching device (relay based for example) constitute the high power battery charger. The charging power is limited by the motor thermal limit and inverter limit that means it will be a high power charger in a typical PHEV. Fig. B.2 shows a simple schematic diagram of the proposed integrated charger. The motor/generator rotates at the synchronous speed, as shown in Fig. B.2, a second clutch is added to the system to disconnect the motor/generator from the transmission system during the charging.

B.2.1 The IPMSM Machine with Split Stator Windings

In a two-pole three-phase IPMSM there are three windings in the stator shifted 120 electrical degrees [7]. Assume that each phase winding is divided into two equivalent parts and moreover they are shifted symmetrically around the stator

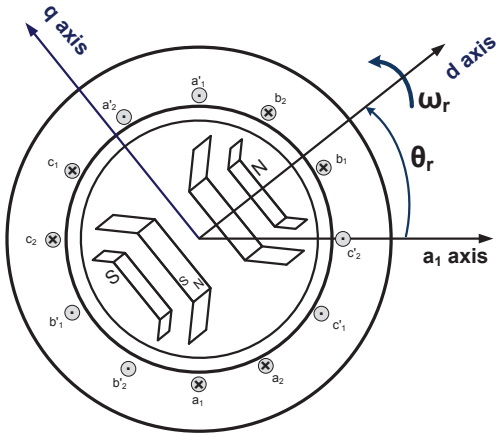

Figure B.3: Cross section of a IPMSM with split stator windings.

periphery. Basically there will be six windings inside the stator instead of three for a two pole machine. Fig. B.3 shows the cross section of the motor in this configuration. As is shown in this figure, there are six windings shifted 30 electrical degrees while the rotor has a two-pole configuration. Other number of pole pairs are also possible for the machine with this integrated charger.

These six windings can be considered as two sets of three-phase windings. Let say a_1, b_1 and c_1 are the first set of windings (the same as classical three-phase windings). a_2, b_2 and c_2 are the second set of three-phase windings. These two sets of three-phase windings are shifted 30 electrical degrees (angle between magnetic axis of $a_1'a_1$ and $a_2'a_2$) in this configuration.

B.2.2 Mathematical Model of the IPMSM with Six Stator Windings

A mathematical model of this machine is developed based on the assumption that all windings magnetomotive force and rotor magnets are sinusoidally distributed. To model this machine with six stator windings, the inductance matrix is first calculated (a 6×6 matrix including self inductances and mutual inductances). Afterwards, the flux and voltage equations are written to model the electrical system [7]. The derivative of the co-energy is calculated to obtain the developed electromagnetic torque. The order of system is eight that is six electrical equations and two mechanical equations in the phase domain. A special *abc* to *dq* transformation is used that is based on the Park transformation but an extended version for six variables instead of three. The system equations in the *dq* frame is reduced to a six order system while all sin and cos terms are eliminated from the equations.

The voltage equations for six windings can be described by the following equations:

$$v_{a_1} = r_s i_{a_1} + \frac{d}{dt}\psi_{a_1} \tag{B.1}$$

$$v_{b_1} = r_s i_{b_1} + \frac{d}{dt}\psi_{b_1} \tag{B.2}$$

$$v_{c_1} = r_s i_{c_1} + \frac{d}{dt}\psi_{c_1} \tag{B.3}$$

$$v_{a_2} = r_s i_{a_2} + \frac{d}{dt}\psi_{a_2} \tag{B.4}$$

$$v_{b_2} = r_s i_{b_2} + \frac{d}{dt}\psi_{b_2} \tag{B.5}$$

$$v_{c_2} = r_s i_{c_2} + \frac{d}{dt}\psi_{c_2} \tag{B.6}$$

where v_{a_1}, v_{b_1}, v_{c_1}, v_{a_2}, v_{b_2}, v_{c_2}, i_{a_1}, i_{b_1}, i_{c_1}, i_{a_2}, i_{b_2}, i_{c_2},ψ_{a_1}, ψ_{b_1}, ψ_{c_1}, ψ_{a_2}, ψ_{b_2}, ψ_{c_2} and r_s are windings voltages, currents, flux linkages and resistance.

The windings flux linkages can be expressed as:

$$\begin{aligned}\psi_{a_1} =& L_{a_1a_1}i_{a_1} + L_{a_1b_1}i_{b_1} + L_{a_1c_1}i_{c_1} + L_{a_1a_2}i_{a_2} + \\ & L_{a_1b_2}i_{b_2} + L_{a_1c_2}i_{c_2} + \psi_{pm}cos(\theta_r)\end{aligned} \tag{B.7}$$

$$\begin{aligned}\psi_{b_1} =& L_{b_1a_1}i_{a_1} + L_{b_1b_1}i_{b_1} + L_{b_1c_1}i_{c_1} + L_{b_1a_2}i_{a_2} + \\ & L_{b_1b_2}i_{b_2} + L_{b_1c_2}i_{c_2} + \psi_{pm}cos(\theta_r - \frac{2\pi}{3})\end{aligned} \tag{B.8}$$

$$\begin{aligned}\psi_{c_1} =& L_{c_1a_1}i_{a_1} + L_{c_1b_1}i_{b_1} + L_{c_1c_1}i_{c_1} + L_{c_1a_2}i_{a_2} + \\ & L_{c_1b_2}i_{b_2} + L_{c_1c_2}i_{c_2} + \psi_{pm}cos(\theta_r + \frac{2\pi}{3})\end{aligned} \tag{B.9}$$

$$\begin{aligned}\psi_{a_2} =& L_{a_2a_1}i_{a_1} + L_{a_2b_1}i_{b_1} + L_{a_2c_1}i_{c_1} + L_{a_2a_2}i_{a_2} + \\ & L_{a_2b_2}i_{b_2} + L_{a_2c_2}i_{c_2} + \psi_{pm}cos(\theta_r - \frac{\pi}{6})\end{aligned} \tag{B.10}$$

$$\begin{aligned}\psi_{b_2} =& L_{b_2a_1}i_{a_1} + L_{b_2b_1}i_{b_1} + L_{b_2c_1}i_{c_1} + L_{b_2a_2}i_{a_2} + \\ & L_{b_2b_2}i_{b_2} + L_{b_2c_2}i_{c_2} + \psi_{pm}cos(\theta_r - \frac{2\pi}{3} - \frac{\pi}{6})\end{aligned} \tag{B.11}$$

$$\begin{aligned}\psi_{c_2} =& L_{c_2a_1}i_{a_1} + L_{c_2b_1}i_{b_1} + L_{c_2c_1}i_{c_1} + L_{c_2a_2}i_{a_2} + \\ & L_{c_2b_2}i_{b_2} + L_{c_2c_2}i_{c_2} + \psi_{pm}cos(\theta_r + \frac{2\pi}{3} - \frac{\pi}{6})\end{aligned} \tag{B.12}$$

where $L_{a_1a_1}$, $L_{b_1b_1}$, $L_{c_1c_1}$, $L_{a_2a_2}$, $L_{b_2b_2}$ and $L_{c_2c_2}$ are windings self inductances. Moreover, $L_{a_1b_1}$, $L_{a_1c_1}$, $L_{a_1a_2}$, $L_{a_1b_2}$, $L_{a_1c_2}$, $L_{b_1bc_1}$, $L_{b_1c_2}$, $L_{c_1b_2}$, $L_{a_2b_2}$, $L_{a_2c_2}$ and $L_{b_2c_2}$ are windings mutual inductances. ψ_{pm} is the permanent magnet flux (the rotor flux) and θ_r is the angel between the rotor d axis and the magnetic axes of winding $a_1'a_1$.

The inductance values are calculates as [7]:

$$L_{a_1a_1} = L_{ls} + \bar{L}_m - L_{\Delta m}cos(2\theta_r) \tag{B.13}$$

$$L_{a_1b_1} = L_{b_1a_1} = -\frac{1}{2}\bar{L}_m - L_{\Delta m}cos2(\theta_r - \frac{\pi}{3}) \tag{B.14}$$

$$L_{a_1c_1} = L_{c_1a_1} = -\frac{1}{2}\bar{L}_m - L_{\Delta m}cos2(\theta_r + \frac{\pi}{3}) \tag{B.15}$$

$$L_{a_1a_2} = L_{a_2a_1} = \frac{\sqrt{3}}{2}\bar{L}_m - L_{\Delta m}cos2(\theta_r - \frac{\pi}{12}) \tag{B.16}$$

$$L_{a_1b_2} = L_{b_2a_1} = -\frac{\sqrt{3}}{2}\bar{L}_m - L_{\Delta m}cos2(\theta_r - \frac{\pi}{3} - \frac{\pi}{12}) \tag{B.17}$$

$$L_{a_1c_2} = L_{c_2a_1} = L_{\Delta m}sin2\theta_r = L_{\Delta m}cos2(\theta_r - \frac{\pi}{4}) \tag{B.18}$$

$$L_{b_1b_1} = L_{ls} + \bar{L}_m - L_{\Delta m}cos2(\theta_r - \frac{2\pi}{3}) \tag{B.19}$$

$$L_{b_1c_1} = L_{c_1b_1} = -\frac{1}{2}\bar{L}_m - L_{\Delta m}cos2\theta_r \tag{B.20}$$

$$L_{b_1a_2} = L_{a_2b_1} = L_{\Delta m}cos2(\theta_r + \frac{\pi}{12}) \tag{B.21}$$

$$L_{b_1b_2} = L_{b_2b_1} = \frac{\sqrt{3}}{2}\bar{L}_m + L_{\Delta m}cos2(\theta_r - \frac{\pi}{4}) \tag{B.22}$$

$$L_{b_1c_2} = L_{c_2b_1} = -\frac{\sqrt{3}}{2}\bar{L}_m - L_{\Delta m}cos2(\theta_r - \frac{\pi}{12}) \tag{B.23}$$

$$L_{c_1c_1} = L_{ls} + \bar{L}_m - L_{\Delta m}cos2(\theta_r + \frac{2\pi}{3}) \tag{B.24}$$

$$L_{c_1a_2} = L_{a_2c_1} = -\frac{\sqrt{3}}{2}\bar{L}_m - L_{\Delta m}cos2(\theta_r + \frac{\pi}{4}) \tag{B.25}$$

$$L_{c_1b_2} = L_{b_2c_1} = L_{\Delta m}cos2(\theta_r + \frac{5\pi}{12}) \tag{B.26}$$

$$L_{c_1c_2} = L_{c_2c_1} = \frac{\sqrt{3}}{2}\bar{L}_m + L_{\Delta m}cos2(\theta_r + \frac{\pi}{12}) \tag{B.27}$$

$$L_{a_2a_2} = L_{ls} + \bar{L}_m - L_{\Delta m}cos2(\theta_r - \frac{\pi}{6}) \tag{B.28}$$

$$L_{a_2b_2} = L_{b_2a_2} = -\frac{1}{2}\bar{L}_m - L_{\Delta m}cos2(\theta_r - \frac{\pi}{2}) \tag{B.29}$$

$$L_{a_2c_2} = L_{c_2a_2} = -\frac{1}{2}\bar{L}_m - L_{\Delta m}cos2(\theta_r + \frac{\pi}{6}) \tag{B.30}$$

$$L_{b_2b_2} = L_{ls} + \bar{L}_m - L_{\Delta m}cos2(\theta_r - \frac{2\pi}{3} - \frac{\pi}{6}) \tag{B.31}$$

$$L_{b_2c_2} = L_{c_2b_2} = -\frac{1}{2}\bar{L}_m - L_{\Delta m}cos2(\theta_r - \frac{\pi}{6}) \tag{B.32}$$

$$L_{c_2c_2} = L_{ls} + \bar{L}_m - L_{\Delta m}cos2(\theta_r + \frac{2\pi}{3} - \frac{\pi}{6}) \tag{B.33}$$

where $\bar{L}_m$, $L_{\Delta m}$ and L_{ls} are average value of magnetization inductance, half-amplitude of the sinusoidal variation of the magnetization inductance and the leakage inductance of each winding. It is assumed that all windings have the same number of turns.

If we define the vectors and matrixes for the inductances, currents, voltages, fluxes, and resistance as following:

$$\mathbf{L_s} = \begin{bmatrix} L_{a_1a_1} & L_{a_1b_1} & L_{a_1c_1} & L_{a_1a_2} & L_{a_1b_2} & L_{a_1c_2} \\ L_{b_1a_1} & L_{b_1b_1} & L_{b_1c_1} & L_{b_1a_2} & L_{b_1b_2} & L_{b_1c_2} \\ L_{c_1a_1} & L_{c_1b_1} & L_{c_1c_1} & L_{c_1a_2} & L_{c_1b_2} & L_{c_1c_2} \\ L_{a_2a_1} & L_{a_2b_1} & L_{a_2c_1} & L_{a_2a_2} & L_{a_2b_2} & L_{a_2c_2} \\ L_{b_2a_1} & L_{b_2b_1} & L_{b_2c_1} & L_{b_2a_2} & L_{b_2b_2} & L_{b_2c_2} \\ L_{c_2a_1} & L_{c_2b_1} & L_{c_2c_1} & L_{c_2a_2} & L_{c_2b_2} & L_{c_2c_2} \end{bmatrix},$$

$$\mathbf{i_s} = \begin{bmatrix} i_{a_1} & i_{b_1} & i_{c_1} & i_{a_2} & i_{b_2} & i_{c_2} \end{bmatrix}^T,$$

$$\mathbf{v_s} = \begin{bmatrix} v_{a_1} & v_{b_1} & v_{c_1} & v_{a_2} & v_{b_2} & v_{c_2} \end{bmatrix}^T,$$

$$\psi_\mathbf{s} = \begin{bmatrix} \psi_{a_1} & \psi_{b_1} & \psi_{c_1} & \psi_{a_2} & \psi_{b_2} & \psi_{c_2} \end{bmatrix}^T \text{ and}$$

$$\mathbf{R_s} = \begin{bmatrix} r_s & 0 & 0 & 0 & 0 & 0 \\ 0 & r_s & 0 & 0 & 0 & 0 \\ 0 & 0 & r_s & 0 & 0 & 0 \\ 0 & 0 & 0 & r_s & 0 & 0 \\ 0 & 0 & 0 & 0 & r_s & 0 \\ 0 & 0 & 0 & 0 & 0 & r_s \end{bmatrix}$$

the voltage and flux equations can be written as [7]:

$$\mathbf{v_s} = \mathbf{R_s i_s} + \frac{d}{dt}\psi_\mathbf{s}. \tag{B.34}$$

The developed electromagnetic torque in the machine can be calculated as [7]:

$$T_e = \frac{P}{2}(\frac{1}{2}\mathbf{i_s^T}\frac{\partial \mathbf{L_s}}{\partial \theta_r}\mathbf{i_s} + \mathbf{i_s^T}\frac{\partial \psi_\mathbf{pm}}{\partial \theta_r}) \tag{B.35}$$

where P is the machine number of poles. $\psi_\mathbf{pm}$ is stator winding fluxes due to rotor magnets. The mechanical dynamical equations describing the machine are:

$$\frac{d\omega_r}{dt} = \frac{P}{2J}(T_e - \frac{2B_m}{P}\omega_r - T_L) \tag{B.36}$$

$$\frac{d\theta_r}{dt} = \omega_r \tag{B.37}$$

where J, B_m, T_L and ω_r are the moment of inertia, viscous friction coefficient, load torque and speed of the machine.

To simplify the machine equations a special version of the Park transformation (it is called extended Park transformation here) is used to reduce the system order and remove all sinusoidal terms. The transformation matrix, $\mathbf{K_s}$, is applied to machine equations to transform them to the synchronous dq0 reference frame. This matrix is defined as:

$$\mathbf{K_s} = \frac{2}{3}\begin{bmatrix} cos\theta_r & cos(\theta_r - \frac{2\pi}{3}) & cos(\theta_r + \frac{2\pi}{3}) & \dots \\ -sin\theta_r & -sin(\theta_r - \frac{2\pi}{3}) & -sin(\theta_r + \frac{2\pi}{3}) & \dots \\ \frac{1}{2} & \frac{1}{2} & \frac{1}{2} & \dots \\ 0 & 0 & 0 & \dots \\ 0 & 0 & 0 & \dots \\ 0 & 0 & 0 & \dots \end{bmatrix}$$

$$\begin{bmatrix} 0 & 0 & 0 \\ 0 & 0 & 0 \\ 0 & 0 & 0 \\ cos(\theta_r - \frac{\pi}{6}) & cos(\theta_r - \frac{2\pi}{3} - \frac{\pi}{6}) & cos(\theta_r + \frac{2\pi}{3} - \frac{\pi}{6}) \\ -sin(\theta_r - \frac{\pi}{6}) & -sin(\theta_r - \frac{2\pi}{3} - \frac{\pi}{6}) & -sin(\theta_r + \frac{2\pi}{3} - \frac{\pi}{6}) \\ \frac{1}{2} & \frac{1}{2} & \frac{1}{2} \end{bmatrix}.$$

The inverse of the matrix $\mathbf{K_s}$,$\mathbf{K_s}^{-1}$, can be calculated as:

$$\mathbf{K_s^{-1}} = \begin{bmatrix} cos\theta_r & -sin\theta_r & 1 & ... \\ cos(\theta_r - \frac{2\pi}{3}) & -sin(\theta_r - \frac{2\pi}{3}) & 1 & ... \\ cos(\theta_r + \frac{2\pi}{3}) & -sin(\theta_r + \frac{2\pi}{3}) & 1 & ... \\ 0 & 0 & 0 & ... \\ 0 & 0 & 0 & ... \\ 0 & 0 & 0 & ... \end{bmatrix}$$

$$\begin{bmatrix} 0 & 0 & 0 \\ 0 & 0 & 0 \\ 0 & 0 & 0 \\ cos(\theta_r - \frac{\pi}{6}) & -sin(\theta_r - \frac{\pi}{6}) & 1 \\ cos(\theta_r - \frac{2\pi}{3} - \frac{\pi}{6}) & -sin(\theta_r - \frac{2\pi}{3} - \frac{\pi}{6}) & 1 \\ cos(\theta_r + \frac{2\pi}{3} - \frac{\pi}{6}) & -sin(\theta_r + \frac{2\pi}{3} - \frac{\pi}{6}) & 1 \end{bmatrix}.$$

By transforming the phase variables to the rotor reference frame by applying the transformation matrix $\mathbf{K_s}$, the machine equations will be simplified with reduced number of equations. In the rotor reference frame the variables are superscripted by letter r and are defined as:

$$\mathbf{i_s^r} = \begin{bmatrix} i_{d_1} & i_{q_1} & i_{0_1} & i_{d_2} & i_{q_2} & i_{0_2} \end{bmatrix}^T,$$

$$\mathbf{v_s^r} = \begin{bmatrix} v_{d_1} & v_{q_1} & v_{0_1} & v_{d_2} & v_{q_2} & v_{0_2} \end{bmatrix}^T \text{ and}$$

$$\psi_\mathbf{s}^\mathbf{r} = \begin{bmatrix} \psi_{d_1} & \psi_{q_1} & \psi_{0_1} & \psi_{d_2} & \psi_{q_2} & \psi_{0_2} \end{bmatrix}^T.$$

The indexes d, q and 0 denote the direct axis, quadrature axis and zero component of the variables. Moreover, there are two set of three-phase quantities that are denoted by the numbers 1 and 2 respectively. For example the voltage can be transformed from the abc domain to the dq domain by $\mathbf{v_s^r} = \mathbf{K_s v_s}$.

By transforming machine voltage, flux linkage and torque equations to the dq reference frame, the following equations describe the dynamical model:

$$v_{d_1} = r_s i_{d_1} + \frac{d}{dt}\psi_{d_1} - \omega_r \psi_{q_1} \tag{B.38}$$

$$v_{q_1} = r_s i_{q_1} + \frac{d}{dt}\psi_{q_1} + \omega_r \psi_{d_1} \tag{B.39}$$

$$v_{d_2} = r_s i_{d_2} + \frac{d}{dt}\psi_{d_2} - \omega_r \psi_{q_2} \tag{B.40}$$

$$v_{q_2} = r_s i_{q_2} + \frac{d}{dt}\psi_{q_2} + \omega_r \psi_{d_2} \tag{B.41}$$

$$\psi_{d_1} = L_d i_{d_1} + L_{md} i_{d_2} + \psi_{pm} \tag{B.42}$$

$$\psi_{q_1} = L_q i_{q_1} + L_{mq} i_{q_2} \tag{B.43}$$

$$\psi_{d_2} = L_{md} i_{d_1} + L_d i_{d_2} + \psi_{pm} \tag{B.44}$$

$$\psi_{q_2} = L_{mq} i_{q_1} + L_q i_{q_2} \tag{B.45}$$

where L_d, L_q, L_{md}, L_{mq} are direct and quadrature axis winding self and mutual inductances respectively. Moreover, $L_d = L_l + L_{md}$ and $L_q = L_l + L_{mq}$. It

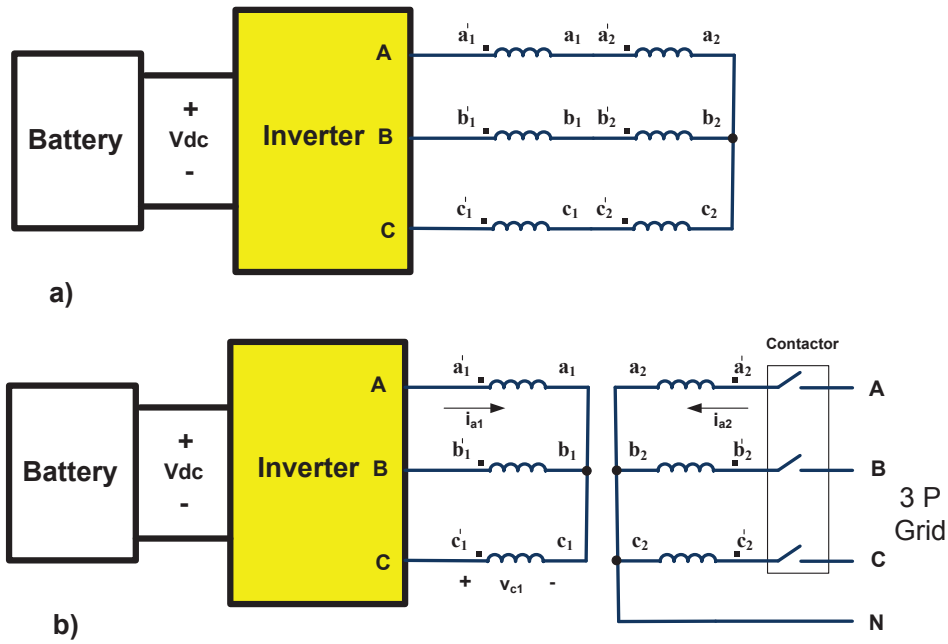

Figure B.4: System modes of operation: a) traction and b) charging.

is assumed that the zero components are zero due to symmetrical three-phase quantities.

The developed electromagnetic torque can be expressed as:

$$T_e = \frac{3}{2}\frac{P}{2}[\psi_{pm}(i_{q_1} + i_{q_2}) + (L_d - L_q)(i_{d_1} i_{q_1} + i_{d_1} i_{q_2} + i_{d_2} i_{q_1} + i_{d_2} i_{q_2}]. \quad \text{(B.46)}$$

B.3 System Modes of Operation: Traction and Charging

As mentioned before, the system has two modes of operation: traction and charging. In the traction mode, each two windings are connected to each other in series to constitute a three-phase winding set. These three windings can be connected to each other in Δ or Y to form a classical three-phase machine. Moreover, the motor is powered by the battery through the inverter. Fig. B.4.a shows the system diagram in this mode. Sensorless schemes for example can be employed to run the motor in the traction mode [9].

For the charging mode the system is reconfigured according to the scheme shown in Fig. B.4.b. A simple relay based device can re-connect the windings and a contactor is needed to connect the system to the utility grid.

If the machine would be kept in standstill as in [10], the magnetization current will be high due to the air-gap. So it is expected to have lower system efficiency depending on the air-gap length. However, if the machine rotates with the grid synchronous speed, the magnets will induce voltages in the inverter-side windings that emulates an isolated PM ac generator for the inverter. The

idea is thus to connect the machine to the grid via the grid-side three-phase windings, a_2, b_2 and c_2. These three windings can be used to run the machine as a classical motor. The inverter side windings, a_1, b_1 and c_1 will pick up the induced voltage due to the developed flux inside the machine (since they are located on the same pole-pair as are the grid-side windings). The inverter can use this isolated voltage source to charge the battery by the means of machine leakage inductances as the converter energy storage component (yielding three-phase boost converter).

To synchronize the machine to the grid, the inverter will run the motor by the means of the battery through the windings a_1, b_1 and c_1. The other windings are open circuited (contactor is open) but the induced voltage will be measured to be synchronized with the grid voltage. When the grid-side winding voltages are synchronized with the grid, the contactor will be closed and the grid voltage will be applied to the grid-side windings. Afterwards, the inverter will control the inverter side winding voltages to charge the battery which is called charge control here.

B.3.1 Motor/Generator Grid Synchronization

The vehicle must be parked while the engine and electric motor are turned off before charging. Then the machine windings are reconfigured by a switching device, like relay. Before connection to the grid, the clutch between the electric machine and mechanical transmission must be opened. The electric machine must be rotated at the synchronous speed and produce the same voltage as the grid does (both amplitude and phase) for the grid connection. Then the contactor is used to connect the grid-side windings to the grid. This process is called grid synchronization for the proposed integrated charger.

At first, the inverter-side windings are used to drive the motor by the means of the battery and proper inverter operation while the grid-side windings are open connected. Before closing the contactor, the dc link voltage, motor/genereator primary side currents and the rotor position/speed are measured to have a classical field oriented speed control of the IPM motor [11]. The position/speed can be estimated instead of using a sensor, but here for simplicity it is assumed that the position and speed signals are available.

Both grid-side winding voltages, and grid voltages are measured and transformed to the dq reference frame. Both voltage vectors magnitude and angle of the grid voltage and motor/generator grid-side windings should be equal as an index of synchronization. The magnitude of voltage is a function of the motor speed and flux (refer to motor/generator equations), so by controlling the flux, the voltage level can be adjusted. In a classical IPM motor usually the reference value for the d component of the machine is zero (for flux weakening operation this value will be modified), but at this scheme this value is used as a control parameter to change the induced voltage magnitude. The d component of the voltage is close to zero so the angle error is replaced by the voltage d components error $(v_{dg} - v_{d2})$ in the controller for the phase synchronization.

The motor/generator will rotate at the synchronous speed to meet the frequency synchronization requirement. So the speed reference will be $2\pi 50\ rad/sec$ for a grid with $50\ Hz$ frequency supply. Moreover, to match the voltage angles, a PI controller is used to adjust the motor/generator speed reference due to

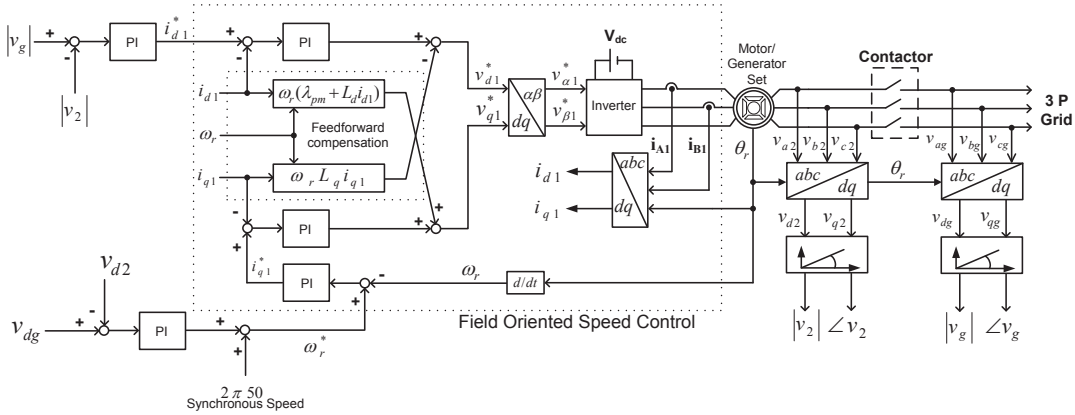

Figure B.5: Grid synchronization scheme of IPM motor/generator set.

the angle error signal. This speed reference will be tracked by the field oriented speed control part of the system. Fig. B.5 shows the schematic diagram of the control system in the synchronization phase.

When both voltage magnitude and angle error signals are small values within predefined bands, the motor/generator set is synchronized and the contactor is closed. Now the system is ready for the charge operation.

B.3.2 Battery Charge Control

Fig. B.6 shows a basic diagram of a three-phase boost converter. This scheme is very similar to the proposed integrated charger system. The voltage equations describing the converter in the dq reference frame are [12]:

$$u_{Ld} = Ri_{Ld} + L\frac{d}{dt}i_{Ld} - \omega L i_{Lq} + u_{Id} \tag{B.47}$$

$$u_{Lq} = Ri_{Lq} + L\frac{d}{dt}i_{Lq} + \omega L i_{Ld} + u_{Iq} \tag{B.48}$$

where u_{Ld}, u_{Lq}, u_{Id} and u_{Iq} are line and inverter dq voltage components respectively. R, L and ω are the resistance, inductance and source frequency also. i_{Ld} and i_{Lq} are d an q components of the line currents. The active and reactive power going to the converter from the grid can be written as [12]:

$$p = \frac{3}{2}(u_{Ld}i_{Ld} + u_{Lq}i_{Lq}) \tag{B.49}$$

$$q = \frac{3}{2}(u_{Lq}i_{Ld} - u_{Ld}i_{Lq}) \tag{B.50}$$

Different control strategies have been proposed for this three-phase boost converter operation [12]. If $i_{Lq} = 0$ and $u_{Lq} = 0$ in the equations above, then the active and reactive power will be simplified to $p = \frac{3}{2}u_{Ld}i_{Ld}$ and $q = 0$. Based on these equations, the feedforward current control method is one of the widely used schemes for power control. Fig. B.7 shows the basic diagram of

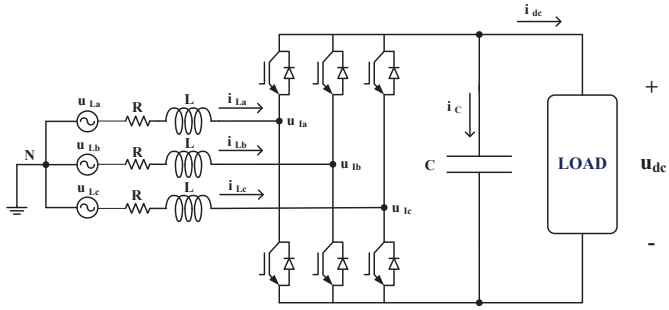

Figure B.6: The power stage of the three-phase boost converter.

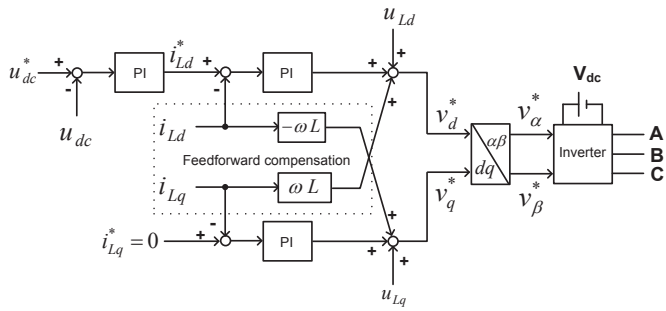

Figure B.7: Decoupled current control of the three-phase boost converter.

the controller. The dq current control and feedforward compensation are main parts of this decoupled control scheme. The controller has an outer loop for the dc bus voltage regulation. This controller output sets the reference value for the d component of the current that will control the power. Two independent PI controllers have been used to generate reference values for the converter, u_α and u_β. The feedforward terms are added to this reference values to the decoupled system in d and q axes to improve the system performance.

At grid synchronization the contactor is closed and the grid voltages are applied to the grid-side motor/generator windings. Thus it is a constant voltage source over the windings. The motor/generator voltage equations can be written as below after some mathematical manipulations:

$$v_{d_2} = r_s(i_{d_2} - i_{d_1}) + L_l \frac{d}{dt}(i_{d_2} - i_{d_1}) - \omega_r L_l (i_{d_2} - i_{d_1}) + v_{d_1} \tag{B.51}$$

$$v_{q_2} = r_s(i_{q_2} - i_{q_1}) + L_l \frac{d}{dt}(i_{q_2} - i_{q_1}) + \omega_r L_l (i_{q_2} - i_{q_1}) + v_{q_1}. \tag{B.52}$$

The equations above are very similar to equations B.47 and B.48 that describe the classical three-phase boost converter. The difference is that currents are replaced by the difference of the primary and secondary winding currents. So the same control strategy is adopted with small modifications (adjusting the currents by the current differences). Moreover, due to existence of a battery in the dc link, the dc bus voltage controller is eliminated from the scheme. Fig. B.8 shows the control system diagram in charging mode. When the system

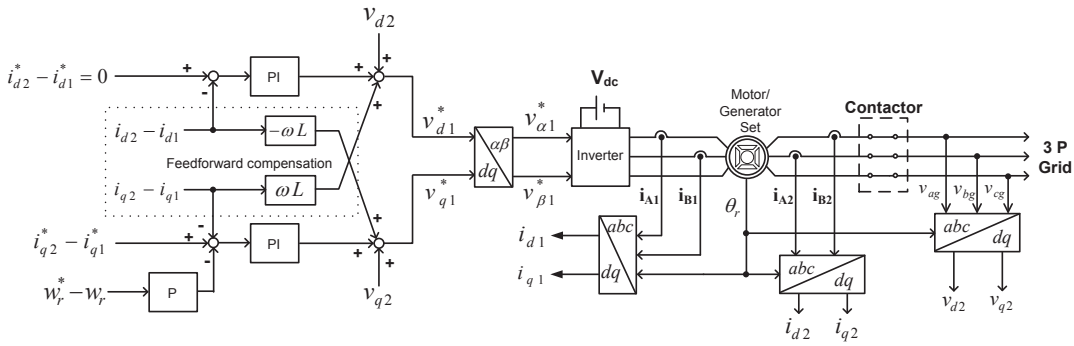

Figure B.8: Block diagram for the charge control of proposed integrated charger.

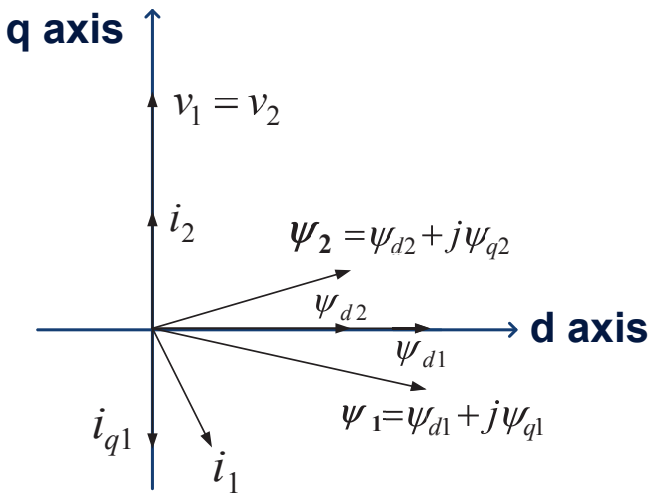

Figure B.9: Motor/generator vector diagram in the charging mode.

start to charge there are some mechanical oscillations in the rotor. The rotor speed error (the difference between the synchronous speed and true speed) is added to the controller by the means a proportional controller to reduce these oscillations.

With assumption of the symmetrical three-phase currents and voltages for the inverter-side and grid-side windings, each three-phase quantity can be represented by a classical two-dimensional vector with the extended dq transformation (there is no coupling in the matrix transformation between the two systems). Fig. B.9 shows the motor/generator vector diagram in steady state operation for the charging mode (assuming that controllers are tuned). The grid voltage is in the q direction and the grid current just has a q component to achieve unit power factor operation from the grid point of view. The inverter-side current is in opposite direction to the grid side current. Further there is a small d component current on the inverter side to adjust the machine voltage

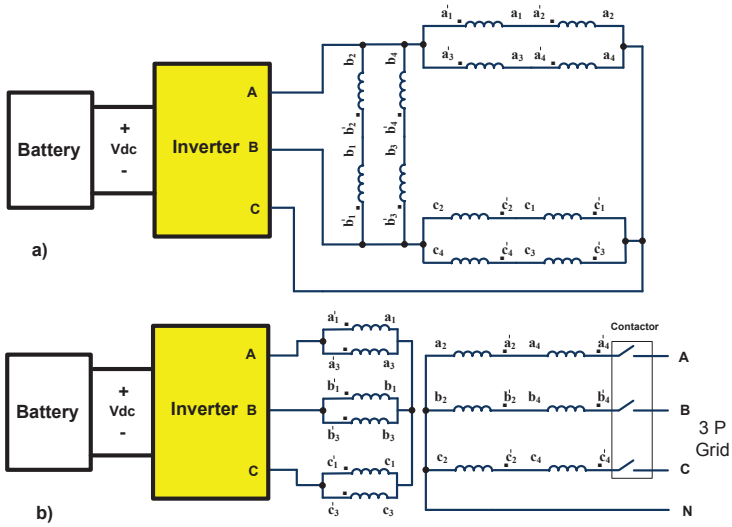

Figure B.10: 25 kW system modes of operation: a) traction and b) charging.

level (proportional to speed and machine flux).

The system has a bidirectional power flow capability that is inherent in the system because of the bidirectional operation of the three-phase inverter. Moreover, by changing the set point of the d component of the current, there is a possibility of production/generation of the reactive power also. The system power limitation is mainly a thermal limitation of the machine in the classical vehicle drive systems. Half of the machine's full power can be used in the charging mode (the converter withstands this power level because it is designed for machine full power operation).

B.4 System Design and Simulation Results

A 4 pole IPM machine is designed and optimized for a 25 kW traction system with a possibility to reconnect the windings for charging [6]. Fig. B.10.a shows the windings configuration (in delta) in the traction mode. The dc bus voltage (battery voltage) is 400 Vdc in this case. The machine base speed is 1500 rpm while the maximum speed is 6000 rpm. For the charging mode, the windings are re-arranged according to Fig. B.10.b. The charge power is limited to 12.5 kW due to the machine thermal limit. The motor parameters are shown in Table B.1. The whole system has been simulated by the use of Matlab/Simulink software based on the before mentioned system equations. The ideal converter is used in the simulation (no PWM or SVM is used for the inverter).

Before simulation starts, it is assumed that the system is reconfigured for the charging operation but the grid contactor is open. The charging process starts with that the inverter starts to rotate the motor by the means of the battery and inverter side motor windings. The motor will then rotate at the grid synchronous speed. The motor voltages and grid voltages are compared

Table B.1: IPM MOTOR PARAMETRS.

Rated power (kW)	25
Rated line voltage (V)	270
Rated phase current (A)	30
Rated speed(rev/min)	1500
No of poles	4
Permanent magnet flux (Wb)	0.6
Stator resistance (Ohm)	0.45
d axis inductance (mH)	12
q axis inductance (mH)	42
Inertia (Kg.m2)	0.1
Viscous friction coefficient (Nms/rad)	0.002

to each other in the $\alpha\beta$ reference frame frame in order to synchronize the grid-side winding voltages to the grid voltage. After 20 seconds the synchronization will be finished (it can be faster) and the contactor is closed. For 5 seconds the system will stay synchronized and then the charge control is started. So the charge control is started after 25 seconds.

Fig. B.11 shows the power from the grid to the charger systems. The system efficiency is around 89%. However, the machine iron losses and inverter losses are neglected in this simulation. The power is negative before the start of the charging since the inverter is powering the system through the battery. Moreover, the three-phase grid currents are shown in Fig. B.12. The unit power factor operation is feasible with aforementioned controller as is shown in Fig. B.13. The rotor electrical speed is shown in Fig. B.14. There are some oscillations in the rotor that the controller adjusts. Fig. B.15 shows the developed electromagnetic torque in the machine that is negligible compared to the machine rated torque in the traction mode(less than 1%).

B.5 Conclusion

It is thoroughly explained how it is possible to use the electric drive system components in a plug-in vehicle for charging purpose, with charging power restricted to half the traction power. The electric motor stator windings are re-configured for the traction and charging modes by the means of a relay-based switching device which together with a clutch are the only extra components needed to yield a very cost-effective and compact on-board three-phase isolated charger with unit power factor capability. The mathematical model of the electric machine in charging mode is presented in detail. Also, the system functional description and controllers are explained for the grid synchronization and charge control. To verify the system operation for the modeled integrated charger, simulation results for a practically designed system are presented, showing that system has high efficiency. The machine is rotating in the charging mode with a zero torque reference and the simulated resulting torque ripple is found to be less than 1% of rated torque.

Acknowledgment

The authors would like to thank Swedish Hybrid Vehicle Center (SHC) for financing the project and support.

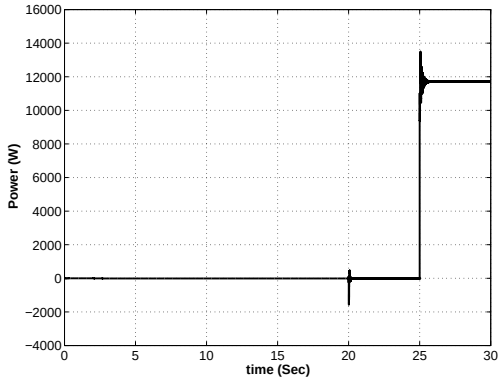

Figure B.11: Grid power to the charger system.

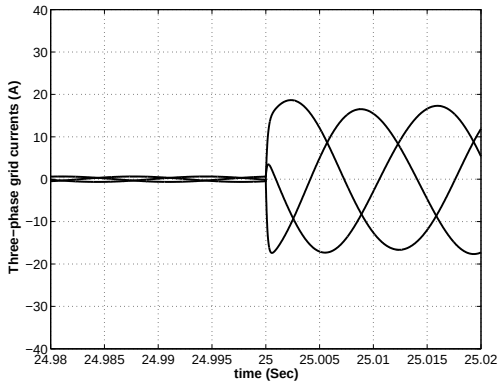

Figure B.12: Grid side windings currents.

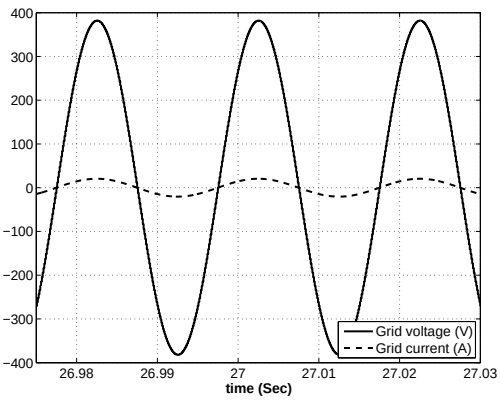

Figure B.13: Grid side phase A voltage and current: unit power factor operation.

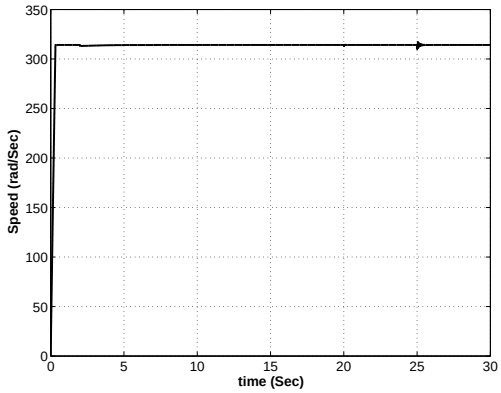

Figure B.14: Electrical speed of the motor/generator.

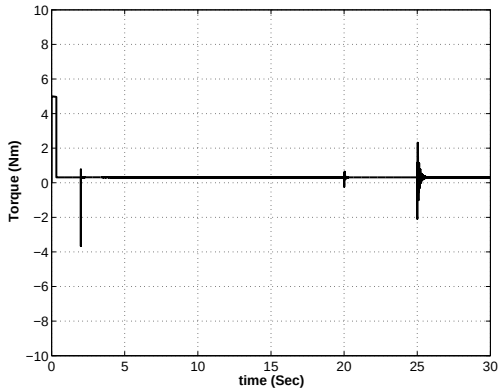

Figure B.15: Machine torque in the charging mode.

References

[1] I.A. Khan, "Battery chargers for electric and hybrid vehicles," Power Electronics in Transportation, Proceedings, 20-21 Oct. 1994, Page(s): 103-112.

[2] J.G. Hayes, "Battery charging systems for electric vehicles, " IEE Colloquium on Electric Vehicles - A Technology Roadmap for the Future, 5 May 1998, pp. 4/1-4/8.

[3] C.C. Chan, and K.T. Chau, "An overview of power electronics in electric vehicles," IEEE Transaction on Industrial Electronics, Vol. 44, Issue 1, Page(s): 3-13, Feb. 1997.

[4] A. Emadi, Joo Lee Young, and Rajashekara Kaushik , "Power electronics and motor Drives in Electric, Hybrid Electric, and Plug-In Hybrid Electric Vehicles," IEEE Transactions on Industrial Electronics, Vol. 55, No.6, June 2008.

[5] Saeid Haghbin, Kashif Khan, Sonja Lundmark, Mats Alakula, Ola Carlson, Mats Leksell and Oskar Wallmark, "Integrated Chargers for EVs and PHEVs: Examples and New Solutions," in International Conference on Electrical Machines (ICEM) proceedings, 2010, Italy.

[6] Kashif Khan, Saeid Haghbin, Mats Leksell and Oskar Wallmark, "Design and Performance Analysis of Permanent-Magnet Assisted Synchronous Reluctance Machines for Integrated Charger," in International Conference on Electrical Machines (ICEM) proceedings, 2010, Italy.

[7] Sergey Edward Lyshevski, "Electromechanical Systems, Electric Machines, and Applied Mechatronics," CRC Press, 1999.

[8] Saeid Haghbin, Mats Alakula, Kashif Khan, Sonja Lundmark, Mats Leksell, Oskar Wallmark and Ola Carlson, "An Integrated Charger for Plug-in Hybrid Electric Vehicles Based on a Special Interior Permanent Magnet Motor," in Vehicle Power and Propulsion Conference (VPPC) Proceedings, 2010, France.

[9] Peter Vas, "Sensorless vector and direct torque control," Oxford Press, 1998.

[10] F. Lacressonniere and B. Cassoret, "Converter used as a battery charger and a motor speed controller in an industrial truck," European Conference on Power Electronics and Applications, 2005.

[11] Bimal K. Bose, "Modern power electronics and ac drives," Prentice Hall, 2001.

[12] M. Malinowski, "Sensorless control strategies for three-phase PWM rectifiers," Ph.D. Thesis, Warsaw Univ. of Technology, Poland, 2001.

Appendix C

Paper III: Performance of a Direct Torque Controlled IPM Drive System in the Low Speed Region

Saeid Haghbin, Sonja Lundmark and Ola Carlson

Published in
Proceedings of IEEE International Symposium on Idustrial Electronics (ISIE), Bari, Iatly, July 2010

The layout has been revised.

Abstract

High power density, high speed operation, high efficiency and wide speed range made the interior permanent magnet (IPM) synchronous motors an interesting choice for ac drive systems. Different control strategies have been proposed to reach a high performance drive system. Direct torque control (DTC) is one of these widely used methods which has fast torque dynamic and a simple structure. Different motor, inverter and controller parameters affect the drive system performance in this scheme. The drive system performance is investigated for four possible inverter switching patterns in terms of the torque ripple, stator current ripple, flux ripple and inverter switching frequency in the low speed region. The results show that the switching pattern in which zero voltage is applied to reduce the torque has better performance compared to the other switching patterns. The analytic solution is provided to quantify the effects of the inverter zero voltage vector on the flux and torque of the machine and how they change when the speed varies.

C.1 Introduction

The overall design process of a modern high performance cost effective drive system is still a complex task. Motor, inverter and controller are the main important parts of a drive system. They should be considered as one package when the whole system is designed. The IPM synchronous motors have recently gained attention by researches for their special features like high power to volume density, wide speed operation range, high speed operation range (robust mechanical structure due to buried magnets inside the rotor) and high efficiency (ideally there is no rotor losses in this machine) [1-3]. Different control methods have been proposed for IPM machines to achieve a high performance adjustable-speed drive system [4]. Sensorless drive systems have become more and more popular as a consequence of sensors price and difficulties [5].

Direct torque control method first introduced by Takahashi [6] and Depenbrock [7] gained a lot of attentions thanks to its simple structure and fast torque dynamics. It was considered as an alternative to the field oriented control (FOC) method by ABB [8]. In the DTC method, six non-zero and two zero voltage vectors generated by the inverter are selected to keep the motor flux and torque within the limits of two hysteresis bands [9]. The DTC method has been widely studied for induction machines. For the induction machines there are four different switching patterns for the selection of the inverter voltage vector [10]. Each switching method affects the drive system performance [11]. The same concept is applied to the IPM synchronous machine [5], so most of the methods developed for DTC based induction motor drive systems can be applied for the DTC based IPM synchronous motor drives.

At low speeds, the stator voltage drop can't be neglected compared to the back-emf so the copper losses will be high compared to the air-gap power (back-emf multiplied by the current) so the system performance will be low.

The purpose of this paper is to investigate the impact of different inverter switching patterns on the performance of a DTC based IPM drive system in terms of the torque ripple, flux ripple, current ripple and inverter switching frequency at low speeds. Applying a zero voltage vector by the inverter has an important role on the overall drive system performance that will be addressed in the sequel. The machine equations are solved for the inverter zero voltage and an analytical solution for the flux trajectory and torque is provided to quantify the machine behavior. The drive system is simulated by the use of Matlab/Simulink package. The simulation results have been used to compare the flux ripple, stator current ripple, torque ripple and inverter switching frequency for each inverter switching algorithm. Moreover, the flux trajectory and developed torque have been presented as the simulation result and compared with the analytical solutions. The results show that when a zero voltage vector is applied to the machine by the inverter, the motor torque will be reduced regardless of the speed.

C.1.1 Dynamic Model of an IPM

The well-known d-q model of AC machines (in the rotor reference frame) is widely used for simulation purposes. The stator voltage equations for the d

and q components are:

$$u_d = Ri_d + L_d\frac{d}{dt}i_d - \omega_r\psi_q \tag{C.1}$$

$$u_q = Ri_q + L_q\frac{d}{dt}i_q + \omega_r\psi_d \tag{C.2}$$

where R is the stator winding resistance,L_d and L_q are direct and quadrature axis winding self inductances and ω_r is the rotor angular speed. ψ_d and ψ_q are the stator components of the flux. The d and q axis components of the flux can be written as:

$$\psi_d = \psi_{pm} + L_d i_d \tag{C.3}$$

$$\psi_q = L_q i_q \tag{C.4}$$

where ψ_{pm} is the permanent magnet flux. The developed electromagnetic torque can be expressed as:

$$T_e = \frac{3}{2}P[\psi_{pm}i_q + (L_d - L_q)i_d i_q] \tag{C.5}$$

where P is the number of pole pairs of the machine.

C.1.2 The Drive System Diagram

Fig. C.1 shows the block diagram of a IPM synchronous motor drive system based on the DTC method. During each sample interval the stator currents, i_A and i_B, are measured along with the dc bus voltage V_{dc}. Using the inverter switching states ($S_A S_B S_C$), the stator voltage and current vector components in the stationary reference frame can be calculated as [9]:

$$u_\alpha = \frac{2}{3}V_{dc}(S_A - \frac{S_A + S_B}{2}) \tag{C.6}$$

$$u_\beta = \frac{1}{\sqrt{3}}V_{dc}(S_B - S_C) \tag{C.7}$$

$$i_\alpha = i_A \tag{C.8}$$

$$i_\beta = \frac{i_A + 2i_B}{\sqrt{3}} \tag{C.9}$$

where u_α, u_β, i_α and i_β are α and β components of the stator voltage and current in the stationary reference frame.

The α and β components of the stator flux, ψ_α and ψ_β, can be obtained by the integration of the stator voltage minus the voltage drop in the stator resistance as:

$$\psi_\alpha = \int_0^t (u_\alpha - Ri_\alpha)dt + \psi_{\alpha|t=0} \tag{C.10}$$

$$\psi_\beta = \int_0^t (u_\beta - Ri_\beta)dt + \psi_{\beta|t=0}. \tag{C.11}$$

The electromagnetic torque, T_e, can be written in terms of quantities in the stationary reference frame as:

$$T_e = \frac{3}{2}P(\psi_\alpha i_\beta - \psi_\beta i_\alpha). \tag{C.12}$$

This equation is used in the drive system to estimate the developed electromagnetic torque [12]. The stator flux vector magnitude and phase are given by:

$$|\overline{\psi}_s| = \sqrt{\psi_\alpha^2 + \psi_\beta^2} \tag{C.13}$$

$$\angle\overline{\psi}_s = \arctan(\frac{\psi_\beta}{\psi_\alpha}). \tag{C.14}$$

As shown in Fig. C.1, estimated values of the stator flux vector magnitude, $|\overline{\psi}_s|$, and the electromagnetic torque, T_e, are compared with their reference values. Afterward, the errors are provided to the flux and torque hysteresis controllers. The goal of the control system is to limit the flux and torque within the hysteresis bands around their reference values. By using the torque error, flux error and stator flux position the control can be done by applying a proper inverter voltage.

For a three phase inverter, there are 6 power switches. It is not possible to turn on the upper and lower switches in a leg simultaneously. So there are 8 possible switching configurations where each state defines a voltage space vector. Fig. C.2 shows six non-zero inverter voltage space vectors (there are two zero voltage vectors, $\overline{u}_7$ and $\overline{u}_8$, that are not shown in this figure). Moreover the $\alpha\beta$ plane can be divided into 6 sectors (k=1, 2, 3, 4, 5 and 6) in which the controller needs to know in what sector the stator flux is located. If two level hysteresis controllers are used for the flux and torque control, there will be four switching strategies for the selection of the appropriate stator voltage vector (these possible switching strategies are proposed for the DTC of induction motors originally). Assume that the stator flux vector is located in sector k, then these four switching strategies are listed in Table C.1 [13]. Effects of the applied voltage vector on the motor flux and torque are summarized in Table C.1 as well. For the DTC system based on the IPM synchronous motor mainly solution A and D are used [14].

Assume that the flux is located in sector k; then, to increase the torque the voltage vectors $\overline{u}_{k+1}$ or $\overline{u}_{k+2}$ will be applied (depending on if the flux increases or decreases, one of the two voltage vectors will be selected). Different voltage vectors can be applied to decrease the torque in different switching possibilities. $\overline{u}_k$, $\overline{u}_{k-1}$, $\overline{u}_{k-2}$, $\overline{u}_{k+3}$, $\overline{u}_7$ and $\overline{u}_8$ can be applied according to Table C.1. As is seen in Table C.1, different switching patterns are only different in the torque decrement case, regardless of the flux increase or decrease demand in the motor. To decrease the torque, the simplest way is applying a zero voltage (solution A). The main difference between switching algorithms is in applying the zero vector or non-zero vector to decrease the torque. The motor current ripple, torque ripple and inverter switching frequency will vary for each switching strategy. This will affect the whole drive system performance for each switching method.

C.1.3 The Drive System Simulation

The whole drive system has been simulated by the use of Matlab/Simulink to study the drive system performance. The motor parameters were selected according to the motor model in [15] and are shown in Table C.2. The controller

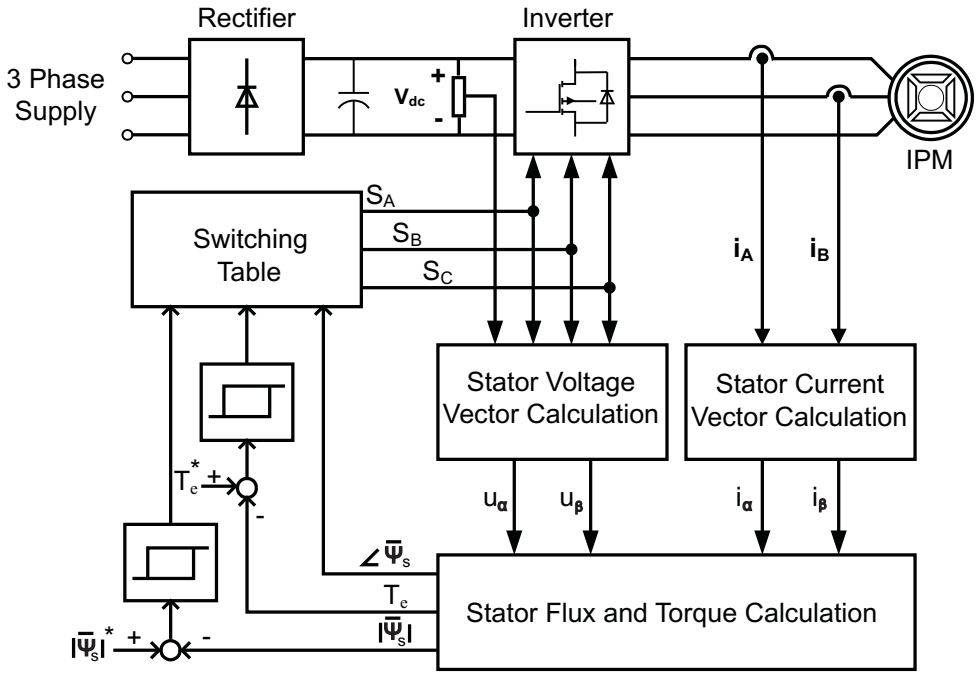

Figure C.1: Block diagram of the direct torque control of IPM synchronous motor.

parameters like sampling frequency, torque reference value, flux reference value and hysteresis band values for the flux and torque have considerable effects on the drive system performance. To investigate the impact of the inverter switching algorithm on the drive system performance, the controller parameters are kept the same for all switching patterns according to Table C.3.

C.2 Impact of Switching Pattern on the Drive System Performance

To evaluate the drive system performance at low speed (100 rpm in this case according to Table C.3 for different inverter switching algorithms according to Table C.1, the motor torque ripple, stator current ripple, stator flux ripple and inverter switching frequency have been considered. Using the same motor, controller and load parameters, simulations have been conducted for different inverter switching patterns. The normalized torque ripple, normalized stator current ripple, normalized stator flux ripple and average inverter switching frequency have been determined. thus, after removing the average part of the signals (torque, magnitude of the stator current and flux vectors), the root mean square (rms) values are calculated. Moreover, the values are normalized by dividing with the related average values. The results are presented in Table C.4.

As is presented in Table C.4, the torque ripple and average inverter switching frequency are lower in solution A compared to the other switching patterns.

Table C.1: SWITCHING STRATEGIES FOR DTC SYSTEM.

	$T_e \uparrow \lvert\overline{\psi}_s\rvert \uparrow$	$T_e \uparrow \lvert\overline{\psi}_s\rvert \downarrow$	$T_e \downarrow \lvert\overline{\psi}_s\rvert \uparrow$	$T_e \downarrow \lvert\overline{\psi}_s\rvert \downarrow$
Solution A	$\overline{u}_{k+1}$	$\overline{u}_{k+2}$	$\overline{u}_7$,$\overline{u}_8$	$\overline{u}_7$,$\overline{u}_8$
Solution B	$\overline{u}_{k+1}$	$\overline{u}_{k+2}$	$\overline{u}_k$	$\overline{u}_7$,$\overline{u}_8$
Solution C	$\overline{u}_{k+1}$	$\overline{u}_{k+2}$	$\overline{u}_k$	$\overline{u}_{k+3}$
Solution D	$\overline{u}_{k+1}$	$\overline{u}_{k+2}$	$\overline{u}_{k-1}$	$\overline{u}_{k-2}$

Table C.2: PARAMETERS OF SYNCHRONOUS RELUCTANCE MOTOR.

Rated power (kW)	2.2
Rated line voltage (V)	380
Rated current (A)	4.1
Rated speed(rev/min)	1750
No of poles	6
Permanent magnet flux (Wb)	0.48
Stator resistance (Ohm)	3.3
d axis inductance (mH)	42
q axis inductance (mH)	57
Inertia (Kg.m2)	0.01
Viscous friction coefficient (Nms/rad)	0.002

Table C.3: CONTROLLER PARAMETERS OF DRIVE SYSTEM.

Reference torque (N-m)	13
Reference flux (Wb)	0.5
Torque hysteresis upper band (N-m)	14
Torque hysteresis lower band (N-m)	12
Flux hysteresis upper band (Wb)	0.55
Flux hysteresis lower band (Wb)	0.45
DC Link voltage (V)	510
Motor steady state speed (rev/min)	100
Sampling frequency (kHz)	20

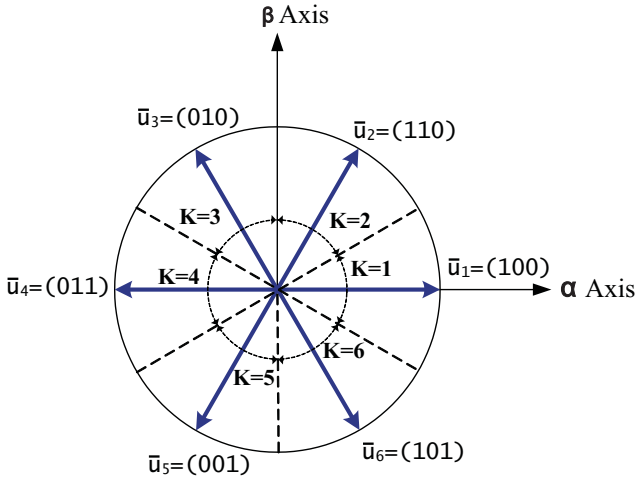

Figure C.2: Inverter voltage space vectors.

The reason for this is explained later in this section. For solution D, the inverter switching frequency is the highest, making inverter loss higher than those of the other switching algorithms. Thus, high values of the torque ripple and inverter switching frequency make this solution (solution D) an unfavorable choice for the drive system at low speeds. The drive system with the switching pattern A has better performance compared to the other methods.

To show high frequency effects, the frequency spectrum of stator current ripple is shown in Fig. C.3 for the four different switching patterns. As can be seen in this figure, the waveform corresponding to solution D shows the lowest harmonics. This is related to the high switching frequency of the inverter producing a more symmetric waveform, especially compared to solution A that applies zero voltage vector in both flux increase and decrease cases.

To explain the situation it is useful to approach the torque control process in terms of rotor reference frame quantities. The developed electromagnetic torque in an IPM synchronous motor in terms of stator and rotor fluxes in the rotor reference frame can be expressed as [14]:

$$T_e = \frac{3P|\overline{\psi}_s|}{8L_dL_q}[2\psi_{pm}L_q \sin\delta - |\overline{\psi}_s|(L_q - L_d)\sin 2\delta] \tag{C.15}$$

where δ is the load angle, the angle between the stator and rotor flux linkage vectors (Fig. C.4). The torque is controlled by regulating the amplitude of the stator flux and its angle with respect to the rotor flux. As expressed in equation C.15 the torque is sensitive to the angle variations. So it is possible to rapidly change the torque by changing the angle δ even with fixed magnitude of the stator flux vector. As mentioned above when a zero voltage is applied the torque has lower ripple compared to the torque ripple when a non-zero voltage vector is applied by the inverter. In other words, the torque has a lower slope when a zero voltage vector is applied to the motor compared to the case when a non-zero voltage vector is applied at low speeds. The reason is that when a non-zero voltage is applied, the flux will change more rapidly

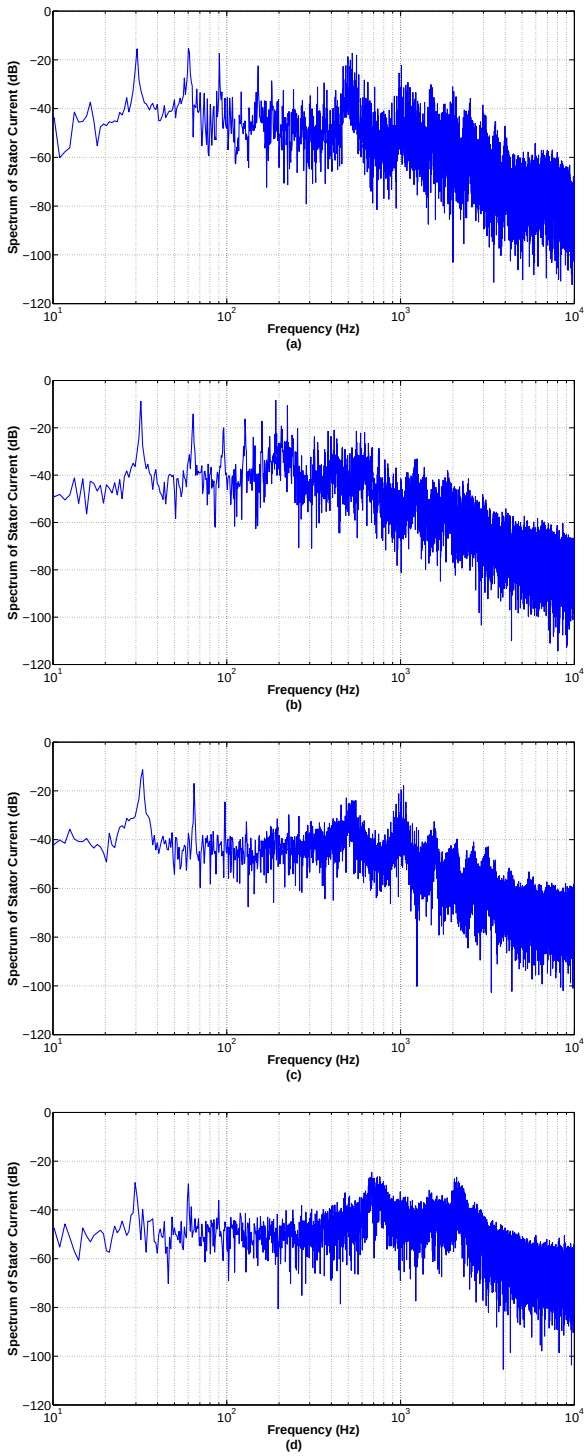

Figure C.3: Stator current ripple frequency spectrum for different switching patterns: (a) solution A, (b): solution B, (c): solution C and (d): solution D.

Table C.4: IMPACT OF SWITCHING ALGORITHM ON THE DRIVE SYSTEM PERFORMANCE.

Switching algorithm	Normalized torque ripple (%)	Normalized stator current ripple (%)	Normalized stator flux ripple (%)	Inverter switching frequency [kHz]
Solution A	5.31	6.81	7.54	0.35
Solution B	11.15	10.36	7.50	0.27
Solution C	10.11	7.81	8.91	1.46
Solution D	8.84	7.48	7.57	2.47

and the load angle will change rapidly compared to the situation when a zero voltage vector is applied [16]. Fig. C.5 shows the torque waveform for the inverter switching pattern A and D. For a torque decrement in solution D, by applying a non-zero vector the torque sharply decreases. In solution A, by applying a zero vector, the torque decreases smoothly which means that the switching frequency will be lower in solution A compared to solution D.

C.3 Impact of the Zero Voltage Vector on the IPM Motor Flux and Torque: Analytical Solution

Simulation results show that applying a zero-voltage vector will reduce the torque (solution A) and the torque will have lower ripple compared to other switching algorithms. More detail analysis is provided in this section to quantify machine flux trajectory and torque by solving the machine equations. During each sampling period the speed of the machine is assumed to be constant. The machine state-space equations in the rotor reference frame with zero voltage can be written as:

$$\begin{bmatrix} \dot{\psi}_d \\ \dot{\psi}_q \end{bmatrix} = \begin{bmatrix} -\frac{R}{L_d} & \omega_r \\ -\omega_r & -\frac{R}{L_q} \end{bmatrix} \begin{bmatrix} \psi_d \\ \psi_q \end{bmatrix} + \begin{bmatrix} \frac{R}{L_d} \\ 0 \end{bmatrix} \psi_{pm}. \tag{C.16}$$

If we assume that the speed is constant then this system will be a time-invariant linear system. The state solutions are [17]:

$$\begin{bmatrix} \psi_d \\ \psi_q \end{bmatrix} = e^{At} \begin{bmatrix} \psi_{d0} \\ \psi_{q0} \end{bmatrix} + e^{At} \int_0^t e^{-A\sigma} \begin{bmatrix} \frac{R}{L_d} \\ 0 \end{bmatrix} \psi_{pm} d\sigma \tag{C.17}$$

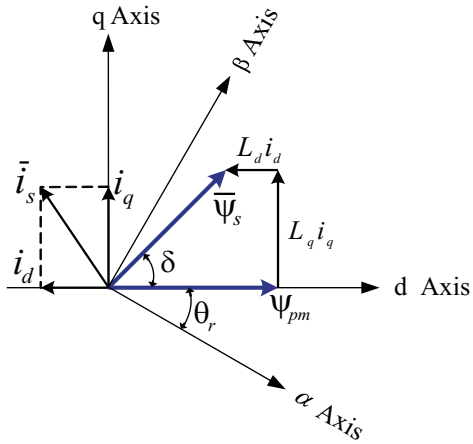

Figure C.4: Vector diagram of IPM synchronous motor.

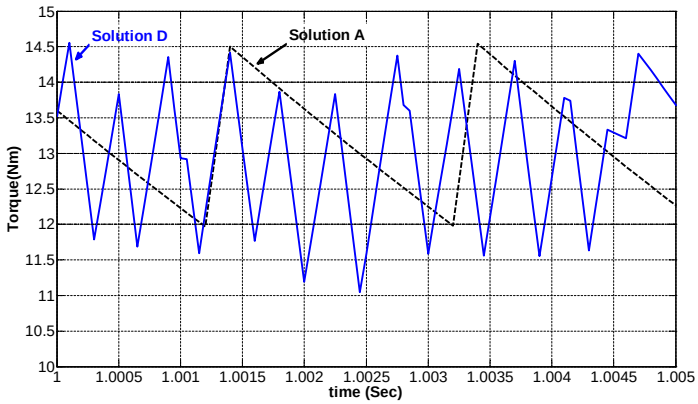

Figure C.5: Torque waveform for switching algorithm A and D.

where $A = \begin{bmatrix} -\frac{R}{L_d} & \omega_r \\ -\omega_r & -\frac{R}{L_q} \end{bmatrix}$.

ψ_{d0} and ψ_{q0} are the rotor flux components in d and q axes at the initial time instant (the time that the zero voltage vector is applied) which here is assumed to be zero for simplicity. The states equilibrium points are points where the time derivatives are zero. These state equilibrium points, ψ_d^e and ψ_q^e, can be calculated as [18]:

$$\psi_d^e = \frac{R^2}{R^2 + \omega_r^2 L_d L_q} \psi_{pm} \tag{C.18}$$

$$\psi_q^e = -\frac{R L_q \omega_r}{R^2 + \omega_r^2 L_d L_q} \psi_{pm}. \tag{C.19}$$

In this case the parametric calculation of the exponential matrix function is difficult but it is possible to describe the system behavior by looking at the

eigenvalues of matrix A. The characteristic function of matrix A is [18]:

$$\lambda^2 + R(\frac{1}{L_d} + \frac{1}{L_q})\lambda + \frac{R^2}{L_d L_q} + \omega_r^2 = 0. \tag{C.20}$$

This equation can be solved to obtain eigenvalues λ. Depending on the speed, the system has two real negative eigenvalues or two complex conjugate eigenvalues with negative real parts. These eigenvalues, λ_1 and λ_2, are:

$$\begin{aligned}\lambda_{1,2} &= -\frac{1}{2}R(\frac{1}{L_d} + \frac{1}{L_q}) \\ &\pm \frac{1}{2}\sqrt{R^2(\frac{1}{L_d} + \frac{1}{L_q})^2 - 4(\omega_r^2 + \frac{R^2}{L_d L_q})} \\ &= -\frac{1}{2}R(\frac{1}{L_d} + \frac{1}{L_q}) \pm \frac{1}{2}\sqrt{R^2(\frac{1}{L_d} - \frac{1}{L_q})^2 - 4\omega_r^2}.\end{aligned} \tag{C.21}$$

If ω_{rc} is defined as $\omega_{rc} = \frac{1}{2}R(\frac{1}{L_d} - \frac{1}{L_q})$, then for $\omega_r < \omega_{rc}$ there are two negative real eigenvalues and for $\omega_r > \omega_{rc}$ there are two complex conjugate eigenvalues with negative real parts. For the machine used in this paper $\omega_{rc} = 10.34\ rad/sec$ which is equivalent to the mechanical speed of 32.9 rpm.

For $\omega_r \ll \omega_{rc}$ the eigenvalues can be approximated as:

$$\lambda_{1,2} = -\frac{1}{2}R(\frac{1}{L_d} + \frac{1}{L_q}) \pm \frac{1}{2}R(\frac{1}{L_d} - \frac{1}{L_q}) \tag{C.22}$$

and for $\omega_r \gg \omega_{rc}$ the eigenvalues can be approximated as:

$$\lambda_{1,2} = -\frac{1}{2}R(\frac{1}{L_d} + \frac{1}{L_q}) \pm j\omega_r. \tag{C.23}$$

For all speeds the real part of eigenvalues are negative so exponential stability of the system (time-invariant system) is guaranteed [18]. Moreover as time increases the trajectory of states will move towards the equilibrium points that are calculated in (18) and (19). The speed is assumed to be constant for a long time to be able to identify the states trajectory treatment. Figure 6 shows the stator flux trajectory for different speeds and how the equilibrium points changes as a function of speed. The time is not shown in this graph so in a real system the trajectory will be different (after a few switching samples a non-zero voltage vector will be applied to increase the torque and this will change the trajectory).

If both eigenvalues are real and negative, say λ_1 and λ_2, then in the state response the terms $e^{\lambda_1 t}$ and $e^{\lambda_2 t}$ tend to zero after a while (λ_1 and λ_2 are negative values)[18]. The state trajectory in ψ_d and ψ_q plane directly moves towards the equilibrium point (that is a function of speed). If eigenvalues are complex conjugate ($\omega_r > \omega_{rc}$) then the state responses includes $e^{\alpha t} cos\omega_r t$ which means that there will be some oscillations in the time response (α is the real part of the eigenvalue λ and is negative also). The oscillation frequency is equivalent to the imaginary part of eigenvalues. The higher the speed, the

higher the time domain oscillations and that will cause circulation in the state plane trajectory (Fig. C.6) [18].

In this simulations (when the zero voltage vector is applied) it has been assumed that the load angle is positive, because the torque should be decreased by applying zero voltage. However this assumption does not affect the results. The magnitude of the stator flux and torque are shown in Fig. C.7 and Fig. C.8. As was expected, both are decreasing when a zero voltage vector is applied to the machine. The decrement of flux magnitude is not sensitive to the speed for a short time (10 sample times in this case) but the torque decrement is very sensitive to the speed. The reason for the fast torque decrement is that the torque is very sensitive to the flux angle (load angle) as can be seen from equation C.15.

When the zero voltage vector is applied, in the low speed region the torque decrement is smoother than that in the high speed region. As a result, for high speed applications, applying a zero voltage vector to decrease the torque will create more torque ripple compared to the low speed region.

C.4 Conclusion

For a DTC based IPM synchronous motor drive system, the effects of the inverter switching pattern on the drive system performance in terms of the torque ripple, stator current ripple, stator flux magnitude ripple and inverter switching frequency was investigated at low speeds. It is shown that the inverter switching pattern A which employs the zero voltage vector to reduce the torque has better performance compared to the other switching methods at low speeds. The analytical analysis of the system was made for the inverter zero-voltage vector to quantify the machine torque and flux. The flux trajectory and torque as a function of time has been presented for different speeds. The analytical results show that applying a zero voltage vector reduces the motor torque for different speeds.

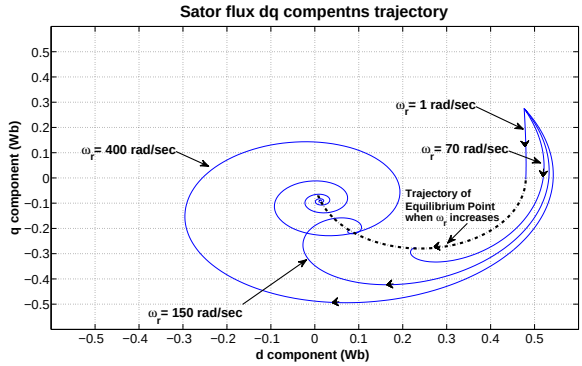

Figure C.6: Stator flux trajectories for different speeds and inverter zero-voltage vector (constant speed assumption).

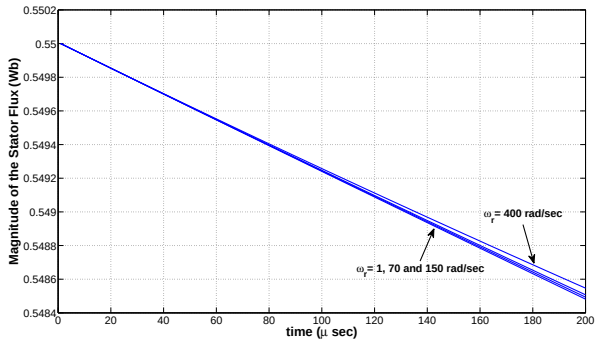

Figure C.7: Magnitude of the stator flux for different speeds as a function of time with the inverter zero-voltage vector (constant speed assumption).

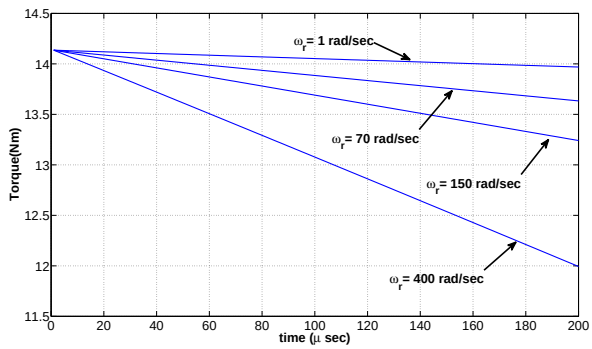

Figure C.8: The developed motor torque for different speeds with the inverter zero-voltage vector (constant speed assumption).

References

[1] H. Murakami, Y. Honda, H. Kiriyama, S. Morimoto and Y. Takeda, "The performance comparison of SPMSM, IPMSM and SynRM in use as air-conditioning compressor," Conf. Rec. IEEE IAS, vol. 2, pp. 840-845, 1999.

[2] Zeraoulia Mounir, Benbouzid Mohamed El Hachemi, Diallo Demba, "Electric motor drive selection issues for HEV propulsion systems : A comparative study," IEEE transactions on vehicular technology ISSN 0018-9545 2006, vol. 55, no6, pp. 1756-1764.

[3] M. A. Rahman, "Recent Advances of IPM Motor Drives in Power electronics word", PDES 2005, pp. 24-31.

[4] T. M. Jahns, G. B. Kliman, and T. W. Neuman, "Interior PM synchronous-motors for adjustable speed drives," IEEE Trans. Ind. Appl., vol. IA-22, no. 4, pp. 738-747, Jul./Aug. 1986.

[5] Li Yongdong and Zhu Hao, "Sensorless Control of Permanent Magnet Synchronous Motor - A Survey," IEEE Vehicle Power and Propulsion Conference (VPPC), September 3-5, 2008, Harbin, China.

[6] I. Takahashi and T. Noguchi, "A new quick-response and high-efficiency control strategy of an induction motor," IEEE Trans. on Industry Applications, vol. 22, no. 5, pp. 820-827, 1986.

[7] M. Depenbrock, "Direct self-control (DSC) of inverter-fed induction machine," IEEE Trans. on Power Electronics, vol. 3, no. 4, pp. 420-429, 1988.

[8] P. Tiitinen and M. Surandra, "The next generation motor control method, DTC direct torque control," Power Electronics, Drives and Energy Systems for Industrial Growth, 1996., Proceedings of the 1996 International Conference on, Vol. 1 (1996), pp. 37-43 vol.1.

[9] Peter.Vas, "Sensorless vector and direct torque control," Oxford Press, 1998.

[10] G. Buja, Domenico Casadei and Giovanni Serra, "Direct torque control of induction motor drives," ISIE'97, Guimaraes, Portugal, IEEE Catalogue Number: 97TH8280.

[11] Y. W. Hu, C. Tian, Y. K. Gu, Z. Q. You, L. X. Tang and M. F. Rahman, "In-depth research on direct torque control of permanent magnet synchronous motor", IEEE Proceedings on industrial electronics society, Vol. 2, pp. 1060-1065, 2002.

[12] L. Zhong, M.F.Rahman, W.Y.Hu, "Analysis of direct torque controlin PMSM drives," IEEE Trans. Power Electronics, vol. 12, no3, pp. 528-536, 1997.

[13] G. Buja, Domenico Casadei and Giovanni Serra, "Direct torque control of induction motor drives," ISIE'97, Guimaraes, Portugal, IEEE Catalogue Number: 97TH8280.

[14] M. F. Rahman and L. Zhong, "Voltage switching tables for DTC controlled interior permanent magnet motor," IECON'99, 25th annual Conference June 1999. p. 1445-51.

[15] Frede Blaabjerg, G. D. Andreescu, C.I. Pitic and I. Boldea, "Combined Flux Observer With Signal Injection Enhancement for Wide Speed Range Sensorless Direct Torque Control of IPMSM Drives," IEEE Transactions on Energy Conversion, vol. 23, no. 2, June 2008.

[16] Saeid Haghbin and Torbjorn Thiringer, "Impact of inverter switching pattern on the performance of a direct torque controlled synchronous reluctance motor drive," International Conference on Power Engineering, Energy and Electrical Drives, POWERENG 09, 18-20 March 2009, Lisboa, Portugal, pp. 337-341.

[17] Wilson J. Rugh, "Linear system theory," second edition, Prentice Hall, 1996.

[18] H. Khalil, "Nonlinear systems," third edition, Prentice Hall, 2002.